International School for Advanced Studies

Physics Area / Condensed Matter

Ph.D. thesis

Non-equilibrium aspects of topological Floquet quantum systems

Candidate
Lorenzo Privitera

Supervisor
Prof. Giuseppe E. Santoro

October 2017
Via Bonomea 265, 34136 Trieste - ITALY

Contents

1. Introduction

The manifestations of topology are ubiquitous in condensed matter physics [1, 2, 3, 4]. One of the most striking examples is the integer quantum Hall effect [5]: the quantization of the Hall conductance for 2D electrons in a constant magnetic field. The standard topological argument [6, 7] says that if the Fermi energy lies in a spectral gap, the Hall conductivity for non-interacting electrons on a lattice is equal to the universal constant e^2/h times an integer number, the *Chern number*. The Chern number is a topological invariant, meaning that it cannot change under smooth variations of the parameters of the system, unless the spectral gap closes and reopens. For this reason, this topological phase is intrinsically robust to perturbations: the underlying physics is not substantially modified by electronic interactions as long as they do not become too strong.

An important theoretical effort towards the extension of these concepts was put forward by Haldane in 1988. He proposed a tight-binding model on the honeycomb lattice without a constant magnetic field, where in some regions of parameter space, a non-zero quantized Hall conductivity could be obtained. He called this phase "Quantum Hall effect without Landau levels". Today it is usually referred to as *Chern insulator*. This work paved the way for what, starting from 2005 [8, 9], has been a revolution in condensed matter. The topological characterization of matter with suitable topological invariants has indeed become a standard tool, and many new materials and phases have been discovered. Limiting ourselves to non-interacting fermionic systems, we mention topological insulators [10, 11], which are the direct generalization of Chern insulators, topological superconductors [12] and Weyl semimetals [13] among others. An important characteristic of these phases is the existence of gapless boundary states in their spectrum [14], whose number depend on the value of the topological invariant, which is a bulk quantity [10, 11, 15]. Because of this *bulk-edge correspondence*, these surface modes are topologically protected from perturbations as the topological invariant is. Their unique properties are indeed at the heart of many of the potential applications of topological materials that have been proposed. Examples include their use in spintronics [16], or as efficient catalysts [17, 18], high-performing components in nanoscale electronic circuits [19, 20], and, most famously, as a basic ingredient for the realization of a fault-tolerant quantum computer [21, 22].

The topological phases that we have mentioned so far are all equilibrium ones. However, it has been realized that topology can manifest itself also in *time-dependent* quantum systems. In this context, a pioneering work was that of Thouless [23], who showed with a topological

argument, that an adiabatic, periodic variation of the parameters of a band insulator leads to a quantized charge transport, a mechanism that is known as *Thouless pump*. This result has had a profound impact in condensed matter physics, ranging from the modern theory of polarization [24, 25], to the field of quantum pumping in mesoscopic systems [26]. Moreover, in 2016, two different experiments have explicitly demonstrated Thouless's idea using ultracold atoms in optical lattices [27, 28].

More recently, a new class of periodically driven systems displaying topological features has been introduced, following the original proposal by Oka and Aoki for a photovoltaic Hall effect in graphene [29], where a single sheet of graphene irradiated by a circularly polarized electric field is show to display a non-zero Hall conductivity without any magnetic field. Soon after [30], it was realized that this model had a non-trivial topological characterization. This can be seen by studying the *Floquet Hamiltonian* of the problem, which can be defined through the evolution operator over one driving period τ as $\hat{U}(\tau + t_0, t_0) \equiv \exp(-\frac{i}{\hbar}\hat{H}_F\tau)$, where $\hat{H}_F$ is an effective Floquet Hamiltonian. At large enough driving frequencies, $\hat{H}_F$ can be shown to have the form of a Haldane model: consequently, this kind of systems is referred to as *Floquet Chern insulators*. Since then, periodic perturbations have gained much attention as a way to induce topological transitions in otherwise "trivial" systems [31, 32, 33]. Several experiments [34] have then tried to prove this concept and most remarkably, an ultracold atoms experiment [35] used this scheme described above to actually map the phase diagram of the Haldane model.

The question that we try to address in this thesis is how much of these topological structures can be harnessed in the realistic dynamics of a closed quantum system. In other words, what are the signatures of topology in the time-evolved state and, consequently, on the observables? Our analysis shows that in both the two kinds of topological periodically driven systems that we have mentioned, Thouless pumping and Floquet Chern insulators, the nonequilibrium occupations of the eigenvalues of the Floquet Hamiltonian, the so called *quasieenergies*, play a crucial role.

In the case of Floquet Chern insulators, to actually achieve a topological state, one would need to populate a quasienergy Floquet-Bloch band having a non-zero Chern number. It is usually assumed that this can be done by slowly turning-on the periodic driving, thanks to a generalized version of the adiabatic theorem. However, our work shows that at the end of the ramping process there is a dichotomy between the bulk and the edge of the system: while the bulk states can be populated in a controlled way, edge states get unavoidable excitations due to exponentially small gaps preventing adiabaticity. These defects reflect in nonequilibrium currents flowing at the edges, that can be manipulated by tailoring the parameters of the periodic driving. Nevertheless, the nonequilibrium state undergoes a generalized form of topological transition, thanks to the controlled population of bulk states. We have been able to characterize this change in the topology of the system by recurring to the Local Chern Marker of Bianco and Resta [36].This is essentially a local measure of the Hall conductivity at equilibrium, and we generalized it to a time-dependent version.

In the case of Thouless pumping we investigated the effects of a driving being not perfectly adiabatic. Having a topological nature, Thouless pumping is generally believed to be robust to many "imperfections", such as disorder [37], finite size effects [38, 39] and finite temperature. Non-adiabatic effects are also believed to be unimportant, specifically to be exponentially small in the frequency of the driving [40, 41]. We analysed the pumped charge averaged over many cycles and discovered that the corrections to perfect quantization of the pumped charge are actually *quadratic* in the frequency of the driving. In particular, exponentially small deviations would be obtained only if one were able to prepare a certain Floquet state, but, analogously to the case of the Floquet Chern insulator, this is physically hard to realize.

The outline of the present thesis will be as follows. In Chap. 2 we will give an overview of Floquet theory for integrable periodically driven quantum systems and discuss their main topological features, trying to put them under a unified framework. Having set the arena for our results, we will start their exposition in Chap 3, where we will study the adiabatic preparation of the Floquet Chern insulator on the honeycomb lattice. After having described our model, we will study the simpler case of the adiabatic dynamics of the driven Haldane model, that will clarify the physical mechanisms behind the Floquet case. We will then return to the periodically driven case, highlighting the properties of the non-equilibrium currents and their dependence on the form of the periodic driving. Special emphasis will be given to the nonequilibrium topological analysis . Finally, we will conclude by examining the more complicated case of resonant driving, where the topological characterization is more intriguing and the adiabatic picture breaks down. Chapter 4 will be devoted to Thouless pumping, studied in the well known Rice-Mele model [42]. We will use analytical and exact numerical methods to demonstrate the non-adiabatic breaking of topological pumping and study its behaviour also far from the adiabatic limit. We will discuss also the role of an initial thermal state and how the pumped charge can be separated into a geometrical component and a dynamical one.

The papers over which the present thesis is based are.

- L. Privitera and G. E. Santoro. "Quantum annealing and nonequilibrium dynamics of Floquet Chern insulators". *Phys. Rev. B*, **93**, 241406, (2016)
- L. Privitera, A. Russomanno, R. Citro and G. E. Santoro. "Non-adiabatic breaking of Thouless pumping". Submitted to *Phys. Rev. Lett.. arXiv preprint arXiv:1709.08457* (2017)

Moreover during my PhD I also published this paper on strongly correlated topological insulators at equilibrium

- A. Amaricci, L. Privitera, F. Petocchi, M Capone, G. Sangiovanni, and B. Trauzettel. "Edge state reconstruction from strong correlations in quantum spin Hall insulators". *Phys. Rev. B*, **95**, 205120 (2017)

2. Floquet theory and topological structures in integrable periodically driven systems

In the present chapter we give a self-contained introduction to some concepts that will be of great importance for this thesis. We will begin in section 2.1 with a basic outline of Floquet theory for periodically driven quantum systems, which we will use to study the generic long-time dynamics of periodically driven systems, elucidating the differences between integrable systems and non-integrable ones. In section 2.2 we will use Fourier series to map Floquet systems into $d+1$ dimensional static ones and show how this "dimensional extension" is effective only for small driving frequencies. Finally in section 2.3, we will introduce the typical topological characteristics of integrable Floquet systems, using models and concepts that we will use in the following chapters.

2.1. Basics of Floquet theory for quantum systems

Floquet theory is the name of the branch of the theory of ordinary differential equations concerning the properties of linear differential equations with periodic coefficients. It takes its name from the 19-th century French mathematician Gaston Floquet. In quantum mechanics, given the linearity of the Schrödinger equation, it finds applications in situations where the Hamiltonian is periodic in space (Bloch's theorem) and/or in time. In the latter case [43, 44, 45, 46], the fundamental theorem of Floquet theory, the *Floquet theorem*, can be stated in the following way. If $\hat{U}(t,t')$ is the evolution operator from time t to time t', and $\tau = 2\pi/\omega$ is the period of the Hamiltonian, then the following relation holds

$$\hat{U}\left(t+n\tau,t_0\right)=\hat{U}\left(t,t_0\right)\left[\hat{U}\left(t_0+\tau,t_0\right)\right]^n . \tag{2.1}$$

It is then evident that the evolution operator over one period, $\hat{U}\left(t_0+\tau,t_0\right)$, is the central object in the study of a periodically driven system, since it contains all the information to study the stroboscopic dynamics of the system (e.g., at times that are integer multiples of the period). It is termed as *Floquet operator* and, being a unitary operator, it is often written as

$$\hat{U}\left(\tau+t_0,t_0\right)=e^{-\frac{i}{\hbar}\hat{H}_F\tau}, \tag{2.2}$$

where $\hat{H}_F$ is an Hermitian operator, the *Floquet Hamiltonian*. $\hat{H}_F$ is an effective Hamiltonian, not in the usual low-energy sense of equilibrium systems, but rather for the dynamics of the

driven system. From now on we will set $t_0 = 0$. The eigenstates $|\phi_\alpha(0)\rangle$ of the Floquet operator are called *Floquet modes* and since the eigenvalues must be complex phases, the spectral representation of $\hat{U}(\tau, 0)$ has the form

$$\hat{U}(\tau, 0) = \sum_\alpha e^{-\frac{i}{\hbar}\varepsilon_\alpha \tau} |\phi_\alpha(0)\rangle \langle\phi_\alpha(0)| \ . \tag{2.3}$$

The real quantities ε_α are the *quasienergies*. They can be translated by an integer multiple of $\hbar\omega$, since they would give rise to the same eigenvalue. In this sense, one can choose a *Floquet Brillouin zone* (FBZ) of size $\hbar\omega$, in analogy with quasimomentum of Bloch states in crystals. We define the Floquet modes at a generic time t as $|\phi_\alpha(t)\rangle = e^{\frac{i}{\hbar}\varepsilon_\alpha t}\, \hat{U}(t, 0)\, |\phi_\alpha(0)\rangle$, where the phase factor in front guarantees that these states are *periodic*, i.e., $|\phi_\alpha(\tau)\rangle = |\phi_\alpha(0)\rangle$. Then, the time-dependent Schrödinger equation will be satisfied by the *Floquet states*

$$|\psi_\alpha(t)\rangle = e^{-\frac{i}{\hbar}\varepsilon_\alpha t}\, |\phi_\alpha(t)\rangle \tag{2.4}$$

at any instant in time, if the initial condition is $|\psi_\alpha(0)\rangle = |\phi_\alpha(0)\rangle$. At this point the analogy with Bloch's theorem is complete. The Floquet states correspond to Bloch states and the Floquet modes to their periodic part. We also remark that the Floquet modes (and states) are orthonormal at any instant in time and therefore form a complete basis of the Hilbert space.

After substituting Eq. (2.4) into the time-dependent Schrödinger equation, we obtain the eigenvalue equation for the quasienergies

$$\hat{\mathcal{K}}(t)\, |\phi_\alpha(t)\rangle = \varepsilon_\alpha\, |\phi_\alpha(t)\rangle \ , \tag{2.5}$$

with the Hermitian operator

$$\hat{\mathcal{K}}\,(t) \equiv \hat{H}(t) - i\hbar \frac{\partial}{\partial t} \ , \tag{2.6}$$

that we call *Floquet extended Hamiltonian*. Since the eigenvectors of $\mathcal{K}$ are periodic in time, it is convenient to consider $\mathcal{K}(t)$ as acting in the extended Hilbert space $\mathscr{H} \otimes \mathscr{T}$ made up of the usual (configuration) Hilbert space $\mathscr{H}$ and the space of time-periodic functions $\mathscr{T}$, where we take as a basis the vectors $\mathrm{e}^{im\omega t}$ [46]. The inner product in $\mathscr{H} \otimes \mathscr{T}$ is taken to be

$$\langle\langle f|g\rangle\rangle = \frac{1}{\tau}\int_0^\tau \langle f|g\rangle \mathrm{d}t \ . \tag{2.7}$$

In this way, as first noticed by Sambe [44], all the properties of the stationary Schrödinger equation (Perturbation theory, Hellmann-Feynman theorem, etc.) are obtained, with the only difference that the role of $\hat{H}$ is played by $\hat{\mathcal{K}}$ and the scalar product is taken in the extended Hilbert space with the definition given above. For example, the Hellmann-Feynman theorem becomes (see appendix E for an explicit demonstration)

$$\frac{d\varepsilon_\alpha\,(\lambda)}{d\lambda} = \frac{\langle\langle\phi_\alpha|\frac{d\hat{\mathcal{K}}(\lambda)}{d\lambda}|\phi_\alpha\rangle\rangle}{\langle\langle\phi_\alpha|\phi_\alpha\rangle\rangle} \ . \tag{2.8}$$

Most importantly for this thesis, a *Floquet adiabatic theorem* can be established [30, 46, 47, 48, 49]. Indeed, if some parameter $\lambda(t)$ of the Hamiltonian is varied on a time scale that is much longer than the period of the periodic driving, the concept of adiabaticity that is introduced for static systems can be recovered in a new form. Let us call $|\psi_\alpha[\lambda(\bar{t})], t\rangle$ the instantantaneous Floquet states at time t for the value $\lambda(\bar{t})$, that is, the Floquet states calculated by keeping fixed λ to its value at time $\bar{t}$. Thus a system that at time $t = 0$ is prepared in a Floquet state $|\psi_\alpha[\lambda(0)], 0\rangle$ will follow the corresponding instantaneous Floquet state at any time, provided that the related quasienergy $\varepsilon_\alpha[\lambda]$ is separated from the other ones, e.g. $\min_{m\in\mathbb{Z},\beta\neq\alpha}(|\varepsilon_\alpha - \varepsilon_\beta + m\hbar\omega|) > 0$ and λ varies sufficiently slowly. The analogy with static systems can be pushed even further since one can then develop an adiabatic perturbation theory [50] to systematically calculate the deviations from perfect adiabatic dynamics. In appendix A we give a very simple application of Floquet adiabatic perturbation theory to the calculation of the Hall conductivity for a 2d periodically driven closed system. A different kind of adiabatic perturbation theory will be instead used in Chapter 4.

2.1.1. Approach to a steady state in closed Floquet systems

The long-time behaviour of periodically driven systems has been extensively investigated in the last years. What is now established is that, in general, expectation values in a closed Floquet system will always reach an asymptotic behaviour that is synchronous with the driving. Only few exceptions exist, such as many-body localized systems. To be a bit more explicit, let us write the state of the system in the Floquet basis: $|\Psi(t)\rangle = \sum_\alpha c_\alpha |\psi_\alpha(t)\rangle$. We consider then the expectation value of a generic operator $\hat{O}$, and call $\mathbb{O}_{\alpha\beta}$ its matrix elements in the Floquet basis. We have

$$\langle\hat{O}\rangle(t) = \langle\Psi(t)|\hat{O}(t)|\Psi(t)\rangle = \underbrace{\sum_\alpha |c_\alpha|^2 \mathbb{O}_{\alpha\alpha}(t)}_{\langle O\rangle_{diag}(t)} + \sum_{\beta\neq\alpha} c_\beta^* c_\alpha e^{\frac{i}{\hbar}(\varepsilon_\beta-\varepsilon_\alpha)t}\mathbb{O}_{\beta\alpha}(t) \ . \tag{2.9}$$

The first term contains only the diagonal matrix elements of the observable and is τ-periodic. The second term instead is not periodic, because of the exponential factors, but it vanishes in the thermodynamic and long time limits, because of destructive interference effects. To see this, we introduce the weighted density of states

$$F_{\hat{O}}(t;\Omega) = \pi \sum_{\beta\neq\alpha} c_\beta^* c_\alpha \mathbb{O}_{\beta\alpha}(t)\delta(\hbar\Omega - \varepsilon_\alpha + \varepsilon_\beta) \ . \tag{2.10}$$

Now we can write Eq. (2.9) as

$$\langle\hat{O}\rangle(t) = \langle\hat{O}\rangle_{diag}(t) + \int_{-\infty}^{+\infty} \frac{\mathrm{d}\Omega}{\pi} F_{\hat{O}}(t;\Omega)\, e^{i\Omega t} \quad \xrightarrow{t\to\infty} \langle\hat{O}\rangle_{diag}(t) \tag{2.11}$$

The last limit is justified by the Riemann-Lebesgue lemma [51], provided that $F_{\hat{O}}(t;\Omega)$ is a smooth function of Ω. This will happen in the thermodynamic limit when the spectrum

becomes a continuum and the infinite sum of Dirac deltas in (2.10) "melts" into a non-singular function. For a detailed discussion (e.g. what happens when the system is disordered and the spectrum discrete) of the conditions under which this happens see [45, 52, 53]. Thus a closed quantum system that is periodically driven evolves in such a way that the expectation values synchronize with the driving. It is usually said that observables converge to the *Floquet diagonal ensemble* value, e.g. the system tends towards a state whose density matrix is diagonal in the Floquet basis.

From the presence of the factors $|c_\alpha|^2 = |\langle\Psi(0)|\,\phi_\alpha(0)\rangle|^2$ in $\langle\hat{O}\rangle_{diag}$, one could argue that the system keeps memory of its initial state forever. This is only an apparent paradox, even though one has to isolate the case of integrable systems [53, 54]. In that case indeed, in analogy with classical mechanics, conserved quantities strongly affect the dynamics of the system in a non-ergodic fashion. Expectation values tend in time towards a τ-periodic function, whose specific form is dictated by the initial conditions. What happens in a non-integrable system, instead, is a generalization of thermalization for an undriven non-integrable system undergoing a quantum quench. In the quantum quench case, the related diagonal ensemble density matrix becomes indistinguishable from a thermal one. This is because, according to the Eigenstate Thermalization Hypothesis [55] the expectation value over an energy eigenstate is equal to a microcanonical thermal expectation value. Moreover the conservation of energy restricts the system to the micro-canonical energy shell: the corresponding thermal density matrix will have matrix elements only between Hamiltonian eigenstates within the energy shell determined by the fixed value of energy. This makes the diagonal density matrix look like a thermal one. In the non-integrable Floquet case instead, the system can continue to absorb energy indefinitely, until it reaches a "trivial" infinite temperature state, e.g., one with all Floquet states being equally probable. This can be seen by introducing an analogue of the Eigenstate Thermalization Hypothesis for driven systems. Its fundamental feature is that in the thermodynamic limit each (many-body) Floquet state is essentially indistinguishable from the others. In this way, the diagonal density matrix approaches a constant $\hat{\rho} \simeq 1/D$, with D being the dimension of the Hilbert space. This signals an infinite temperature state: expectation values of observables will be not only periodic in time but also constant. This hypothesis has been explicitly verified in many cases [56, 57, 58, 59].

In this thesis we will anyway deal only with integrable systems, and non-integrability will be a subject only of marginal considerations.

2.2. Fourier representation of a periodically driven system.

The calculation of Floquet states guarantees full knowledge of the dynamics of our system. In particular, finding them at the initial time, is equivalent to diagonalizing the Floquet operator $\hat{U}(\tau, 0)$ and Hamiltonian $\hat{H}_F$, which are a tool to access the stroboscopic part of the dynamics. As we mentioned in section 2.1, the quasienergies and Floquet modes at all

times can also be found from another eigenvalue equation, the one for the Hermitian operator $\hat{\mathcal{K}}(t)$, see Eq. (2.5). This equation in turn, can be made time-independent by expanding the Floquet modes, which are time-periodic, in Fourier series [43, 44, 46]:

$$|\phi_\alpha(t)\rangle = \sum_{m=-\infty}^{+\infty} |\chi_{\alpha,m}\rangle \, \mathrm{e}^{im\omega t} \, . \tag{2.12}$$

Plugging this expression into Eq. (2.5), multiplying by $e^{-im\omega t}$ and integrating over one period gives us

$$\sum_{m'=-\infty}^{\infty} \hat{H}_{m-m'} \left|\chi_{\alpha,m'}\right\rangle + m\hbar\omega \, |\chi_{\alpha,m}\rangle = \varepsilon_\alpha \, |\chi_{\alpha,m}\rangle \ , \tag{2.13}$$

where $\hat{H}_{m-m'}$ is the $(m-m')$-th Fourier component of the Hamiltonian:

$$\hat{H}_n = \frac{1}{\tau} \int_0^\tau \mathrm{d}t \ \hat{H}(t) \, \mathrm{e}^{-in\omega t} \, . \tag{2.14}$$

The harmonics index m can be regarded as a label of lattice sites in an additional fictitious spatial dimension. From this point of view, the matrix elements[1] $\hat{\mathcal{K}}_{m',m} = \hat{H}_{m-m'} + m\hbar\omega\delta_{m,m'}$ are the ones of a Hamiltonian with hoppings $\hat{H}_{m-m'}$ connecting sites with coordinates m and m' and a linear "potential" $m\hbar\omega\delta_{m,m'}$, such as the one derived from an electric field. At a first glance, one could think that the number of solutions is equal to the number of "Fourier" lattice sites (which is actually infinite) times the dimension of the Hilbert space of $\hat{H}$. Nevertheless, as we have already discussed in section 2.1, if ε_α is an eigenvalue with corresponding Fourier amplitudes $|\chi_{\alpha,m}\rangle$, then $\tilde{\varepsilon}_\alpha = \varepsilon_\alpha + p\hbar\omega$ is another eigenvalue whose corresponding eigenvector has Fourier amplitudes $|\tilde{\chi}_{\alpha,m}\rangle = |\chi_{\alpha,m+p}\rangle$, in a way that is totally analogue to what is known as *Wannier-Stark ladder* in the electric field case. Therefore they will give the same (Floquet state) solution of the Schrödinger equation. Summarizing, from the d-dimensional time-dependent problem of Eq. (2.5) we arrive at the $d+1$-dimensional one of Eq. (2.13), describing particles under the influence of a static "electric field" along the extra (Fourier) dimension. This problem has been studied intensively since the advent of modern solid state theory [60, 61]. What concerns us most is that the eigenfunctions of the Wannier-Stark problem are *localized* by the electric field in real space [62, 63].

For the sake of concreteness, we consider a 1d non-interacting translationally-invariant tight-binding Hamiltonian $\hat{H}_0$ driven by one monochromatic time-periodic field:

$$\hat{H}(t) = \hat{H}_0 + \hat{A}e^{i\omega t} + \hat{A}^\dagger e^{-i\omega t} \, . \tag{2.15}$$

[1] Actually these are not numbers, but operators acting only on the Hilbert space $\mathscr{H}$, rather than the composite space $\mathscr{H} \otimes \mathscr{T}$. See the discussion in section 2.1.

In Fourier space this reads

$$\begin{pmatrix} \ddots & \hat{A} & & & & \\ \hat{A}^\dagger & \hat{H}_0 + \hbar\omega & \hat{A} & & & \\ & \hat{A}^\dagger & \hat{H}_0 & \hat{A} & & \\ & & \hat{A}^\dagger & \hat{H}_0 - \hbar\omega & \hat{A} & \\ & & & \hat{A}^\dagger & \ddots & \end{pmatrix} . \tag{2.16}$$

We call x the real space direction and y the Fourier one. While there is translational invariance along x, the scalar potential $m\hbar\omega$ breaks it along y and competes with the hopping along the same direction induced by $\hat{A}$. In the limit where $\omega \to 0$ (very slow, *adiabatic* driving), the Hamiltonian in extended space will be translationally invariant along both axis and, consequently, the eigenstates will be Bloch states, with the role of quasimomentum along y k_y played by $\varphi = \omega t$. Moreover both ε_α and $|\phi_\alpha(\varphi(t)\rangle$ will coincide with the eigenstates of $\hat{H}(\varphi(t))$. When ω is finite instead, the "electric field" will localize the eigenstates along y, the α-th eigenstate centred around the α-th site along y[2]. This fact is called *Wannier-Stark localization*. When $\omega \to \infty$ the hoppings along y will be completely ineffective, breaking the systems into uncoupled 1d chains. The spectrum will be therefore made of copies of the spectrum of $\hat{H}_0$ translated by $m\hbar\omega$. In general, when $\hbar\omega$ is larger than any of the energy scales in $\hat{H}_0$, we can still describe the system by focusing on one of the chains and then adding the coupling as a perturbation. Restricting ourselves to the subspace of the chain with $m = 0$, we consider virtual hopping processes and add them to our "low-energy" description with second-order perturbation theory. Indeed, if ε is the energy associated to an eigenstate of $\hat{H}_0$, going from $m = 0$ to $m = 1$ and coming back is described by a term $\hat{A}\frac{1}{(\varepsilon+\hbar\omega)-\varepsilon}\hat{A}^\dagger$, while going from $m = 0$ to $m = -1$ gives $\hat{A}^\dagger\frac{1}{(\varepsilon-\hbar\omega)-\varepsilon}\hat{A}$. This means that the Hamiltonian for the Floquet modes is the original one-dimensional Hamiltonian $\hat{H}_0$ with no dimensional extension, but simply with some additional terms, that at first order in $1/\omega$ read $\left[\hat{A}, \hat{A}^\dagger\right]/(\hbar\omega)$. This expansion in $1/\hbar\omega$ can be also developed for $\hat{H}_F$ in a systematic way, as we will see in the next chapters.

Summarising, periodically driven systems in d dimension can be seen as static systems in $d + 1$ dimension. However, the bigger is the driving frequency, the less effective is this dimensional extension. At very high frequencies indeed it is more convenient to include the effects of the driving as a perturbative modification of the Hamiltonian in the original d dimensional system. This Fourier-based dimensional extension is convenient also because it allows to treat multiple periodic drivings that are mutually incommensurate [65] (hence Floquet theory would not apply).

[2] In our simple case, the wavefunction of the α-th eigenstate at Fourier site m is proportional to $J_{|m-\alpha|}(t/(\hbar\omega))$, where J_n is the Bessel function of the first kind of order n and t is the hopping matrix element between nearest neighbour sites along y direction, which depends on the specific form of the driving operator $\hat{A}$ [64].

2.3. Appearance of topology in Floquet systems

Although possessing an intrinsically non-equilibrium nature, periodically driven systems can have a topological characterisation, as static systems do. Let us consider the case of free fermions. In the time-independent case, one usually constructs many-body states, e.g. Slater determinants, out of the single particle Hamiltonian eigenstates and compute the appropriate associated topological invariant, which sometimes corresponds to a specific observable quantity. This construction can be naturally extended by replacing Hamiltonian eigenstates with Floquet states. In the prototypical situation of static systems, the Slater determinant is the one of a Bloch band separated in energy from the others and the choice of the invariant depends on the symmetries and dimensionality of the Hamiltonian [66]. The most immediate generalisation for Floquet systems [31, 67] is to build a Slater determinant of the Floquet modes at the initial time, which govern the stroboscopic dynamics and are eigenstates of $\hat{H}_F$. One can then choose those modes that correspond to a *quasienergy* Bloch band that is separated in quasienergy from the others for a given choice of the Floquet Brillouin zone. Another possibility is instead to consider the Floquet modes at all times. As we have discussed, these are the eigenvectors of a d+1-dimensional static operator and this dimensional extension is particularly effective at low frequencies. In this case, it is instead natural to characterise topologically the system with the invariants of static $d+1$ systems [68].

In what follows, we are going to give some examples that elucidate the ways topology enters Floquet systems and that are relevant for the rest of this thesis. We stress that our goal is not to give a complete overview of the subject, nor to elucidate the ways to classify all of the symmetry-protected topological phases in integrable Floquet systems [67, 69, 70, 71]. We want instead to highlight the main analogies and differences with static systems and prepare the presentation of our results, which are reported in the next chapters.

As a first example, we will see how it is possible to design an effective Hamiltonian for the Floquet modes having specific topological properties with a high-frequency periodic driving. Secondly we will show how Thouless pumping [23] realizes the dimensional extension of the previous section. Finally, as a last example, we will see how the periodicity by $\hbar\omega$ translations of the quasienergies modifies the standard bulk-edge correspondence of static systems [10, 11, 15, 72] in the case of Floquet spectra.

2.3.1. High frequency Floquet engineering of topological properties

In this paragraph we give a short glimpse of how the extended Floquet Hamiltonian $\hat{\mathcal{K}}$ of a graphene sheet subjected to a specific high-frequency periodic driving takes the form of a Chern insulator, the simplest kind of topological insulator in $2d$. This class of insulators, in the static case, is topologically characterised by an integer number, the Chern number C, which is of fundamental importance because the Hall conductivity σ_{xy} of $2d$ band insulators, in

the thermodynamic limit and with periodic boundary conditions, is proportional to C [6, 7]. Indeed $\sigma_{xy} = \frac{e^2}{h}\sum_{\nu}^{occ} C_\nu$, where C_ν is the Chern number of the ν-th band, implying a quantization in units of e^2/h. The Chern number of a given ν-th band can be expressed as the integral of the Berry curvature $\mathcal{F}^{\nu}_{k_x k_y}(\mathbf{k})$ [73] over k-space

$$C_\nu = \frac{1}{2\pi}\int_{\mathrm{BZ}} \mathrm{d}^2\mathbf{k}\, \mathcal{F}^{\nu}_{k_x k_y}(\mathbf{k}) = i\frac{1}{2\pi}\int_{\mathrm{BZ}} \mathrm{d}^2\mathbf{k}\left[\langle\partial_{k_x} u_{\mathbf{k},\nu}|\partial_{k_y} u_{\mathbf{k},\nu}\rangle - \langle\partial_{k_y} u_{\mathbf{k},\nu}|\partial_{k_x} u_{\mathbf{k},\nu}\rangle\right], \quad (2.17)$$

where $|u_{\mathbf{k},\nu}\rangle$ is the periodic part of the Bloch wavefunction for the ν-th band. Chern numbers can change their value only by closing and reopening of a gap.

As we mentioned in the introduction of this thesis, the prototypical tight-binding model of a Chern insulator is the Haldane model [74]. It describes free spinless fermions on the honeycomb lattice with a sublattice-dependent *complex* next-nearest neighbours hopping. Its Hamiltonian reads

$$\hat{H}_H = t_1\sum_{(i,j)}\hat{c}_i^\dagger\hat{c}_j + t_2\sum_{((i,j))}\mathrm{e}^{-i\phi_H\nu_{ij}}\hat{c}_i^\dagger\hat{c}_j + \Delta_{AB}\left(\sum_{i\in\mathcal{A}}\hat{c}_i^\dagger\hat{c}_i - \sum_{j\in\mathcal{B}}\hat{c}_j^\dagger\hat{c}_j\right). \quad (2.18)$$

Here $\hat{c}_j^\dagger$ creates a fermion at site j, while (i,j) and $((i,j))$ denote nearest and next-nearest neighbours summation respectively. ϕ_H is the Haldane flux and $\nu_{i,j} = \pm 1$ depending on which of the two sublattices the sites i and j belong to. Δ_{AB} is an energy offset between the two triangular sublattices $\mathcal{A}$ and $\mathcal{B}$ of the honeycomb lattice, but it is not the fundamental ingredient for topology. Indeed, in the parameters space $(\Delta_{AB}/t_2, \phi_H)$, the region with Chern numbers $C = \pm 1$ is the surface $|\Delta_{AB}/t_2| < \left|3\sqrt{3}\sin(\phi_H)\right|$. Thus for a topologically non-trivial phase, we must have $\phi_H \neq 0$. Naturally, such a peculiar Hamiltonian is very difficult to realize in equilibrium systems (see [75] for a recent theoretical proposal.) However, following a suggestion of Ref. [29], it was understood in Ref. [30] that a circularly polarized electric field of sufficiently high frequency irradiating a graphene sheet would result in an *extended Floquet Hamiltonian* $\hat{\mathcal{K}}$ having the form of the Haldane model. We will analyse this model in full detail in Sec. 3.1.2 with a high frequency expansion for the Floquet Hamiltonian $\hat{H}_F$ rather than $\hat{\mathcal{K}}$, but let us just say here that the idea is the same of Sec. 2.2: at high driving frequencies, the effects of the driving can be treated pertubatively by going to Fourier space. The first order expansion in $1/\hbar\omega$ is given by $\hat{\mathcal{K}} \approx \hat{H}_0 + \left[\hat{H}_1, \hat{H}_{-1}\right]/\hbar\omega$, where $\hat{H}_n$ is the n-th Fourier component of the Hamiltonian (2.14). The 0-th order term $\hat{H}_0$ consists only of normal nearest neighbour hopping terms. Instead , the result of the first order term commutator for a spatially uniform electric field is exactly a Haldane next-nearest neighbour hopping term with $t_2 = -\frac{\sqrt{3}t_1^2 J_1^2(\lambda)}{\hbar\omega}$ and a polarization-dependent flux $\phi_H = \pm\frac{\pi}{2}$. λ is a dimensionless quantity proportional to the electric field amplitude that we will properly define in Chap. 3.

The bands of $\hat{\mathcal{K}}$ have non-zero Chern number. For this reason, this phase goes under the name of *Floquet Chern insulator*. It is only one of the many proposals for the realization of high-frequency Floquet Hamiltonians with topological structures in integrable models. These

include Chern insulators and other kinds of topological insulators in different dimensions [68, 76, 77], topological superconductors and superfluids[78, 79, 80, 81, 82], Weyl semimetals [83, 84, 85, 86, 87, 88, 89, 90, 91, 92], Hopf insulators [93].

2.3.2. Thouless pumping

One of most striking examples of topological effects in condensed matter is given by the celebrated Thouless pump [23] and, to our knowledge, it is also the first example of topological effects in a periodically driven system. Here topology dictates the rule that the charge transported after a cyclic adiabatic driving of a 1d band insulating system is an integer number. Let us see briefly why.

The pumped charge is defined as the total particle current carried by the time-evolved state $|\Psi(t)\rangle$ of the system, integrated over one driving period τ and normalized by the system length L:

$$Q = \lim_{L\to\infty} \frac{1}{L} \int_0^\tau \mathrm{d}t \, \langle \Psi(t)|\widehat{J}_x|\Psi(t)\rangle \, . \tag{2.19}$$

In Thouless pumping, the driving is adiabatic, so that $|\Psi(t)\rangle$ stays always arbitrarily close to the instantaneous ground state. However, even if we are in the adiabatic limit $\tau \to \infty$, we must anyway look for the corrections of order $1/\tau$ to the perfect adiabatic evolution of $|\Psi(t)\rangle$ because we are integrating over a "long" time τ in Eq. (2.19): The integration will compensate for the "smallness" of these corrections, yielding a finite result. With a standard adiabatic perturbation theory calculation [23], if we suppose that the initial state is the initial ground state $|0(t)\rangle$, one finds that these corrections are given by

$$|\Psi(t)\rangle = \mathrm{e}^{i\gamma_0(t)} \, \mathrm{e}^{-\frac{i}{\hbar}\int_0^t dt' E_0(t')} \left[|0(t)\rangle + i\hbar \sum_{n\neq 0} \frac{|n(t)\rangle\langle n(t)|\partial_t 0(t)\rangle}{E_n(t) - E_0(t)} \right] , \tag{2.20}$$

where $E_n(t)$ and $|n(t)\rangle$ are the instantaneous n-th (many-body) energy and eigenstate at time t, while γ_n is the Berry phase relative to the n-th eigenstate $\gamma_n = i\int_0^\tau \langle n(t)|\,\partial_t n(t)\rangle \mathrm{d}t$. We suppose that the system is translationally invariant[3] so that the instantaneous ground state is a Slater determinant of Bloch waves

$$|0(t)\rangle = \prod_{\nu}^{\mathrm{occ}} \prod_{k}^{\mathrm{BZ}} \hat{c}^\dagger_{\nu,k}(t) \, |0\rangle \, , \tag{2.21}$$

where $\hat{c}^\dagger_{\nu,k}(t)$ creates a particle in the instantaneous periodic part of a Bloch wavefunction in the band ν, $u_{\nu,k}(x,t) = \langle x|\hat{c}^\dagger_{\nu,k}(t)|0\rangle$. If Φ_0 is a magnetic flux piercing our $1d$ system, the current operator can be written as $\widehat{J}_x = \partial_\kappa \hat{H}/\hbar$, where $\kappa = \frac{2\pi}{L}\frac{\Phi}{\Phi_0}$ ad Φ_0 is the flux quantum (see Ref. [94] and the discussions in App. F.1). The energies and the wavefunctions $|u_{\nu,k}\rangle$

[3]The disordered case is more complicated but is characterized by the same physics [37].

depend on $k+\kappa$, thus we can take derivative with respect to κ or k. With these facts in mind, if we insert Eqs. (2.21) and (2.20) in (2.19), then use the identity

$$\frac{\langle 0(t)|\partial_\kappa \hat{H}(t)|n(t)\rangle}{(E_n(t)-E_0(t))} = -\langle \partial_\kappa 0(t)|n(t)\rangle$$

and the Hellmann-Feynman theorem $\langle 0(t)|\,\widehat{J}_x\,|0(t)\rangle = \sum_k \sum_\nu^{occ} \partial_k E_{k,\nu} = 0$ we arrive at the final formula

$$Q(\tau) = \sum_\nu^{\text{occ}} \int_{-\frac{\pi}{a}}^{\frac{\pi}{a}} \frac{dk}{2\pi} \int_0^\tau \underbrace{i\Big(\langle \partial_k u_{\nu,k}|\,\partial_t u_{\nu,k}\rangle - \text{c.c.}\Big)}_{\mathcal{F}^\nu_{k,t}} = \sum_\nu^{occ} C_\nu\ . \tag{2.22}$$

In the end, the pumped charge is equal to the sum of the Chern numbers of the (time-dependent) occupied bands. At variance with Eq. (2.17), here the Berry curvature $\mathcal{F}$ depends on k and t, rather than k_x and k_y. This is an example of what we have discussed in section 2.2. At low frequency the system with a periodic driving can be reinterpreted as one in which the Fourier index m plays the role of an extra space index and the phase ωt (if the dependence on time is linear) the role of quasimomentum. Thus in both this case and the case of irradiated graphene discussed previously, the possible phases are characterized by a Chern number, but the physical observable associated to topology is different. In the genuinely $2d$ case, the Chern number is proportional to the Hall conductivity, while here, in $(1+1)d$, is equal to the charge pumped in a period. Pictorially, the pumping of charge can also be seen in the Fourier lattice setting as the transverse current response in the physical direction to the action of the electric field $\hbar\omega$ in the Fourier direction. In the adiabatic limit this is equal to the Hall conductance, that is, the Chern number of the occupied bands, see Eq. (2.22).

2.3.3. Anomalous bulk-edge correspondence at low frequencies.

A distinctive trait of topological insulators is the direct link between the value of the topological invariant and the existence of metallic surface states with specific properties. Since the topological invariant is a property of the bulk of the system (it is usually calculated with periodic boundary conditions), this phenomenon goes under the name of bulk-edge correspondence. For example, in the case of a $2d$ Chern insulator, a ground state Chern number equal to ± 1 means that there are two *chiral* (i.e., with a definite sign of the group velocity) edge states that cross the bulk gap between valence and conduction bands. More generally, it is possible to calculate the number of edge modes in each one of the spectral gaps by calculating the Chern number of the various Bloch bands. This behaviour is reproduced also in Floquet systems at high-frequency, such as the driven graphene model described in Sec. 2.3.1, which will be the subject of chapter 3 . In the left panel of Fig. 2.1 we show a typical spectrum for this model in the high-frequency regime in a cylindrical geometry (PBC in the y direction and open boundary conditions in the x direction). Fourier-Bloch transform

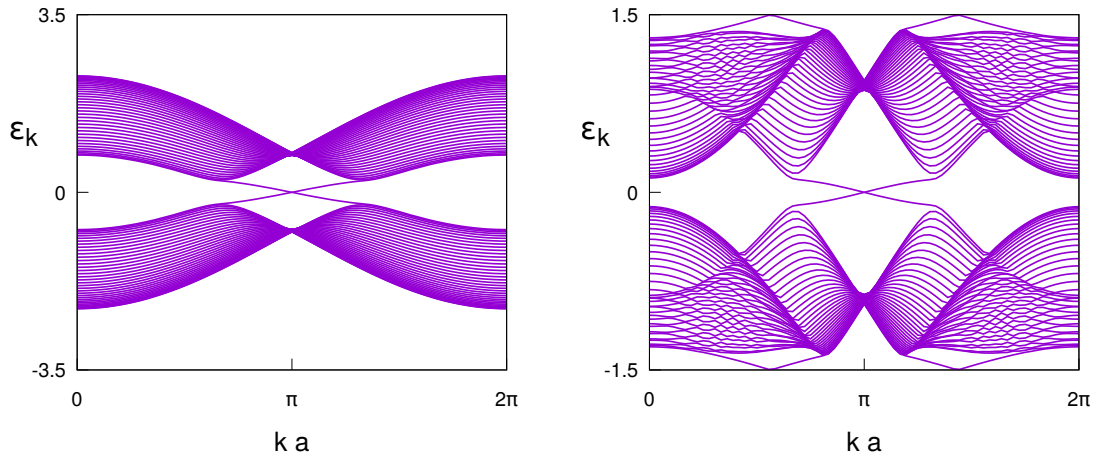

Figure 2.1.: Quasienergy spectra (in units of the nearest nieghbour hopping $|t_1|$)for the driven graphene model of Sec. 2.3.1 and Chap 3 on a strip geometry with 72 sites in the x-direction. Boundary conditions are open along x and periodic along y. The FBZ is $[-\hbar\omega/2, \hbar\omega/2]$. Left: High frequency regime, $\hbar\omega = 7\,|t_1|$. Chern number is equal to -1. Right: Low frequency regime, $\hbar\omega = 3\,|t_1|$. Chern number is equal to -3 and there are anomalous edge states.

is performed only along the y direction. The wavefunctions of the two metallic branches that cross the gap are situated on the two opposite edges of the sample: states with the same chirality are situated on the same edge.

The bulk-edge correspondence can however become more complicated for Floquet systems with a low driving frequency. The reason is that for quasienergy spectra there is no notion of "lowest" band, because of the periodicity of the quasienergies under translation by $\hbar\omega$. Therefore, all of the bands in the quasienergy spectrum have one gap below them and one above it. This means that for a natural choice of the FBZ, $[-\hbar\omega/2, \hbar\omega/2]$, additional edge state branches can be present in the gap at $\pm\hbar\omega/2$. An example is shown in the right panel of Fig. 2.1, where we plot the quasienergy spectrum of the driven graphene model, with the same parameters of the left panel, but with a lower frequency. Two pairs of edge modes have appeared in the gap at $\pm\hbar\omega/2$. The Chern number of the lowest band is -3, giving the correct number of edge states, but this is not always the case: Chern numbers are not in general a good edge states-indicator in quasienergy spectra. In particular in Ref. [95], it was constructed a periodically driven model that host a phase where all the bands have zero-Chern number but there are edge states in each quasienergy gap.

Let us see why these additional edge states appear when the frequency is sufficiently low. Consider, for simplicity a two-band periodically driven Chern insulator with particle-hole symmetry, e.g. with the lower band having the same eigenvalues of the upper one but with opposite sign. We choose as FBZ the interval $[-\hbar\omega/2, \hbar\omega/2]$. At $\omega \to \infty$ the quasienergy spectrum coincide with that of time-averaged Hamiltonian which can only have edge states

in the gap around $\varepsilon = 0$. In order to get the anomalous edge state we must then have a gap closing and reopening around $\pm\hbar\omega/2$, which can only happen when the frequency becomes low enough, e.g. $\hbar\omega \lesssim W$, with W being the total bandwidth of the time-averaged Hamiltonian. In this situation we have already seen that the system is characterized by invariants that are defined in $d+1$ dimensions. This is in line with was demonstrated in Ref. [95]. The number of chiral edge states for a Floquet Chern insulator gap at quasienergy ε is obtained with another bulk topological invariant. It is a winding number of the map from the 3-torus composed by $(\omega t, k_x, k_y)$ to the space of unitary operators. For completeness we report here its expression:

$$W_\varepsilon = \frac{1}{8\pi^2}\int \mathrm{d}k_x \mathrm{d}k_y \mathrm{d}t\, \mathrm{Tr}\left(\hat{U}_\varepsilon^\dagger\, \partial_t \hat{U}_\varepsilon \left[\hat{U}_\varepsilon^\dagger\, \partial_{k_x}\hat{U}_\varepsilon,\, \hat{U}_\varepsilon^\dagger\, \partial_{k_y}\hat{U}_\varepsilon\right]\right) . \tag{2.23}$$

In the formula above the unitary operator $\hat{U}_\varepsilon$ depends on $\mathbf{k}$ and t. It is defined by the following construction: for $t = \tau$ we have $\hat{U}_\varepsilon(\mathbf{k}, \tau) = \mathbb{1}$ while for other times it is obtained from the actual evolution operator at quasimomentum $\mathbf{k}$, $\hat{U}(\mathbf{k}, t)$ by continuously deforming it in such a way that the gap at quasienergy ε is shifted at $\hbar\omega/2$ without ever closing it.

3. Adiabatic preparation of a Floquet Chern insulator

In this chapter we will deal with a model for free fermions in a graphene-like system subjected to periodic driving. Most importantly, the time dependence of this model resides in the *phase* of the hopping terms, e.g. $t_{ij}e^{i\Phi_{ij}(t)}\hat{c}_i^\dagger\hat{c}_j$. The phases $\Phi_{ij}(t)$ — making the hoppings complex, hence generally breaking time-reversal — may result from different physical mechanisms: in the neutral cold atoms experiments [35] they are due to a time-periodic modulation of the optical lattice; in more traditional electronic systems, they originate from the Peierls' substitution minimal coupling of the electrons with the (classical) electromagnetic field of a laser beam. If $\mathbf{A}(\mathbf{r},t)$ is the vector potential of the electromagnetic field, it enters the Hamiltonian via

$$t_{ij}\hat{c}_i^\dagger\hat{c}_j \to t_{ij}e^{-\frac{ie}{\hbar c}\int_{\mathbf{r}_i}^{\mathbf{r}_j} d\mathbf{l}\cdot\mathbf{A}(\mathbf{r},t)}\hat{c}_i^\dagger\hat{c}_j \ .$$

A circularly polarised $\mathbf{A}$ results in topologically non-trivial Floquet Hamiltonian. In particular for off-resonant frequencies, e.g. $\hbar\omega$ greater than the energy bandwidth W, $\hat{H}_F$ will be an Haldane model. We will anyway be considering only the two lowest energy bands of graphene, so $\hbar\omega$ must not be too large in order to avoid resonance with high-lying bands.

We study here what happens when the amplitude of the vector potential is slowly turned on, while keeping the frequency ω fixed. The goal of this scheme is to make the original unperturbed ground state adiabatically evolve into a Floquet Chern insulating state. A perfect adiabatic preparation would have many consequences. First of all, in an ideal system with no dissipation and no boundaries, the Hall conductivity of such a state is quantized as in static Chern insulators. We show this in App. A with the use of Floquet adiabatic perturbation theory. Moreover, given the possibilities offered by the easy tunability of the driving parameters, it would be possible to manipulate edge states and currents.

We begin this chapter with a detailed description of the periodically driven model (on a strip geometry) and then prove with a Magnus expansion (see App. B) that its Floquet Hamiltonian at high frequencies correspond to the one of the Haldane model. We will then introduce the idea of adiabatic preparation of the *Floquet ground state* and the full model that we study: the driven honeycomb lattice with a slow turn-on of the driving amplitude. In Sec. 3.2 we will study the simpler case of the adiabatic dynamics of the Haldane model: we will show that it already contains all the elements to understand the dynamics in the periodically driven case for $\hbar\omega > W$. This will be the subject of Sec. 3.3. Here we will

analyse one of the hallmarks of this dynamics, namely the resulting nonequilibrium currents flowing at the edges. Their manipulation with a spatially varying driving field will be also discussed. In Sec. 3.4 we will introduce a time-dependent *local* indicator of the topological transition, which is a generalization of the Chern Marker [36]. Finally, in Sec.3.5, we will discuss how the picture changes completely in the resonant case $\hbar\omega < W$. The topological features are more interesting, but an adiabatic preparation is practically impossible.

3.1. Model and idea

3.1.1. Periodically driven graphene

We describe here in full detail the model for a Floquet Chern insulator in a graphene-like system. Our model consists of free spinless fermions on the honeycomb lattice, coupled to a circularly polarized electric field. Inspired by the usual tight-binding description of graphene [96], we consider only one orbital per site and to be a bit more general, we include also an energy offset Δ_{AB} between the two triangular sublattices $\mathcal{A}$ and $\mathcal{B}$ that constitute the honeycomb lattice, as it happens in boron nitride. The lattice is characterized (see left panel of Fig. 3.1) by the vectors connecting nearest neighbours (n.n.)

$$\mathbf{d}_1 = d\left(\frac{1}{2}, -\frac{\sqrt{3}}{2}\right), \quad \mathbf{d}_2 = d\left(\frac{1}{2}, \frac{\sqrt{3}}{2}\right), \quad \mathbf{d}_3 = d\,(-1, 0)\ , \tag{3.1}$$

where d is the n.n. distance. Then, if we call $a = \sqrt{3}d$, the second neighbour vectors are

$$\mathbf{a}_1 = \mathbf{d}_2 - \mathbf{d}_3 = a\left(\frac{\sqrt{3}}{2}, \frac{1}{2}\right)\ ; \tag{3.2a}$$

$$\mathbf{a}_2 = \mathbf{d}_3 - \mathbf{d}_1 = a\left(-\frac{\sqrt{3}}{2}, \frac{1}{2}\right)\ ; \tag{3.2b}$$

$$\mathbf{a}_3 = \mathbf{d}_1 - \mathbf{d}_2 = a\,(0, -1)\ . \tag{3.2c}$$

Given the importance of edge states physics in topological phases, we put ourselves on a strip geometry with periodic boundary conditions (PBC) along the y-direction and open boundary conditions (OBC) with zigzag edges along x. The sites are labelled with two integers, $\mathbf{r}_{i,j}$ (rather than just one as in Eq. (2.18)) with $i = 1 \cdots N_x$ and $j = 1 \cdots N_y$, along zigzag lines at 30° from the x-direction, as shown in Fig. 3.1. In terms of the n.n. vector $\mathbf{d}_2 = d(\frac{1}{2}\hat{\mathbf{x}} + \frac{\sqrt{3}}{2}\hat{\mathbf{y}})$ and the lattice vector $\mathbf{a}_1 = a(\frac{\sqrt{3}}{2}\hat{\mathbf{x}} + \frac{1}{2}\hat{\mathbf{y}})$ we then write: $\mathbf{r}_{1,1} = \mathbf{0}$, $\mathbf{r}_{2,1} = \mathbf{d}_2$, and $\mathbf{r}_{i\geq 2,j} = \mathbf{r}_{i-2,1} + \mathbf{a}_1 + a(j-1)\hat{\mathbf{y}}$. We assume the strip width N_x to be even, and the origin to belong to the $\mathcal{A}$-sublattice.
For the moment, we leave aside the periodic driving and consider the static Hamiltonian

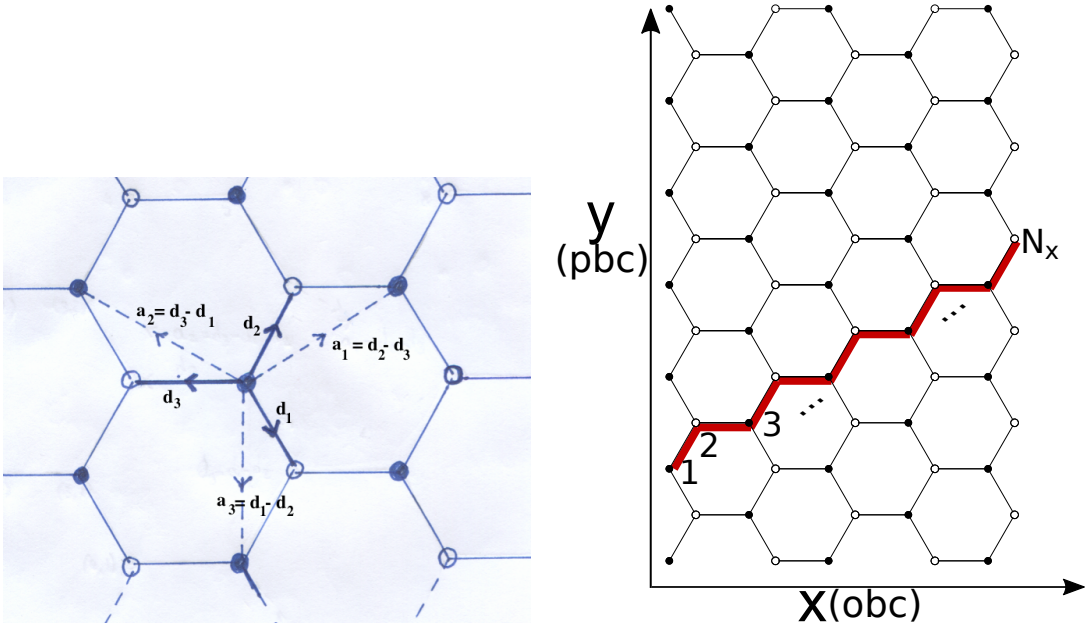

Figure 3.1.: The honeycomb lattice with first and second nearest neighbours lattice vectors(left), and a zigzag strip with the lattice numbering that we have chosen(right). Filled (empty) dots constitute sublattice $\mathcal{A}$ ($\mathcal{B}$).

$$\hat{H} = t_1 \sum_{(ij,i'j')} \hat{c}^\dagger_{i,j}\hat{c}_{i',j'} + \Delta_{AB}\sum_{i,j}(-1)^{i+1}\hat{c}^\dagger_{i,j}\hat{c}_{i,j}\ , \tag{3.3}$$

where $\hat{c}^\dagger_{i,j}$ creates a particle at site $\mathbf{r}_{i,j}$ and $(ij, i'j')$ denotes sums over n.n.. If we had PBC on both sides, the spectrum could be easily found by going to momentum space: $E_{\pm,\mathbf{k}} = \pm t_1\sqrt{3 + 2\cos(\mathbf{k}\cdot\mathbf{a}_1) + 2\cos(\mathbf{k}\cdot\mathbf{a}_2) + 2\cos(\mathbf{k}\cdot(\mathbf{a}_2+\mathbf{a}_1)) + \Delta^2_{AB}}$. When Δ_{AB} is zero, the the spectrum is gapless at the two Dirac points $\mathbf{K}_\pm = (\frac{2\pi}{\sqrt{3}a}, \pm\frac{2\pi}{3a})$. However, translational invariance is present only along y, allowing the use of only $k_y \equiv k$ as a quantum number. Introducing Bloch transformations

$$\hat{c}^\dagger_{i,k} = \frac{1}{\sqrt{N_y}}\sum_{j=1}^{N_y} \mathrm{e}^{ikaj}\hat{c}^\dagger_{i,j}\ ,$$

with $ka = \frac{2\pi n}{N_y}$ $(n = 0, \cdots, N_y - 1)$, the Hamiltonian 3.3 can be rewritten as

$$\hat{H} = \sum_{k}^{\mathrm{BZ}_y}\sum_{i,i'=1}^{N_x} \mathbb{H}_{ii'}(k)\ \hat{c}^\dagger_{i,k}\hat{c}_{i',k}\ . \tag{3.4}$$

where $\mathbb{H}(k,t)$ is an $N_x \times N_x$ Hermitean matrix with elements on the diagonal (the on-site terms $\pm\Delta_{AB}$) and at n.n.. It can be diagonalized numerically and an energy spectrum for the

case $\Delta_{AB} = 0$ is plotted in Fig. (F.1). We notice that besides being gapless at the projection of the two Dirac points $K_+ = 2\pi/3a$, $K_- = 4\pi/3a$, there are two degenerate branches of non dispersive states that connect the two points. These are actually states localized on the edge and their existence can be explained on topological grounds, but is not related to the Chern number. When $\Delta_{AB} \neq 0$ the two branches are lifted in energy together with the Dirac cones, but remain flat.

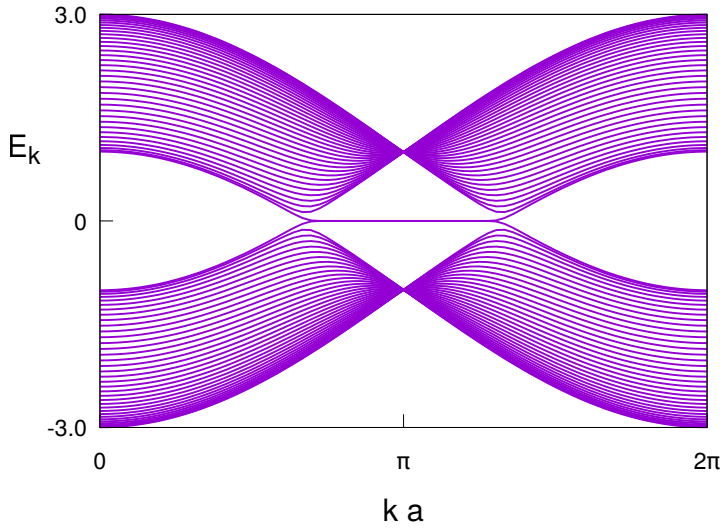

Figure 3.2.: Energy dispersion in the strip geometry with $N_x = 72$ and $\Delta_{AB} = 0$. The unit of energy (from now on) is $|t_1|$.

We introduce now the periodic driving. It models the action of an elliptically polarized monochromatic laser beam propagating along a direction normal to the lattice plane. We treat it as a classical field and use the paraxial approximation [97], so that the electric field[1] $\mathcal{E}$ will be a plane wave e^{ikz} modulated by some envelope function depending on x, y and t. We choose a gauge in which there is no scalar potential and we allow only spatial variations along x, so that translation invariance along y is not lost. A choice for the vector potential is

$$\mathbf{A}(\mathbf{r}, t) = A_0 w(x) \left[\hat{\mathbf{x}} \sin(\omega t) + \hat{\mathbf{y}} \sin(\omega t - \varphi)\right] \ , \tag{3.5}$$

where the dimensionless function $w(x) \leq 1$ describes the modulations of the field along x. The tight-binding model gets modified by the vector potential through the standard Peierls' substitution: the hopping operator $t_1 \hat{c}^\dagger_{i,j} \hat{c}_{i',j'}$ from site $\mathbf{r}_{i',j'}$ to site $\mathbf{r}_{i,j}$ get multiplied by the complex phase factors $\exp(-i\lambda\Phi^{ij}_{i'j'}(t))$, with the definitions

$$\Phi^{ij}_{i'j'}(t) = \frac{1}{dA_0} \int_{\mathbf{r}_{i',j'}}^{\mathbf{r}_{i,j}} d\mathbf{l} \cdot \mathbf{A}(\mathbf{r}, t) \tag{3.6}$$

[1] We will neglect magnetic fields

$$\lambda = \frac{e}{\hbar c} dA_0 \ . \tag{3.7}$$

In the case of a uniform driving and circular polarization $\phi = \pm\pi/2$, the phases associated to going from sublattice $\mathcal{A}$ to sublattice $\mathcal{B}$ are

$$\frac{e}{\hbar c}\int_{\mathbf{r}_{i,j}}^{\mathbf{r}_{i,j}+\mathbf{d}_1} \mathbf{A}\cdot\mathbf{dl} = \lambda\left(\frac{1}{2}\sin(\omega t) - \frac{\sqrt{3}}{2}\sin\left(\omega t \mp \frac{\pi}{2}\right)\right) = \lambda\sin\left(\omega t \pm \frac{\pi}{3}\right) \tag{3.8a}$$

$$\frac{e}{\hbar c}\int_{\mathbf{r}_{i,j}}^{\mathbf{r}_{i,j}+\mathbf{d}_2} \mathbf{A}\cdot\mathbf{dl} = \lambda\left(\frac{1}{2}\sin(\omega t) + \frac{\sqrt{3}}{2}\sin\left(\omega t \mp \frac{\pi}{2}\right)\right) = \lambda\sin\left(\omega t \mp \frac{\pi}{3}\right) \tag{3.8b}$$

$$\frac{e}{\hbar c}\int_{\mathbf{r}_{i,j}}^{\mathbf{r}_{i,j}+\mathbf{d}_3} \mathbf{A}\cdot\mathbf{dl} = \lambda\sin(\omega t + \pi) \ . \tag{3.8c}$$

Clearly, the phases relative to the Hermitean process (from $\mathcal{B}$ to $\mathcal{A}$) have a minus sign in front. These equations can be summed up in one single expression:

$$\Phi^{ij}_{i',j'}(t) = (-1)^i \sin\left(\omega t + \theta^{i'j'}_{ij}\right) \ , \qquad \theta^{i'j'}_{ij} = \left(\pm\frac{\pi}{3}, \mp\frac{\pi}{3}, \pi\right) \ . \tag{3.9}$$

The phase $\theta^{i'j'}_{ij}$ is chosen depending on which one of the three n.n. bonds (enumerated according to the vectors $\pm\mathbf{d}_l$ of Eq. (3.1)) connects the sites $\mathbf{r}_{i,j}$ and $\mathbf{r}_{i',j'}$. In the end, the periodically driven Hamiltonian is

$$\hat{H}(t) = t_1 \sum_{(ij,i'j')} \mathrm{e}^{-i\lambda\Phi^{ij}_{i',j'}(t)}\hat{c}^\dagger_{i,j}\hat{c}_{i',j'} + \Delta_{AB}\sum_{i,j}(-1)^{i+1}\hat{c}^\dagger_{i,j}\hat{c}_{i,j} \ . \tag{3.10}$$

We conclude by saying that this Hamiltonian has been obtained in the optical lattice experiment of Ref. [35], with the difference that electrons are substituted by neutral atoms. The circularly polarized field is recreated by rotating the lattice elliptically. A canonical transformation into the rest frame of the atoms will make the Hamiltonian assume exactly the same of form of Eq. (3.10).

3.1.2. Floquet Hamiltonian at high frequencies

We want to show here, as first realized in ref. [30]that, for large ω and to the lowest non-trivial order in $t_1^2\lambda^2/(\hbar\omega)$, the Floquet Hamiltonian H_F relative to the driven problem of Eq. (3.10) with uniform driving (Eq. (3.9)) is essentially the one of the Haldane model, the prototypical Chern insulator [74]. The starting point of our analysis is the Magnus expansion at first order, Eq. (B.3), which we reproduce here:

$$\hat{H}_F = \hat{H}_0 + \sum_{n\neq 0}\frac{1}{n\hbar\omega}\left\{\hat{H}_n\hat{H}_{-n} + \left[\hat{H}_0, \hat{H}_n\right]\right\} + \mathcal{O}\left(\frac{1}{(\hbar\omega)^2}\right) \ . \tag{3.11}$$

Here $\hat{H}_0$ and $\hat{H}_n$ are Fourier components of the time-dependent Hamiltonian

$$\hat{H}_n = \frac{1}{\tau}\int_0^\tau \hat{H}\,(t)\, e^{-in\omega t} dt\ , \tag{3.12}$$

and the Floquet Hamiltonian is defined as $\hat{U}(\tau,0) = \mathrm{e}^{(-\frac{i}{\hbar}\hat{H}_F\tau)}$. The crucial ingredient we need comes from the following Bessel function identity:

$$\mathrm{e}^{i\lambda\sin(\omega t+\theta)} = \sum_{n=-\infty}^{+\infty} J_n(\lambda)\ \mathrm{e}^{in(\omega t+\theta)}\ , \tag{3.13}$$

where $J_n(\lambda)$ is the nth-order Bessel function, and $J_{-n}(\lambda) = (-1)^n J_{+n}(\lambda)$. It is then straightforward to calculate that:

$$\hat{H}_0 = t_1 J_0(\lambda) \sum_{(ij,i'j')} \hat{c}^\dagger_{i,j}\hat{c}_{i',j'} + \Delta_{AB}\sum_{i,j}(-1)^{i+1}\hat{c}^\dagger_{i,j}\hat{c}_{i,j}\ , \tag{3.14}$$

while the other components read:

$$\hat{H}_{n\neq 0} = -t_1 J_n(\lambda) \sum_{(ij,i'j')} \mathrm{e}^{in\theta^{ij}_{i'j'}}\hat{c}^\dagger_{i,j}\hat{c}_{i',j'}\ . \tag{3.15}$$

At this point we can calculate the first-order correction to $\hat{H}_0$ in Eq. (3.11). Let us consider only the H_n, H_{-n} term. It can be written as a sum of commutators $\sum_n [H_n, H_{-n}]/\hbar\omega$, with $n \geq 1$. A simple calculation [2] shows that:

$$\frac{1}{\hbar\omega}\sum_{n=1}^{\infty}\left[\hat{H}_{+n}, \hat{H}_{-n}\right] = -2it_1^2 J_n^2(\lambda) \sum_{((ij,i'j'))} \sin\left(n(\theta^{lm}_{ij} - \theta^{i'j'}_{lm})\right)\hat{c}^\dagger_{i,j}\hat{c}_{i',j'}\ . \tag{3.16}$$

Here $((ij,i'j'))$ denotes a sum of next-nearest neighbours and $\mathbf{r}_{l,m}$ is the intermediate site between $\mathbf{r}_{i,j}$ and $\mathbf{r}_{i',j'}$. By this we mean that if for example $\mathbf{r}_{i,j} = \mathbf{r}_{i',j'} + \mathbf{a}_1$, then $\mathbf{r}_{l,m} = \mathbf{r}_{i,j} + \mathbf{d}_2$ since $\mathbf{a}_1 = \mathbf{d}_2 - \mathbf{d}_3$. It is remarkable that the various differences $\theta^{lm}_{ij} - \theta^{i'j'}_{lm}$ are all equal to $\theta^{lm}_{ij} - \theta^{i'j'}_{lm} = \pm 2\pi/3(-1)^{(i+1)}$, with the sign $\pm$ depending on the polarization $\varphi = \pm\frac{\pi}{2}$. In this way, the hopping changes sign depending on the sublattice that is involved. Now, for small enough λ we can consider only the first addendum in the infinite sum (3.16), since close to zero $J_n(|\lambda|) \sim |\lambda|^n$. This means that the Hamiltonian has the form of the Haldane model with the identification:

$$t_2 = -\frac{\sqrt{3}t_1^2 J_1^2(\lambda)}{\hbar\omega}\ . \tag{3.17}$$

[2] We use:

$$\left[\hat{c}^\dagger_{i,j}\hat{c}_{i',j'}, \hat{c}^\dagger_{l,m}\hat{c}_{l',m'}\right] \delta_{(i',j'),(l,m)}\hat{c}^\dagger_{i,j}\hat{c}_{l',m'} - \delta_{(i,j),(l',m')}\hat{c}^\dagger_{l,m}\hat{c}_{i',j'}\ .$$

Since the hopping operators $\hat{c}^\dagger_{i,j}\hat{c}_{i',j'}$ were between n.n. sites, the operators on the r.h.s. will refer to two sites that are next-nearest neighbours, thanks to the Kronecker's deltas.

and a polarization-dependent flux $\phi_H = \pm\frac{\pi}{2}$.

As far as the $[H_0, H_n]$ term of Eq. (3.11) is concerned, we have discussed in App. B that it does not affect the quasienergy spectrum if we consider only corrections of order $1/\hbar\omega$. This means that the gap at the two Dirac cones will not close and the topology of the bands will be the same as before. The same reasoning can also be applied to higher harmonics terms in the sum of Eq. (3.16). Therefore for sufficiently large ω and small λ we can consider the Floquet Hamiltonian of our problem to be very close to the one of the Haldane model.

We conclude this paragraph by saying that the Chern numbers of the two bands of $\hat{H}_F$ do not depend on the initial time of the driving. Indeed Floquet Hamiltonians with different definitions of initial time are related by a unitary transformation (see appendix B). This implies that they have the same spectrum and therefore one cannot close the bulk gap and induce a topological transition by changing the initial time.

3.1.3. Adiabatic switching of the driving: the full model

In the previous sections we have discussed the topological structures of the Floquet Hamiltonian. In particular, we have seen how the Slater determinants made up of the Floquet states of a quasienergy Bloch band can have a non-zero Chern number. A fundamental question is how the actual time-evolved state $|\Psi(t)\rangle$ of our system can reach this many-body Floquet state. Indeed, in general, the solution of the time-dependent Schrödinger equation with a Hamiltonian periodic in time will be a superposition of Floquet states depending on the specific initial conditions. The only way for $|\Psi(t)\rangle$ to reach a Floquet state is to be prepared in such a state at the initial time of the driving. The most common strategy[3] to prepare a Floquet state is to resort to the Floquet adiabatic theorem, described in Sec. 2.1. The key observation is that when the driving is turned off, e.g. the dimensionless driving amplitude is 0, it is obvious from the definition in Eq. (2.2) that $\hat{H}_F[\lambda = 0] = \hat{H}$. Therefore, the Floquet modes will coincide with the (time-independent) eigenstates of $\hat{H}$. In particular, if we fix the choice of the FBZ to $[-\hbar\omega/2, \hbar\omega 2]$, the Slater determinant ground state (GS) of $\hat{H}(0)$, $|\Psi_{GS}(0)\rangle$ will coincide with the Slater determinant of the lowest quasienergy band, which we term *Floquet ground state* (FGS) $|\Psi_{\mathrm{FGS}}[\lambda = 0], t = 0\rangle$, provided that $\hbar\omega$ is larger than the unperturbed energy bandwidth W. Assuming that we prepare our system in the GS of $\hat{H}(0)$, $|\Psi(0)\rangle = |\Psi_{GS}(0)\rangle$, if we turn on the driving, we will have at any time $|\Psi(t)\rangle \approx |\Psi_{\mathrm{FGS}}[\lambda(t)]; t\rangle$, as long as the variation of λ are "slow" compared to the quasienergy gap (which we remark is defined modulo $\hbar\omega$) with the upper band. This strategy is precisely the one used in the experiment of Ref. [35].

As λ is slowly increased, the Floquet Hamiltonian will cross a critical point, characterized by a closing and reopening of a (quasienergy) gap and a change in the topology of the FGS. This is, in essence, the typical setting of a quantum annealing (QA) dynamics [98, 99, 100,

[3] We remark again that we do not consider any form of dissipation.

101]. For this reason, we dab τ_{QA} the time over which $\lambda(t)$ is increased.

The complete form of the Hamiltonian that we are going to study is therefore a modified version of the one in Eq. (3.10)

$$\hat{H}(t) = t_1 \sum_{(ij,i'j')} \mathrm{e}^{-i\lambda(t)\Phi_{ij}(t)} \hat{c}^\dagger_{i,j}\hat{c}_{i',j'} + \Delta_{AB}(t) \sum_{i,j} (-1)^{i+1} \hat{c}^\dagger_{i,j}\hat{c}_{i,j} \ , \tag{3.18}$$

with

$$\lambda(t) = \begin{cases} \dfrac{t}{\tau_{\mathrm{QA}}}\lambda_f, & t < \tau_{\mathrm{QA}} \\ \lambda_f & t \geq \tau_{\mathrm{QA}} \end{cases} \ . \tag{3.19}$$

We have also included a Δ_{AB} that changes in time, a possibility that can be realized in optical lattices. One can for example think of turning on the driving without entering the topological phase of H_F of interest and then go into it with a variation of Δ_{AB}.

If the frequency of the driving is instead smaller than the bandwidth, the folding of the original energy levels inside the FBZ implies that $|\Psi(0)\rangle = |\Psi_{\mathrm{GS}}(0)\rangle \neq |\Psi_{\mathrm{FGS}}[\lambda = 0], 0\rangle$. We leave aside for the moment this issue, but we will return to it in Sec. 3.5.

3.2. Quantum annealing of the Haldane model

As the dimensionless amplitude $\lambda(t)$ of the phase modulation is slowly turned-on — and/or the on-site difference $\Delta_{AB}(t)$ is slowly decreased towards 0 — we are effectively driving the parameters of the Haldane model, $\hat{H}_H(t)$, and can in principle cross the critical point $(\Delta_{AB}/t_2)_c$ separating the trivial from non-trivial insulating state in its equilibrium phase diagram [74]. For this reason, before studying the quantum annealing of the periodically driven honeycomb lattice, it is very instructive to study the QA of the Haldane model itself. In this way, we will neglect for the moment all the complications that come from dealing with the adiabatic tracking of a Floquet state, rather than an Hamiltonian eigenstate.
The Hamiltonian that we are going to study is

$$\hat{H} = t_1 \sum_{(ij,i'j')} \hat{c}^\dagger_{i,j}\hat{c}_{i',j'} + t_2 \sum_{((ij,i'j'))} \mathrm{e}^{i\phi_H \nu_{ij}^{i'j'}} \hat{c}^\dagger_{i,j}\hat{c}_{i',j'} + \Delta_{AB}(t) \sum_{i,j} (-1)^{i+1} \hat{c}^\dagger_{i,j}\hat{c}_{i,j} \ , \tag{3.20}$$

where

$$\nu_{ij}^{i'j'} = (-1)^{i+1} \times \begin{cases} +1, & \mathbf{r}_{i,j} - \mathbf{r}_{i',j'} = \mathbf{a}_l \ \forall l \\ -1, & \mathbf{r}_{i,j} - \mathbf{r}_{i',j'} = -\mathbf{a}_l \ \forall l \end{cases} \ .$$

and

$$\Delta_{AB}(t) = \begin{cases} \Delta^0_{AB} + \dfrac{t}{\tau_{\mathrm{QA}}}\left(\Delta^f_{AB} - \Delta^0_{AB}\right), & t < \tau_{\mathrm{QA}} \\ \Delta^f_{AB} & t \geq \tau_{\mathrm{QA}} \end{cases} . \tag{3.21}$$

In analogy with the Floquet Hamiltonian of section 3.1.2, we will set $\phi_H = \pm\frac{\pi}{2}$. The initial state $|\Psi(0)\rangle$ is the initial ground state at half filling $|\Psi_{\mathrm{GS}}(0)\rangle$; we want to investigate how close can $|\Psi(t \geq \tau_{\mathrm{QA}})\rangle$ get to $|\Psi_{\mathrm{GS}}(t)\rangle$ after having crossed the critical point.

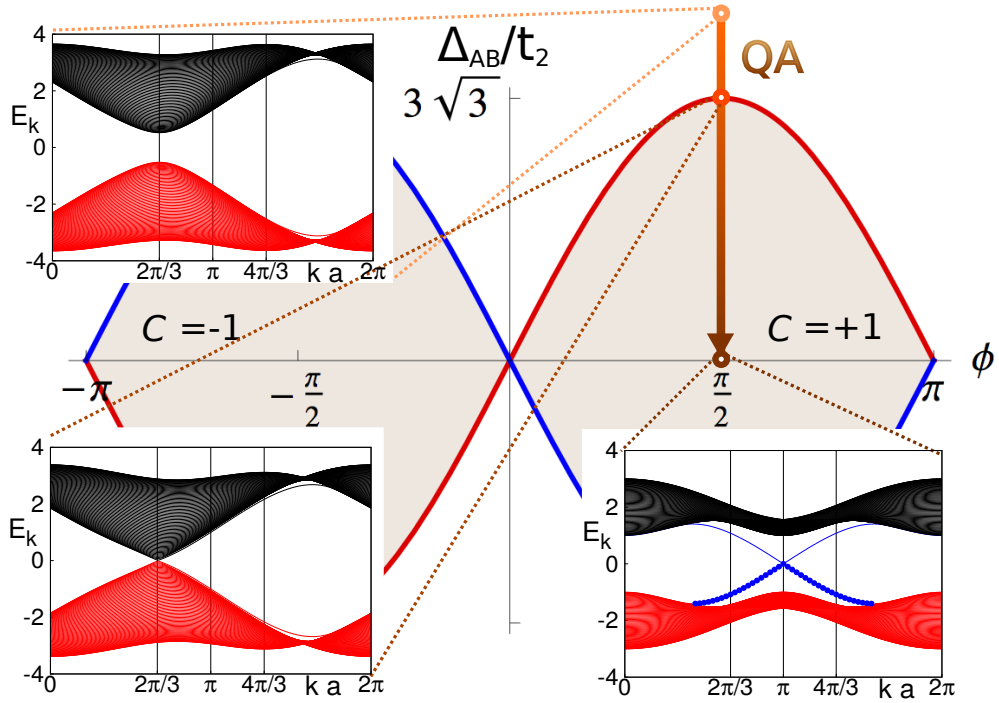

Figure 3.3.: The equilibrium phase diagram of the Haldane model with three representative zigzag spectra along the path in parameters space within one quantum annealing evolution. At the beginning, $\Delta_{AB}/t_2 = 4\sqrt{3}$ For the critical value $\Delta_{AB}/t_2 = 3\sqrt{3}$ the bulk gap closes at the Dirac point and edge states start appearing. Finally, in at the end of the annealing $\Delta_{AB}/t_2 = 0$, the spectrum is symmetric and the two edge states branches cross at $k = \pi/a$. Blue lines represent edge state; if filled blue circles are present, they are occupied in the ground state.

The equilibrium phase diagram in the Δ_{AB}/t_2 vs ϕ plane is shown in Fig. 3.3, the coloured regions denoting the topologically non-trivial phases with Chern number $C = \pm 1$. The insets show three representative strip spectra along a QA evolution: a trivial insulator, the critical point $\Delta_{AB}/t_2 = 3\sqrt{3}$, and the point in the non-trivial region with $\Delta_{AB} = 0$. Filled blue circles represent edge states occupied in the ground state. Edge states cross the bulk gap in the non-trivial phase, left-edge states with a positive k-dispersion and right-edge ones with a negative k-dispersion. The crossing point between the two branches moves from $K_+ =$

$2\pi/(3a)$ towards $K_{\rm f} = \pi/a$ as Δ_{AB}/t_2 decreases from the critical point $(\Delta_{AB}/t_2)_c = 3\sqrt{3}$ towards $\Delta_{AB}/t_2 = 0$. As a matter of fact, the crossing is really an *anti-crossing* Landau-Zener (LZ) point [102, 103, 104], with an extremely small gap separating the two states, indeed a gap which is *exponentially small* in the strip width N_x, $\sim e^{-N_x/\xi}$, due to the localization length ξ of the relevant edge states. Consider now the QA evolution of Fig. 3.3 driven by $\Delta_{AB}/t_2(t)$. In the initial part, the Dirac point (bulk) gap Δ_{K_+} closes at the critical point in a simple way $\Delta_{K_+} \sim 1/N_x$, as it can be seen from Fig. 3.4. This results in a standard Kibble-

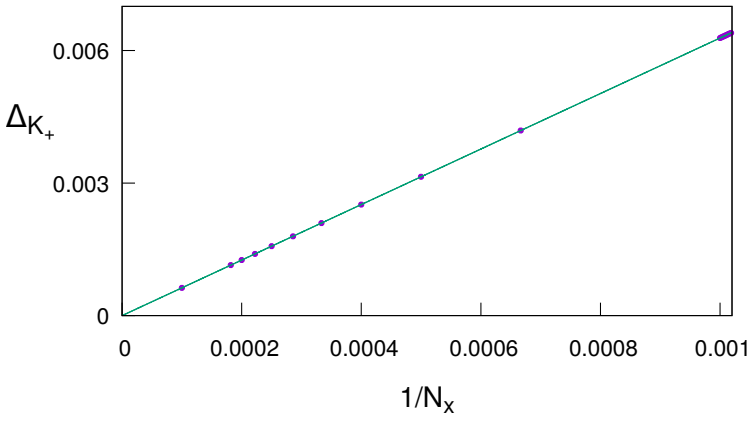

Figure 3.4.: Gap at the Dirac point K_+ for the critical value of the ratio $(\Delta_{AB}/t_2)_c = 3\sqrt{3}$, as a function of the inverse of the system size N_x. The smooth line is $6.2845/N_x$

Zurek (KZ) [105, 106] excitation mechanism: defects are created by the out-of-equilibrium excitation of critical point electrons, unable to adiabatically follow the ground state, into the conduction band [101]. The excitation energy with respect to instantaneous ground state one $E_{\rm GS}(t)$

$$E_{\rm res}(t) = \langle \Psi(t)|\hat{H}(t)|\Psi(t)\rangle - E_{\rm GS}(t) \ , \tag{3.22}$$

when computed at the end of the annealing process, $t = \tau_{\rm QA}$, should decrease in a characteristic universal way as the annealing time $\tau_{\rm QA}$ is increased. The scaling predicted by the KZ theory [107] for a finite size sample with $L = N_x = N_y$ is $\mathscr{E}_{\rm res} = E_{\rm res}(\tau_{\rm QA})/L^2 \sim \tau_{\rm QA}^{\frac{d\nu}{1+z\nu}}$. In the present case, the equilibrium critical point exponents are $\nu = 1$ and $z = 1$, because the gap closes like $\Delta_{K_+} \sim (\Delta_{AB}/t_2) - (\Delta_{AB}/t_2)_c$ and exactly at the critical point we have $\Delta_{K_+} \sim 1/N_x$. Therefore, since $d = 2$, the KZ scaling is $\mathscr{E}_{\rm res} \sim \tau_{\rm QA}^{-1}$. The bare data for $\mathscr{E}_{\rm res}(\tau_{\rm QA})$, shown as black stars in the left plot of Fig. 3.5, strongly depart from this KZ scenario. The reason for such a disagreement is simple to understand, and sheds light onto a universal mechanism of edge-state selective excitation which we now discuss. As previously mentioned, the "anti-crossing" point, with its exponentially-small LZ gap, sweeps to the right, towards the $ka = \pi$ point, for the QA evolution we are considering. Consider now

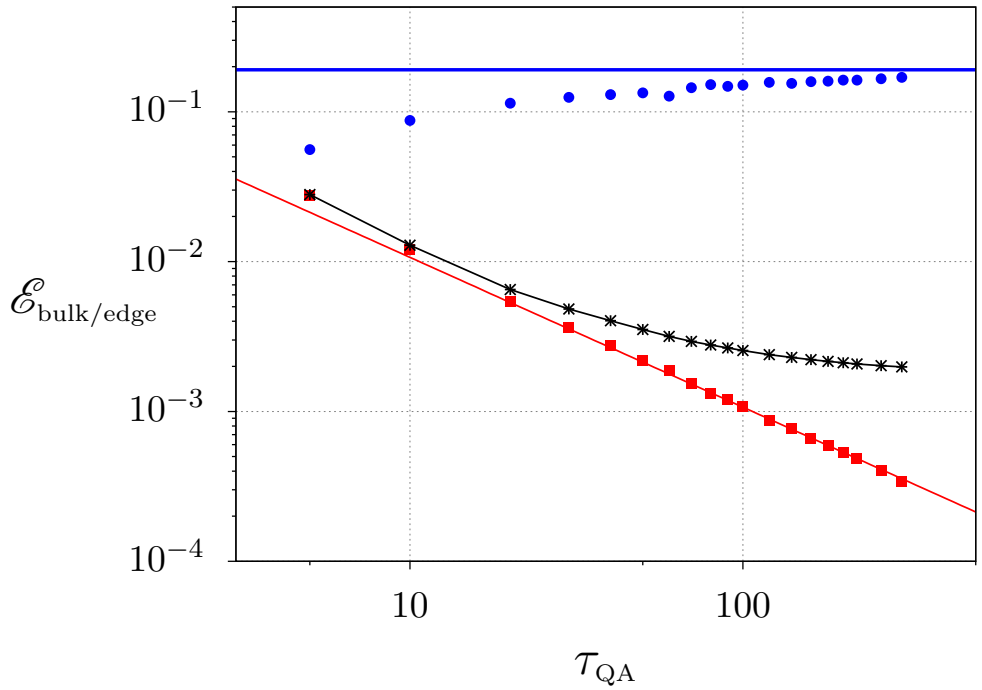

Figure 3.5.: Residual energy $\mathscr{E}_{\mathrm{res}}$ (stars), separated into bulk $\mathscr{E}_{\mathrm{bulk}}$ (squares) and edge $\mathscr{E}_{\mathrm{edge}}$ (circles) contributions, vs the annealing time τ_{QA}. The solid horizontal blue line is $\mathscr{E}_{\mathrm{edge}}^{\mathrm{LZ}}$ of Eq. (3.23). Here data with $L = N_x = N_y = 6n$ from 18 to 102 were used to get $\varepsilon_{\mathrm{bulk/edge}}$ for each τ_{QA}.

the right-edge electron sitting immediately to the right of the LZ gap in the left panel of Fig. 3.6 (we have here a "small" $N_y = 72a$ to better show the discrete occupied k-points): as the LZ-gap sweeps towards larger k-momenta, this right-edge electron will be *unable to follow the ground state* due to the exponentially small LZ gap, and will remain in the right-edge band, but now *excited*, since the corresponding equilibrium lowest-energy state sits in the left-edge band. In essence: there cannot be any LZ tunnelling across the opposite edges of the sample. Hence, left-edge states remain, one after the other, selectively unoccupied, while their fellow on the right-edge are occupied. If we account for this edge-state residual energy — which scales as $\mathscr{E}_{\rm edge}L$, as opposed to the bulk residual energy, scaling as $\mathscr{E}_{\rm bulk}L^2$ — and analyse the data as $E_{\rm res} = \mathscr{E}_{\rm bulk}L^2 + \mathscr{E}_{\rm edge}L + \cdots$, we find that $\mathscr{E}_{\rm bulk}(\tau_{\rm QA}) \sim \tau_{\rm QA}^{-1}$ (filled squares in left plot of Fig. 3.5), while $\mathscr{E}_{\rm edge}(\tau_{\rm QA})$ (solid circles) slowly increases, approaching the value expected from the previous LZ analysis:

$$\mathscr{E}_{\rm edge}^{\rm LZ} = \int_{K_+}^{K_{\rm f}} \frac{{\rm d}k}{2\pi} \, [E_{k,+} - E_{k,-}] \ , \tag{3.23}$$

indicated by the solid horizontal line in Fig. 3.5)C. A detailed analysis of the scaling of the excitation energy can be found in appendix D.2.

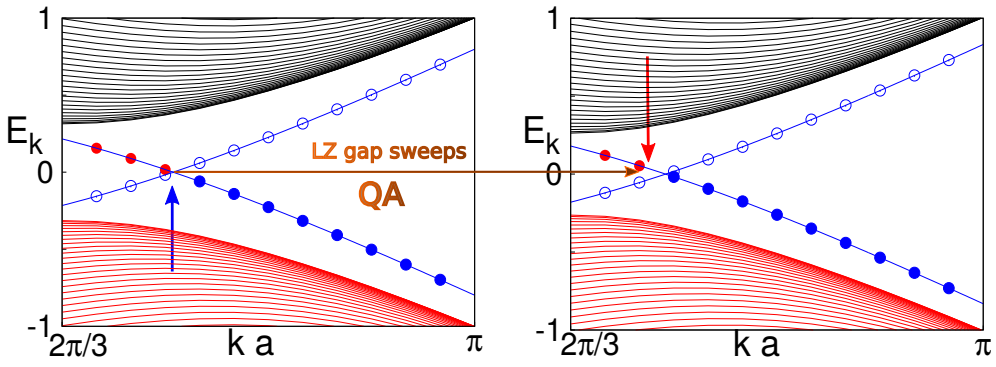

Figure 3.6.: The mechanism by which right-edge states get selectively populated as the exponentially-small LZ gap sweeps to larger values of k during the QA evolution. The (equilibrium) edge states shown refer to $\Delta_{AB}/t_2 = 2.5$ (left) and $\Delta_{AB}/t_2 = 2.4$ (right). Filled/empty circles denote occupied/empty edge states. The blue vertical arrow in the left panel points to an occupied right-edge electron that remains occupied (red vertical arrow in the right panel) after the Landau-Zener event.

The side where excited electrons will be found at the end of the annealing depends on the sign of the initial $(\Delta_{AB}(0))$, which decides which one of the sublattices is energetically favourite. When the Hamiltonian enters the non-trivial phase, the instantaneous ground state will have more edge states on the side of the sample determined by $\Delta_{AB}(t)$. As $\Delta_{AB}(t)$ is decreased, this unbalance is less and less evident in $|\Psi_{\rm GS}(t)\rangle$, but the LZ excitations will not allow the symmetry restoration in $|\Psi(t)\rangle$. In the case shown in the previous figures an opposite initial Δ_{AB} would have meant a gap closing at K_- and a final population of the other edge-states branch (whose wavefunctions are localized on the opposite edge with respect to the states of the other branch).

3.3. Periodically driven model: non-resonant case

We now return to our Floquet QA, Eq. (3.18), with a circularly polarized driving "adiabatically" turned on $\lambda(t) = (t/\tau_{\rm QA})\lambda_{\rm f}$ in a time $\tau_{\rm QA} = n_{\rm QA}\tau$, followed by an evolution with constant $\lambda_{\rm f}$ for $\tau_{\rm f} = n_{\rm f}\tau$. Technical details on the simulation are given in App. D.1. The role of Δ_{AB} deserves a few comments. Leaving aside for the moment cold atoms, in principle, $\Delta_{AB} = 0$ in graphene, while $\Delta_{AB} \neq 0$ in systems like Boron-Nitride, where inversion symmetry is broken. Graphene, however, is a gapless critical system, and its adiabatic evolution towards a Floquet Chern insulator does not fit into the previous standard KZ scenario. Nevertheless, a zigzag graphene nanoribbon has a very small finite-size gap separating non-dispersive edge states, which in principle allows for a well defined initial Slater determinant to be formed. Unfortunately, these edge states turn out to be somewhat unphysical: they are symmetric/antisymmetric combinations of left-right edge wavefunctions, a very delicate quantum mechanical creature, likely destroyed by many physical mechanisms, including decoherence effects, interactions, disorder. To get rid of such quantum mechanical superpositions of left-right edge states, we will always add a very small symmetry-breaking Δ_{AB} when describing "graphene", which in principle should be sent to 0 after the thermodynamic limit is taken. As soon as a very small Δ_{AB} is included, the nature of the edge wavefunctions changes, and the lower lying states become localized at the right edge (if $\Delta_{AB} > 0$) or at the left edge (if $\Delta_{AB} < 0$). We have verified that the value of the small symmetry-breaking Δ_{AB} is not important (only the sign matters) for the results we are going to describe. Anyway, we will also have in mind ultracold atoms, thus, as we have anticipated in Sec. 3.1.3, we have included in our model (3.18) a Δ_{AB} that can vary in time. We will hence perform evolutions both with a time-independent Δ_{AB}, and with $\Delta_{AB}(t)$ switched-off to 0 during the annealing time $\tau_{\rm QA}$.

The results we find are perfectly described by the Haldane physics we have illustrated, provided the driving field is spatially uniform, and, most importantly, the frequency $\hbar\omega$ of the perturbation is larger then the unperturbed bandwidth $W = 6|t_1|$. We have verified this by monitoring the occupations $n_{k,\alpha}$ of the instantaneous single-particle Floquet modes $|\phi_{k,\alpha}\rangle$: the state $|\Psi(\tau_{\rm QA})\rangle$ after the annealing is "close" to $|\Psi_{\rm FGS}(\lambda(\tau_{\rm QA}))\rangle$, apart from bulk KZ excitations near the Dirac points, and the previously discussed selective excitation of edge states, see Fig. 3.7.

The dynamics of the Hall current is interesting. As customary, in a Laughlin cylinder geometry the total current in the y-direction is given by

$$\hat{J}_y = \frac{1}{\hbar}\frac{\partial \hat{H}}{\partial \kappa_y}\Big|_{\kappa_y=0} ,$$

where $\kappa_y = \frac{2\pi}{N_y a}\frac{\Phi_L}{\phi_0}$ is related to the flux Φ_L, piercing the PBC-cylinder along the x-axis, and ϕ_0 is the flux quantum [108]. As we discussed in Sec. 3.1.1, PBC along y, allow us to write $\hat{H}(t) = \sum_k^{\rm BZ_y} \sum_{ii'} \mathbb{H}_{ii'}(k,t)\, \hat{c}^\dagger_{i,k}\hat{c}_{i',k}$, where $\mathbb{H}(k,t)$ is the k-resolved strip Hamiltonian and $\hat{c}^\dagger_{i,k}$

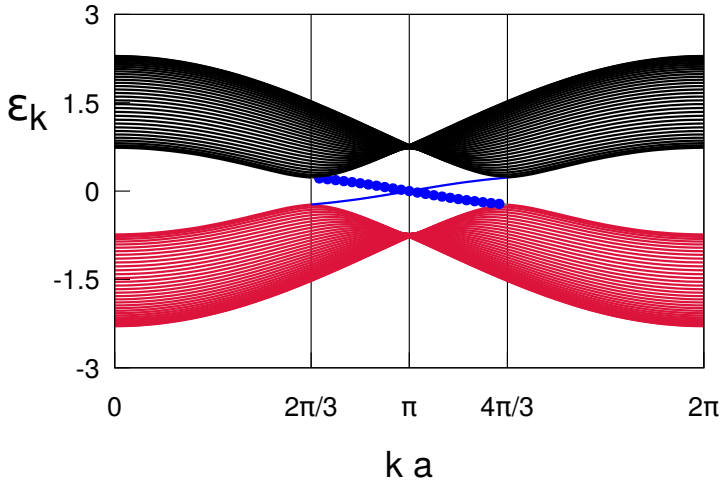

Figure 3.7.: Final Floquet quasi-energy bands for a uniform driving with $\phi = -\pi/2$, $\hbar\omega = 7|t_1| > W$, $\Delta_{AB} = 10^{-3}|t_1|$ (effectively representing graphene), and $\lambda(t)$ linearly ramped up to $\lambda_f = 1$ in $\tau_{QA} = 100\tau$, with $\tau = 2\pi/\omega$. Here the topological transition occurs at $\lambda_{cr} \approx 0$. Valence states (in red) are filled, conduction states (in black) empty. Filled circles denote occupied edge states.

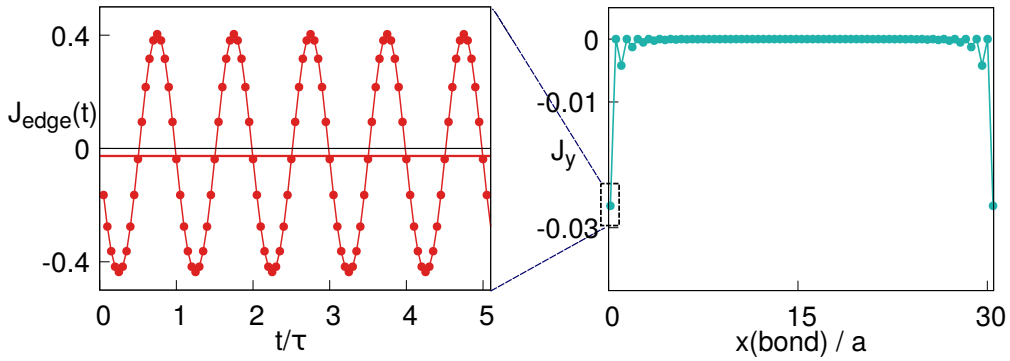

Figure 3.8.: Right: Time-averaged bond currents calculated with a periodic evolution at constant λ_f for $\tau_f = 100\tau$. Left: the large intra-period oscillations for the first bond on the left. The parameters are same of Fig. 3.7

.

creates an electron of momentum k at site i along the zigzag line sketched in Fig. 3.1-**b′**. Hence, bond-resolved y-currents are

$$J_{i,i+1}(t) = \langle\Psi(t)|\sum_{k}^{\mathrm{BZ}_y} \mathbb{J}_{i,i+1}(k,t)\ \hat{c}^{\dagger}_{i,k}\hat{c}_{i+1,k}|\Psi(t)\rangle\ ,$$

with

$$\mathbb{J} = \frac{1}{\hbar}\frac{\partial\mathbb{H}}{\partial\kappa_y}\Big|_{\kappa_y=0}\ .$$

Now since after the annealing $|\Psi(t>\tau_{\mathrm{QA}})\rangle$ is basically a Slater determinant of Floquet modes, e.g. the occupations are basically all 0 or 1, the observables will immediately converge to diagonal ensemble value. The circles in the right plot of Fig. 3.8 denote the time-average of $J_{i,i+1}(t)$ during the constant-λ_{f} evolution,

$$[J_{i,i+1}]_{\mathrm{av}} = \frac{1}{n_{\mathrm{f}}\tau}\int_{\tau_{\mathrm{QA}}}^{\tau_{\mathrm{QA}}+n_{\mathrm{f}}\tau}\mathrm{d}t\ J_{i,i+1}(t)\ .$$

Currents are concentrated at the edges, but with large periodic oscillations, shown in the left plot. Therefore the stroboscopic averages are not representative of the true time-averages and period-averages are necessary. Notice that the edge currents have left/right symmetry, while one would naively expect currents only on the edge which is selectively occupied by the out-of-equilibrium dynamics (the right edge, for Fig. 3.7). This behaviour originates from specific symmetries — previously noted in equilibrium for the Haldane model at $\phi_H = \pm\pi/2$ [109, 110] — whereby the GS value of $\hat{J}_y$ is *zero everywhere* due to an exact compensation between currents due to edge states and edge-current contributions due to *bulk* states. Since the out-of-equilibrium dynamics brings a lack of current-carrying edge states (Fig. 3.7), the corresponding bulk contribution is uncompensated and gives rise to a left-flowing current of the same sign and amplitude as that at the right-edge. We notice that the sign of the currents can be changed by changing the sign of the polarisation φ. An opposite φ implies an opposite Haldane flux in the Floquet Hamiltonian: the bulk gap closing and reopening will happen at the other Dirac-cone. In this case there will be an excess of populated edge states that carry a positive current.

This left/right symmetry can be removed by a space inhomogeneity of the perturbation, e.g., a laser focused off-centrer. As we explained in Section 3.1.1, we find here expedient to retain translational invariance along y, assuming a y-independent Gaussian modulation in the amplitude $w(\mathbf{x},t) = \mathrm{e}^{-(x-x_c)^2/2\sigma^2}$, where x_c is the focus centre, and σ the beam width. All the previous results remain valid for a central focusing, $x_c = L_x/2$, provided σ is not too small ($\sigma \gtrsim 0.4L_x$). But the interesting new feature is the ability to control the edge current to flow on either edge of the sample by moving the focus off-centrer. The left panel of Fig. 3.9 illustrates the final Floquet quasi-energy bands when the laser is focused on the right edge ($x_c = L_x$), with $\sigma = 0.4L_x$. Notice that only the irradiated right-edge states show a k-dispersion: unirradiated left-edge states stay flat and carry no current. Non-equilibrium currents flow only at the irradiated edge, see the right panel of Fig. 3.9.

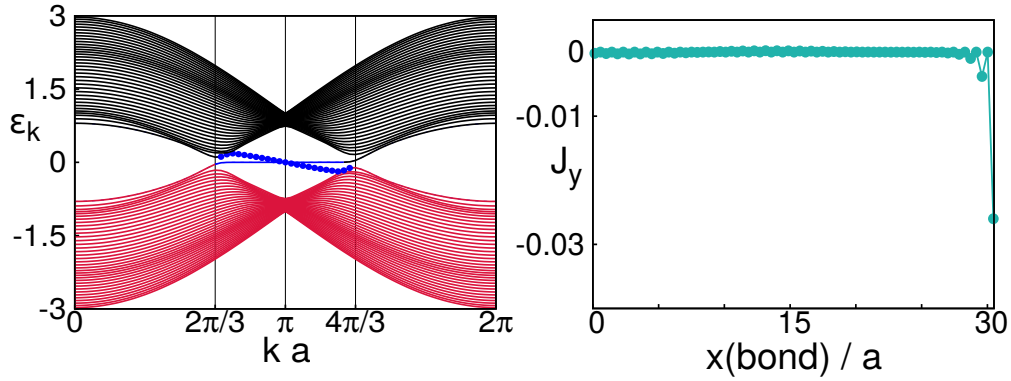

Figure 3.9.: Quasienergy bands with occupations (left) and time-averaged bond currents calculated with a periodic evolution at constant $\lambda_{\rm f}$ for $\tau_{\rm f} = 100\tau$ for an inhomogeneous driving focused on the right edge ($x_c = L_x$) of width $\sigma = 0.4L_x$ and the same parameters of Fig.3.8: $\phi = -\pi/2$, $\hbar\omega = 7|t_1| > W$, $\Delta_{AB} = 10^{-3}|t_1|$ (effectively representing graphene), and $\lambda(t)$ linearly ramped up to $\lambda_{\rm f} = 1$ in $\tau_{\rm QA} = 100\tau$, with $\tau = 2\pi/\omega$.

3.4. A local indicator of dynamical topological transitions

It is interesting to address the issue of an "indicator" of non-trivial topology in a non-equilibrium translationally-non-invariant setting. For translational invariant systems (with PBC), it was shown that the usual Chern number C is conserved during a unitary evolution [109, 111]: the time evolved state cannot undergo a topological transition in a closed quantum system in such a setting. However, since for $\hbar\omega > W$ the non-trivial final bulk states are adiabatically populated in a controlled way, we would expect to be able to "see" the topological transition by looking only at the "bulk" of the sample. We find that the local Chern marker (CM) $\mathfrak{C}(\mathbf{r})$ introduced in Ref. [36] at equilibrium, essentially a local measure of the Hall conductivity, works also in our non-equilibrium context: it signals if the sample bulk is *locally* a topologically non-trivial insulator, $\mathfrak{C}(\mathbf{r}) \sim \pm 1$. $\mathfrak{C}$ can be expressed as a physically appealing commutator of position operators [36]:

$$\mathfrak{C}(\mathbf{r},t) = -2\pi i \,\langle \mathbf{r}| \left[\hat{x}_{\mathcal{P}(t)}, \hat{y}_{\mathcal{P}(t)}\right] |\mathbf{r}\rangle \ . \tag{3.24}$$

Here $\hat{x}_{\mathcal{P}} = \hat{\mathcal{P}}\hat{x}\hat{\mathcal{P}}$ and $\hat{y}_{\hat{\mathcal{P}}} = \hat{\mathcal{P}}\hat{y}\hat{\mathcal{P}}$ are position operators projected on the occupied states, $\hat{\mathcal{P}}(t)$ being the projector on the time-evolved Slater determinant $|\Psi(t)\rangle$. An explanation of this formula can be found in Appendix C.

Fig. 3.10 illustrates, with a colour-code map, the dynamics of $\mathfrak{C}(\mathbf{r},t)$ as the system evolves from a trivial insulating phase at $\lambda = 0$ (left), towards a final non-trivial point with $\lambda_{\rm f} = 1$ (right). Notice that at all edges (including those imposed by the PBC along y) the CM deviates strongly from its bulk behaviour, in such a way that $\int_V \mathrm{d}\mathbf{r}\ \mathfrak{C}(\mathbf{r}) = 0$ on any finite sample [36], regardless of the edge states excitations that characterize the dynamics. Fig. 3.11 shows more in detail the dynamics of $\mathfrak{C}(\mathbf{r},t)$, averaged over a central "bulk" portion of the

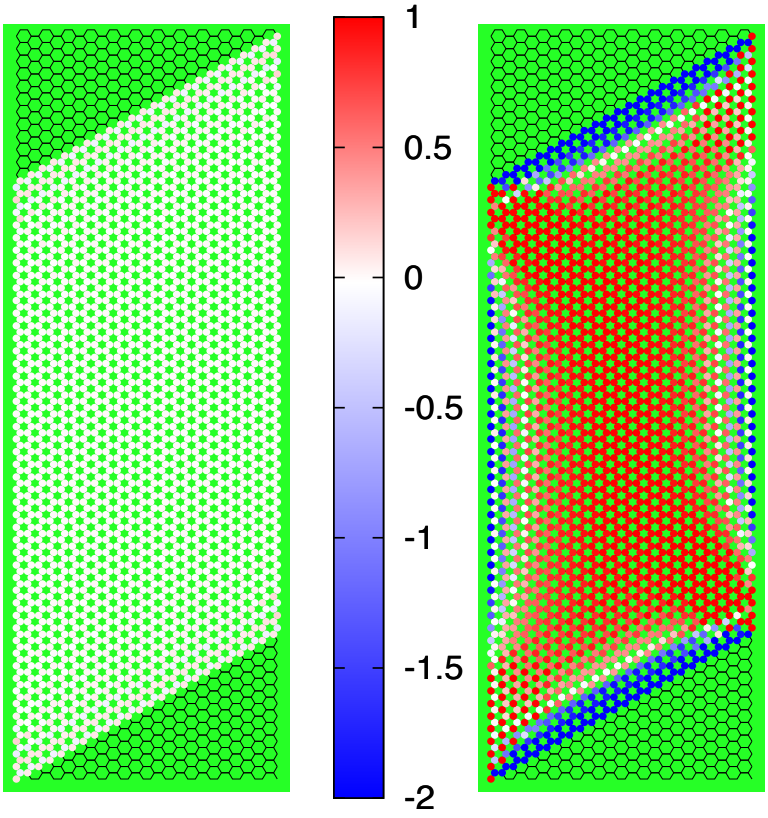

Figure 3.10.: The local value of the Chern marker $\mathfrak{C}(\mathbf{r}, t)$ at two different time shots during a QA evolution with $\tau_{\mathrm{QA}} = 300\tau$ and $\Delta_{AB}(t) = 0.1\,|t_1|$for a zigzag strip with $N_x = N_y = 48$ sites (PBC in the y-direction): the initial trivial insulator (left, with $\mathfrak{C}(\mathbf{r}) \sim 0$) and the non-trivial insulator after the end of the annealing, $t = \tau_{\mathrm{QA}} + 50\tau$ (right, with $\mathfrak{C}(\mathbf{r}) \sim +1$ in the bulk and finite-size effects at the edges).

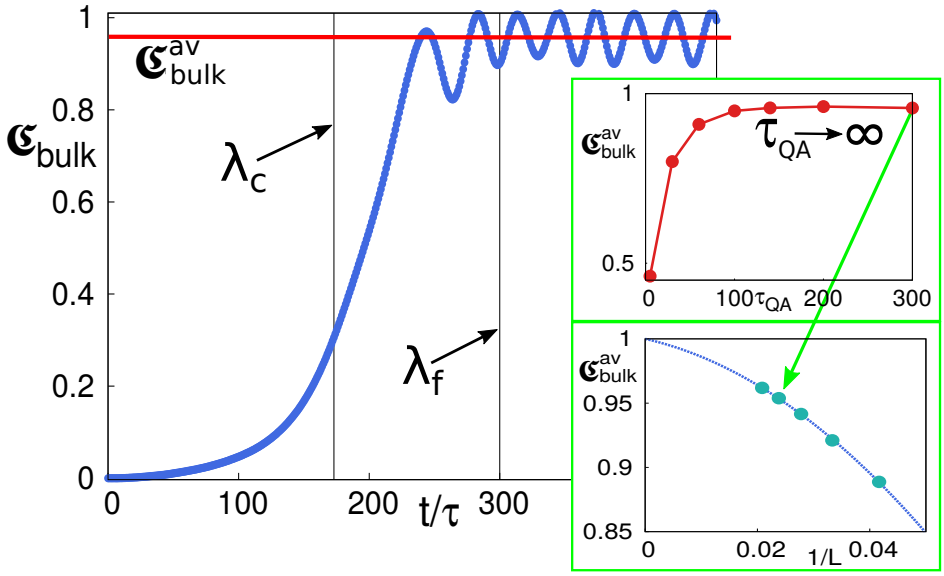

Figure 3.11.: The bulk average $\mathfrak{C}_{\rm bulk}(t)$ of the local Chern marker $\mathfrak{C}(\mathbf{r},t)$ for a uniform driving with $\phi=-\pi/2$, $\hbar\omega=7|t_1|>W$, $\Delta_{AB}=0.1|t_1|$, and $\lambda(t)$ linearly ramped up to $\lambda_{\rm f}=1$ in $\tau_{\rm QA}=300\tau$, followed by a constant-$\lambda_{\rm f}$ evolution for $\tau_{\rm f}=220\tau$, with $\tau=2\pi/\omega$. The topological transition occurs at $\lambda_{\rm c}\approx 0.57$. Here $L=N_x=N_y=48$, and we average on a central square of size 12×12. The horizontal line at ≈ 0.96 is the time-average $\mathfrak{C}^{\rm av}_{\rm bulk}$, calculated from $t=\tau_{\rm QA}$ to $t=\tau_{\rm QA}+\tau_{\rm f}$. The upper inset shows the saturation of $\mathfrak{C}^{\rm av}_{\rm bulk}(L,\tau_{\rm QA}\to\infty)$ to a limiting value that, see lower inset (where we fit points with standard power-law corrections $1+c_1/L+c_2/L^2$), goes to 1 for $L\to\infty$.

sample (a macroscopic average)

$$\mathfrak{C}_{\rm bulk}(t)=\frac{1}{N_{\rm bulk}}\sum_{\mathbf{r}\in{\rm bulk}}\mathfrak{C}(\mathbf{r},t)\;, \tag{3.25}$$

as the system evolves from a trivial insulator at $\lambda=0$, towards the non-trivial point with $\lambda_{\rm f}=1$. Upon time-averaging the oscillations after $\tau_{\rm QA}$, we obtain a quantity

$$\mathfrak{C}^{\rm av}_{\rm bulk}(L,\tau_{\rm QA})=\frac{1}{n_{\rm f}\tau}\int_{\tau_{\rm QA}}^{\tau_{\rm QA}+n_{\rm f}\tau}{\rm d}t\;\mathfrak{C}_{\rm bulk}(t)$$

approaching the correct integer value 1 as $\tau_{\rm QA}\to\infty$ and $L\to\infty$ (see insets in Fig. 3.11):

$$\lim_{L\to\infty}\lim_{\tau_{\rm QA}\to\infty}\mathfrak{C}^{\rm av}_{\rm bulk}(L,\tau_{\rm QA})=1\;.$$

In order to further clarify the nature of the dynamical topological transition we compare these results for the Floquet case with those obtained in the simpler case of the Haldane model. The behaviour of the local CM is captured by its macroscopic average in the bulk [36].

Fig. 3.12-**a** illustrates the time evolution of $\mathfrak{C}_{\rm bulk}(t)$, in the Haldane case, along the evolution arrow of Fig. 3.3, for $L = N_x = N_y = 48$, by considering the bulk portion to be a central square of size 12×12. Starting from zero, $\mathfrak{C}_{\rm bulk}(t)$ begins to grow near the equilibrium topological transition, until it reaches a value $\simeq 0.98$. Afterwards, it fluctuates very weakly around this final value. We find that the time-average of $\mathfrak{C}_{\rm bulk}(t)$, $\mathfrak{C}^{\rm av}_{\rm bulk}(L, \tau_{\rm QA})$, reaches, for long annealing times $\tau_{\rm QA}$, the value corresponding to the ground state of the final Hamiltonian, $\mathfrak{C}^{\rm eq}_{\rm bulk}$, which, in turn, approaches 1 as the size L increases, as shown in Fig. 3.12-**c**. Moreover, the amplitude of the time fluctuations

$$\mathfrak{C}^{\rm rms}_{\rm bulk}(L, \tau_{\rm QA}) = \sqrt{\frac{1}{\tau_{\rm f}} \int_{\tau_{\rm QA}}^{\tau_{\rm QA}+\tau_{\rm f}} {\rm d}t \ \left(\mathfrak{C}_{\rm bulk}(t) - \mathfrak{C}^{\rm av}_{\rm bulk}\right)^2} \tag{3.26}$$

goes to 0 as $\tau_{\rm QA} \to \infty$, see Fig. 3.12-**b**. These facts shed a light on the nature of the adiabatic transition. As explained above, excitations of the bulk states are of the standard KZ-type and can be controlled by making the annealing time $\tau_{\rm QA}$ larger and larger, while edge states are occupied in a characteristic non-equilibrium way no matter how large $\tau_{\rm QA}$ is. However, due to the localized nature of an insulating state [112, 113], the bulk "does not know" about the excited edge states. Thus $\mathfrak{C}^{\rm av}_{\rm bulk} \sim 1$ signals that the bulk correlations are of the insulating type, and that the time-evolved state has managed to follow the instantaneous ground state also in its topological aspects, contrary to what might be expected on the basis of the conservation the total Chern number [111]. When the annealing time is too short, $\mathfrak{C}^{\rm av}_{\rm bulk}$ fluctuates strongly around some value between 0 and 1, indicating that the bulk should be considered to be in a non-equilibrium "metallic" phase.

In the Floquet case, we observe that smooth oscillations appear on top of the behaviour illustrated for the Haldane case. For instance, Fig. 3.12-**a′** shows the result (already presented in Fig. 3.11) for the case of a periodically driven insulator with a finite constant $\Delta_{AB} = 0.1|t_1|$ and size $L = N_x = N_y = 48$. Fig. 3.12-**b′** shows that by increasing the annealing time $\tau_{\rm QA}$, the time-average $\mathfrak{C}^{\rm av}_{\rm bulk}$ tends to $\mathfrak{C}^{\rm av}_{\rm bulk} \simeq 0.96$, while the time-fluctuation $\mathfrak{C}^{\rm rms}_{\rm bulk}$ settles down to a small but non-vanishing value $\mathfrak{C}^{\rm rms}_{\rm bulk} \sim 0.04$. However, as shown in Fig. 3.10-**c′**, not only $\lim_{L\to\infty} \lim_{\tau_{\rm QA}\to\infty} \mathfrak{C}^{\rm av}_{\rm bulk}(L, \tau_{\rm QA}) = 1$, but also $\lim_{L\to\infty} \lim_{\tau_{\rm QA}\to\infty} \mathfrak{C}^{\rm rms}_{\rm bulk}(L, \tau_{\rm QA}) = 0$.

3.5. Periodically driven model: resonant case

It would be extremely interesting to be able to stabilize the non-trivial Floquet-Chern insulator states that can arise when the frequency of the driving becomes smaller than the bandwidth: $\hbar\omega < W$. Indeed, as we have mentioned in section 2.3.3, it is possible to realize phases where the Floquet Ground state has higher Chern numbers and the bulk-edge correspondence become highly non-trivial, with the possibility that the number of edge modes can not be deduced from the value of the Chern number.

However, obtaining such non-trivial Floquet-Chern insulating states seems very difficult in

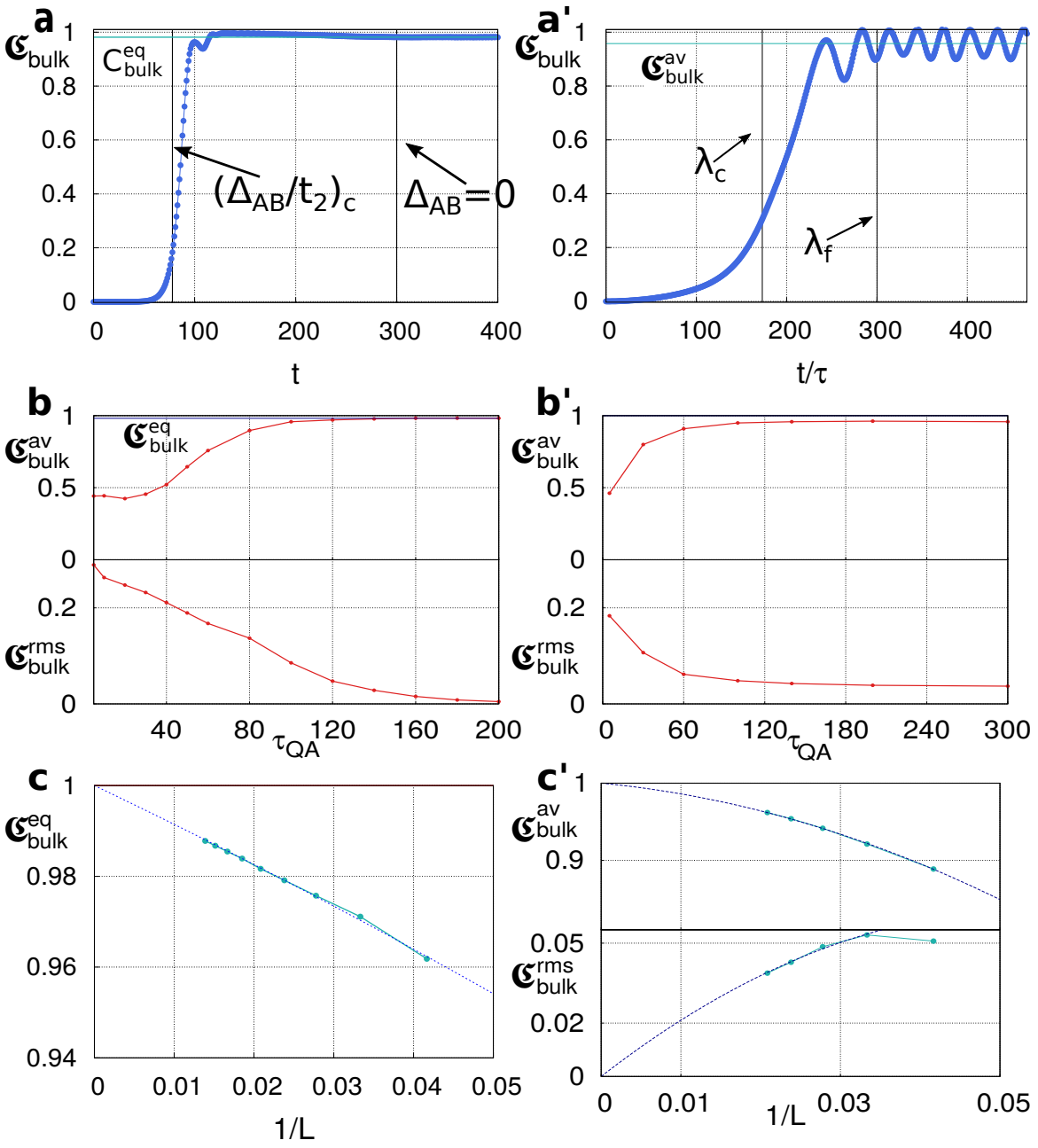

Figure 3.12.: Dynamics of the Chern marker. Bulk Chern marker $\mathfrak{C}_{\text{bulk}}$ for a strip of size $L = N_x = N_y = 48$, calculated on the central square of size 12×12 sites, as a function of time, for the Haldane model (**a**, **b** and **c**) and for the graphene-Floquet model (**a**′, **b**′ and **c**′).

(continued)

Figure 3.12.: (*Continued*) (**a**): Annealing of a Haldane model from $\Delta_{AB}/t_2 = 4\sqrt{3}$ to $\Delta_{AB}/t_2 = 0$, with $\tau_{\rm QA} = 300\hbar/|t_1|$, followed by an evolution with $\Delta_{\rm AB} = 0$ for a time $\tau_{\rm f} = 220\hbar/|t_1|$. A vertical indicates the critical value $(\Delta_{AB}/t_2)_c$. The horizontal line at ≈ 0.98, is the bulk Chern marker of the ground state $\mathfrak{C}^{\rm eq}_{\rm bulk}$ of the Haldane model with $\Delta_{\rm AB} = 0$. (**b**): the long time average $C^{\rm av}_{\rm bulk}$ of the CM and the long time rms $\mathfrak{C}^{\rm rms}_{\rm bulk}$ as a function of $\tau_{\rm QA}$ in the Haldane case with the same parameters of (**a**). (**c**): the equilibrium $\mathfrak{C}^{\rm eq}_{\rm bulk}$ for the Haldane model with $\Delta_{\rm AB} = 0$ versus the size L of the system. (**a′**): Annealing of the driven graphene model with $\lambda(t) = (t/\tau_{\rm QA})\lambda_{\rm f}$ and $\lambda_{\rm f} = 1$, followed by a periodic evolution with fixed $\lambda_{\rm f}$ for $\tau_{\rm f} = 220\tau$; here $\tau_{\rm QA} = 300\tau$, $\hbar\omega = 7|t_1| > W$ and $\Delta_{AB} = 0.1|t_1|$. The horizontal line at ≈ 0.96 is the long time average $\mathfrak{C}^{\rm av}_{\rm bulk}$. (**b′**): $\mathfrak{C}^{\rm av}_{\rm bulk}$ and $\mathfrak{C}^{\rm rms}_{\rm bulk}$ as a function of $\tau_{\rm QA}$ with the same parameters of (**a′**). (**c′**): $\mathfrak{C}^{\rm av}_{\rm bulk}$ and the $\mathfrak{C}^{\rm rms}_{\rm bulk}$ for $\tau_{\rm QA} = 200\tau$ versus L. In **a** and **a′**, the first vertical line on the left indicates the closing of the gap in the instantaneous (energy or quasi-energy) spectrum, the second one the end of the annealing. The $\mathfrak{C}^{\rm av}_{\rm bulk}$ points in **c** and **c′** are fitted by a parabola passing through $(0, 1)$, while $\mathfrak{C}^{\rm rms}_{\rm bulk}$ data are fitted by a parabola passing through $(0, 0)$.

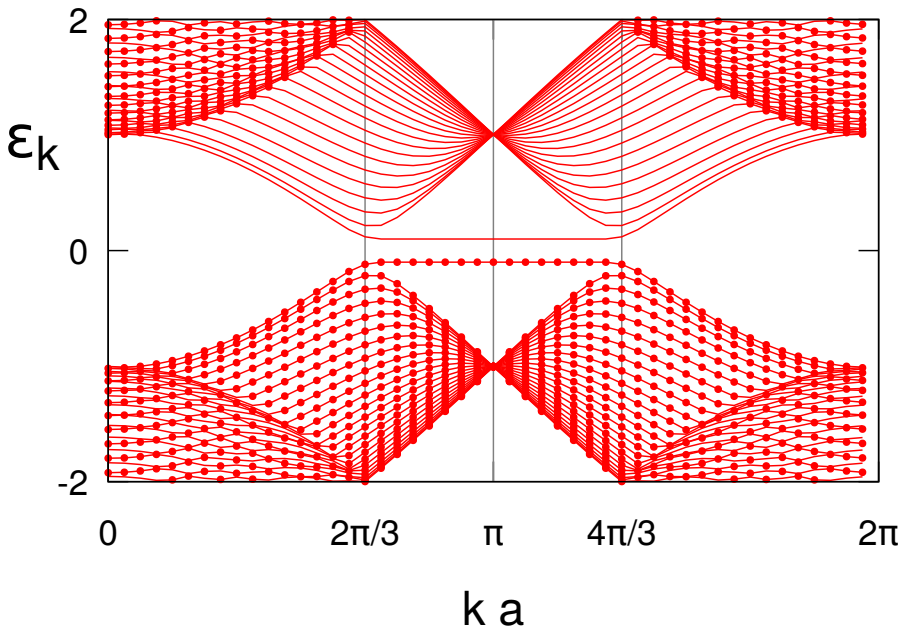

Figure 3.13.: Initial ($\lambda = 0$) quasienergy spectrum in the case of $\hbar\omega = 4\,|t_1|$ and $\Delta_{AB}(0) = |0.1|$. The quasienergies are equal modulo $\hbar\omega$ to the energies of $\hat{H}(0)$, but due to the fact that $\hbar\omega < W$, they get partially folded inside the FBZ $[-\hbar\omega/2, \hbar\omega/2]$. Filled dots indicate the populated levels, e.g. the original GS energy levels.

absence of dissipation effects due to an environment. Indeed, when $\hbar\omega$ is *smaller* than the bandwidth W, intra-band resonances between valence states at E_α and conduction ones at $E_\beta \approx E_\alpha + \hbar\omega$ change the physics completely, breaking the Floquet adiabatic picture. The whole crux is, in essence, that the starting point at $\lambda(0) = 0$ — the usual Slater determinant

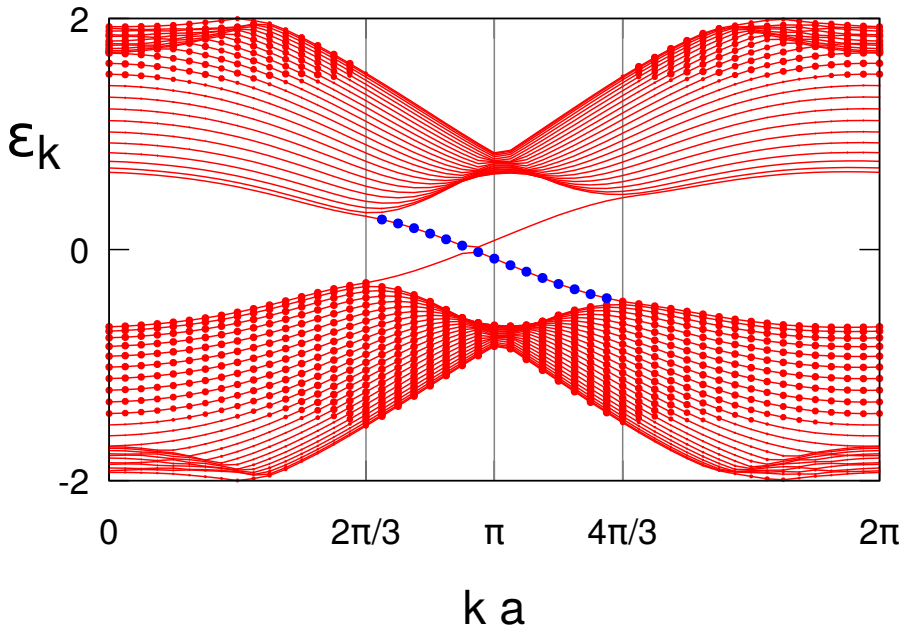

Figure 3.14.: Final Floquet quasi-energies $\varepsilon_{k,\alpha}$ and occupations $n_{k,\alpha}$ (dot size proportional to the occupation $n_{k,\alpha}$) for $\phi = -\pi/2$, $\hbar\omega = 4|t_1| < W$, $\Delta_{AB} = 0.1|t_1|$ (constant), and $\lambda(t)$ linearly ramped up to $\lambda_{\rm f} = 1$ in $\tau_{\rm QA} = 300\tau$.

$|\Psi(0)\rangle$ — does not coincide with the Floquet GS, $|\Psi(0)\rangle \neq |\Psi_{\rm FGS}(\lambda = 0), 0\rangle$, for any choice of the Floquet BZ. As we show in Fig. 3.13, upon folding the original $[-W/2, W/2]$ spectrum in e.g., $[-\hbar\omega/2, \hbar\omega/2]$, we see that the lower Floquet quasi-energy band is only partially filled, with empty conduction-band-originated states intermixed with filled valence-band ones. These filled-empty pairs with small Floquet gaps [47, 48] $\min_{m\in\mathbb{Z}}(|\epsilon_\alpha - \epsilon_\beta + m\hbar\omega|)$ lead to a proliferation of *bulk* LZ events as $\lambda(t)$ is ramped up, with a complex redistribution of electronic occupations of the states: the final Floquet GS $|\Psi_{\rm FGS}(\lambda(\tau_{\rm QA})\rangle$ is *never* reached, even for $\tau_{\rm QA} \to \infty$. Fig. 3.14 shows the final Floquet quasi-energy bands, with the corresponding population indicated by a variable-size dot, for $\hbar\omega = 4|t_1| < W$ and $\lambda(t)$ linearly ramped up to $\lambda_{\rm f} = 1$ in $\tau_{\rm QA} = 300\tau$. The final state reached is a non-equilibrium metal, rather than an insulator with Chern number $C = 3$ as the final FGS is. This aspect is important in devising pump-probe photoemission experiments in graphene [114].

3.6. Conclusions

We found a non-equilibrium mechanism which selectively populates edge states when performing an adiabatic switching-on of a periodic perturbation towards a topologically non-trivial insulating phase. The mechanism we illustrated requires edge states (hence OBC)

whose electronic occupation is unable to follow instantaneous equilibrium as they become topologically non-trivial and cross the bulk gap. It is general enough, and is at the root of the deviations from KZ scaling in $1d$ topological transitions, as seen in [115, 116]. In the present $2d$ context, it adds flexibility to the control of the edge currents flowing at the boundaries of the sample, including the ability to have currents flowing only at one edge, by appropriate focusing of the ac field. We have also discovered that a dynamical generalization of the Chern Marker [36] is able to detect locally the topological transition of the time-evolved state, marking a net difference with Chern number dynamics in systems with no boundaries [111]. Finally, we have shown that for $\hbar\omega < W$ intra-band resonances ruin the adiabatic picture and the resulting state is a non-equilibrium metal. Our findings should be amenable to experimental tests both with ultra-cold atoms in optical lattices [35], and with laser irradiated electronic systems.

4. Non-adiabatic effects in Thouless pumping

In this chapter we study Thouless pumping without the assumption of perfectly adiabatic driving, by using the tools of Floquet theory. In all the aspects that we will analyse, we will refer to the periodically driven Rice-Mele model as an example, which is a minimal tight-binding model for topological quantum pumping and has now become one of the most used models for the study of general properties of Thouless pumping [39, 117, 118, 119, 120]. Its static version [42] was originally introduced in the study of linearly conjugated polymers. The driven version is strictly related to the original practical proposal by Thouless for the realization of topological quantum pumping through a spatially sliding potential. Indeed, the recent experimental demonstrations of Thouless pumping with cold atoms [27, 28] were also based on this idea and in some regimes are described by the Rice-Mele model. Specifically, they used two one-dimensional superimposed optical lattice potentials with one of the two slowly translated in time, e.g. $V(x,t) = V_s \sin^2\left(\frac{\pi x}{d_s} + \frac{\pi}{2}\right) + V_l \sin^2\left(\frac{\pi x}{d_l} - \frac{\varphi(t)}{2}\right)$.

In the following sections, we will begin with a short introduction to the Rice-Mele model. Then in Sec. 4.2 we will explore a Floquet point of view on Thouless pumping, different from the dimensional extension of Chapter 2, namely that the quantized pumping in the adiabatic limit can be seen as a topological property of the *quasienergies*, rather than the Floquet states. In order to investigate the non-adiabatic effects we will then study the diagonal ensemble value of the charge, e.g. the average over many pumping cycles. We will argue with both numerical and analytical insights, that one of the ingredients of the long-time limit pumped charge, the occupations of Floquet modes, are responsible for what we might call *non-adiabatic breaking* of Thouless pumping. By this we mean the fact that corrections to quantization are at lowest order *quadratic* in the frequency ω and not exponentially small as previously supposed. This is reflected also in the charge pumped in a single period, which displays a non-analytic behaviour on top of an overall quadratic decrease. We will show that exponentially small corrections to quantization are obtained only if one was able to prepare a specific Floquet band Slater determinant. After this, thanks to the analysis of the diagonal ensemble pumped charge, we will study Thouless pumping also for frequencies very far from the adiabatic limit. We will also address in section 4.4 the effects of an initial thermal state. In the end we will conclude by showing some results on the separation of pumped charge between geometrical and dynamical contributions.

4.1. The Rice-Mele model

The Rice-Mele model is a minimal tight-binding model describing a $1d$ lattice constituted of two alternating sublattices, A and B. The two sublattices can have different on-site energy and the hopping between the two is asymmetric. We consider its periodically driven version, e.g. where the tight-binding matrix elements vary periodically in time. The Hamiltonian in real space reads

$$\begin{aligned}\hat{H}_{\mathrm{RM}}(t) = &- J_1(t)\sum_{j=1}^{N}\left(\hat{c}^{\dagger}_{j,B}\hat{c}_{j,A} + \mathrm{H.c.}\right) - J_2(t)\sum_{j=1}^{N}\left(\hat{c}^{\dagger}_{j+1,A}\hat{c}_{j,B} + \mathrm{H.c.}\right) + \\ &+ \sum_{j=1}^{N}\Delta(t)\left(\hat{n}_{j,A} - \hat{n}_{j,B}\right)\end{aligned} \quad . \tag{4.1}$$

Here $\hat{c}^{\dagger}_{A/B}$ creates a particle in cell j at sublattice, A/B. We imagine all the atoms to be

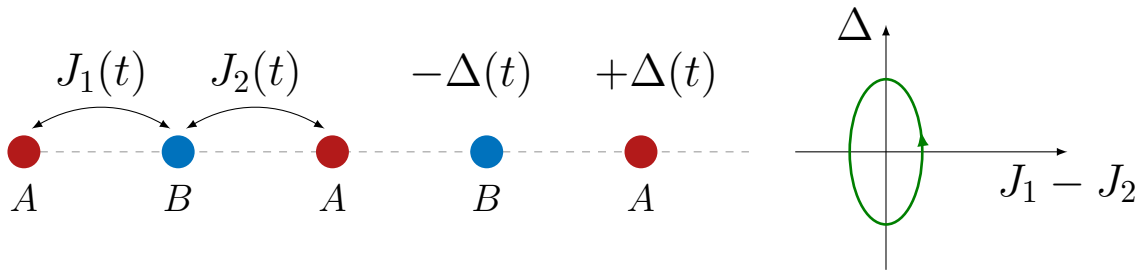

Figure 4.1.: Left: cartoon representation of Rice-Mele model. Right: a path in parameter space.

separated by the same distance $a/2$, regardless of which bond is considered. If we apply periodic boundary conditions and there is translational invariance, we can diagonalize the Hamiltonian by going into momentum space.

$$\begin{cases} \hat{c}^{\dagger}_{k,A} = \dfrac{1}{\sqrt{N}}\displaystyle\sum_{j=1}^{N} \mathrm{e}^{ikaj}\hat{c}^{\dagger}_{j,A} \\ \hat{c}^{\dagger}_{k,B} = \dfrac{1}{\sqrt{N}}\displaystyle\sum_{j=1}^{N} \mathrm{e}^{ikaj}\hat{c}^{\dagger}_{j,B} \end{cases} \qquad \begin{cases} \hat{c}^{\dagger}_{j,A} = \dfrac{1}{\sqrt{N}}\displaystyle\sum_{k}^{\mathrm{BZ}} \mathrm{e}^{-ikaj}\hat{c}^{\dagger}_{k,A} \\ \hat{c}^{\dagger}_{j,B} = \dfrac{1}{\sqrt{N}}\displaystyle\sum_{k}^{\mathrm{BZ}} \mathrm{e}^{-ikaj}\hat{c}^{\dagger}_{k,B} \end{cases} \quad . \tag{4.2}$$

This gives

$$\hat{H}_{\mathrm{RM}}(t) = \sum_{k}^{\mathrm{BZ}} \begin{bmatrix} \hat{c}^{\dagger}_{k,A} & \hat{c}^{\dagger}_{k,B} \end{bmatrix} \begin{bmatrix} \mathbb{H}(k,t) \end{bmatrix} \begin{bmatrix} \hat{c}_{k,A} \\ \hat{c}_{k,B} \end{bmatrix} \tag{4.3}$$

where, for each $k \in \mathrm{BZ}$, the Hamiltonian $\mathbb{H}(k,t)$ is a 2×2 Hermitean matrix, which one can always parametrize, in terms of the identity $\mathbb{1}$ and the three Pauli matrices $\hat{\boldsymbol{\sigma}}$. Here, as the

trace of the matrix is zero, we can write $\hat{\mathbb{H}}(k,t) = \mathbf{R}(k,t)\cdot\hat{\boldsymbol{\sigma}}$, or, more explicitly:

$$\mathbb{H}(k,t) = \begin{bmatrix} R_z & R_x - iR_y \\ R_x + iR + y & -R_z \end{bmatrix} = R_x(k,t)\hat{\sigma}_x + R_y(k,t)\hat{\sigma}_y + R_z(k,t)\hat{\sigma}_z \ . \tag{4.4}$$

A simple calculation shows that:

$$\begin{aligned} R_x(k,t) &= -J_1(t) - J_2(t)\cos ka \\ R_y(k,t) &= -J_2(t)\sin ka \\ R_z(k,t) &= \Delta(t) \ . \end{aligned} \tag{4.5}$$

The instantaneous spectrum is then given by

$$E_{k,1/0}(t) = \pm|\mathbf{R}(k,t)| = \pm\sqrt{J_1^2 + J_2^2 + 2J_1J_2\cos ka + \Delta^2} \ . \tag{4.6}$$

The form of the driving that we choose is

$$\begin{aligned} J_1(t) =& J_0 + \delta_0\cos\frac{2\pi t}{T} = J_0 + \delta(t) \\ J_2(t) =& J_0 - \delta_0\cos\frac{2\pi t}{T} = J_0 - \delta(t) \\ \Delta(t) =& \Delta_0\sin\frac{2\pi t}{T} \ . \end{aligned} \tag{4.7}$$

In this way, paths in parameters space $(J_1 - J_2, \Delta)$ will be ellipses around the metallic point $(0,0)$. For what concerns topology, this is one of the two possible paths for an adiabatic driving: paths can either contain the origin or not. In the first case they cannot be shrunk to a point because they would encounter a non-adiabatic trajectory, in the other it is possible. The first kind of path is the only one that leads to a non-zero quantized pumping [117].

4.2. Charge pumped by a Floquet state

In this section we show how Thouless formula for the charge pumped in an adiabatically periodically driven insulator is a particular case of topological charge pumping in a Floquet framework. We follow Ref. [67], but similar results are present also in Ref. [41, 121, 122].
We suppose, generically, that our initial state is a Slater determinant of some (filled) Bloch bands in 1D. The expectation value of the current operator $\widehat{J} = \frac{1}{\hbar}\partial_\kappa\hat{H}$, where we defined as usual $\kappa = \frac{2\pi}{L}\frac{\Phi}{\Phi_0}$ (see App.F.1), is

$$\begin{aligned} \langle\Psi(t)|\,\widehat{J}(t)\,|\Psi(t)\rangle =& \frac{1}{\hbar}\,\langle\Psi(t_0)|\,\hat{U}^\dagger(t,0)\partial_\kappa\hat{H}(t)\hat{U}(t,0)\,|\Psi(t_0)\rangle \\ =& \frac{1}{\hbar}\,\mathrm{Tr}\left\{\hat{\mathcal{P}}\hat{U}^\dagger(t,0)\partial_\kappa\hat{H}(t)\hat{U}(t,0)\right\} \ , \end{aligned} \tag{4.8}$$

where $\hat{\mathcal{P}}$ is the Projector over the initially occupied bands. Now consider the derivative of the evolution operator with respect to some parameter, κ in our case. If $\{t_p\}$ is a sequence of $N+1$ ordered times between 0 and τ separated by an interval Δt, it follows that

$$\begin{aligned}\partial_\kappa \hat{U}(\tau,0) =&\partial_\kappa \mathcal{T} \mathrm{e}^{-\frac{i}{\hbar}\int_0^\tau \hat{H}(t)dt} = \partial_\kappa \prod_{p=N}^{1} \hat{U}(t_p,t_{p-1}) = \partial_\kappa \lim_{N\to\infty} \prod_{p=N}^{1} \mathrm{e}^{-\frac{i}{\hbar}\hat{H}(t_{p-1})\Delta t} = \\ =&-\frac{i}{\hbar}\lim_{N\to\infty}\Delta t \sum_{p=0}^{N}\left(\prod_{j=N}^{p+1}\mathrm{e}^{-\frac{i}{\hbar}\hat{H}(t_j)\Delta t}\partial_\kappa \hat{H}(t_p)\prod_{l=p}^{0}\mathrm{e}^{-\frac{i}{\hbar}\hat{H}(t_l)\Delta t}\right) = \\ =&-\frac{i}{\hbar}\int_0^\tau dt \hat{U}(\tau,t)\left[\partial_\kappa \hat{H}(t)\right]\hat{U}(t,0)\ .\end{aligned} \tag{4.9}$$

The charge pumped after a period τ is given by the integral of Eq. 4.8 over one period divided by the system's length:

$$Q(\tau) = \frac{1}{L}\int_0^\tau \langle\Psi(t)|\,\widehat{J}(t)\,|\Psi(t)\rangle\, dt\ .$$

Making use of Eq. 4.9 and of the fundamental property $\hat{U}^\dagger(t,0) = \hat{U}(0,t) = \hat{U}(0,\tau)\hat{U}(\tau,t)$, we arrive at

$$Q(\tau) = \frac{1}{L}\,\mathrm{Tr}\left(\hat{\mathcal{P}}\hat{U}^{-1}(\tau,0)\left[i\partial_\kappa \hat{U}(\tau,0)\right]\right)\ . \tag{4.10}$$

This last expression for the pumped charge is still slightly more general than Thouless's one, since we have not specified the initial state and whether the driving is adiabatic or not. We can write the evolution operators above in the spectral (Floquet) representation, that is

$$\hat{U}(\tau,0) = \sum_\alpha \mathrm{e}^{-\frac{i}{\hbar}\varepsilon_\alpha \tau}\,|\phi_\alpha(0)\rangle\langle\phi_\alpha(0)|\,.$$

Thus we get[1]

$$\begin{aligned}Q(\tau) =& \frac{1}{L}\,\mathrm{Tr}\Bigg\{\mathcal{P}\sum_{\alpha\alpha'}\Bigg(|\phi_\alpha\rangle\langle\phi_\alpha|\,\delta_{\alpha\alpha'}\frac{\tau}{\hbar}\partial_\kappa\varepsilon_\alpha + \\ &+\mathrm{e}^{\frac{i}{\hbar}(\varepsilon_{\alpha'}-\varepsilon_\alpha)\tau}\,|\phi_{\alpha'}\rangle\langle\phi_{\alpha'}|\,\partial_\kappa\phi_\alpha\rangle\langle\phi_\alpha| + |\phi_\alpha\rangle\langle\partial_\kappa\phi_\alpha|\,\delta_{\alpha\alpha'}\Bigg)\Bigg\} = \\ =& \frac{1}{L}\,\mathrm{Tr}\Bigg\{\mathcal{P}\sum_\alpha\left(\frac{\tau}{\hbar}\partial_\kappa\varepsilon_\alpha\,|\phi_\alpha\rangle\langle\phi_\alpha| + \sum_{\alpha'\neq\alpha}\mathrm{e}^{\frac{i}{\hbar}(\varepsilon_{\alpha'}-\varepsilon_\alpha)\tau}\,|\phi_{\alpha'}\rangle\langle\phi_{\alpha'}|\,\partial_\kappa\phi_\alpha\rangle\langle\phi_\alpha|\right)\Bigg\}\ .\end{aligned} \tag{4.11}$$

At first, we consider the situation in which the initially filled bands are the Floquet modes coming from the cyclic variation of the parameters, e.g. our initial state is an eigenstate of the Floquet operator, rather than the initial Hamiltonian as in the usual (Thouless) pumping.

[1] The last simplification comes from manipulating the terms for which $\alpha = \alpha'$ in the second addendum as $\sum_\alpha |\langle n|\,\phi_\alpha\rangle|^2\langle\phi_\alpha|\,\partial_\kappa\phi_\alpha\rangle = -\sum_\alpha |\langle n|\,\phi_\alpha\rangle|^2\langle\partial_\kappa\phi_\alpha|\,\phi_\alpha\rangle$, where we wrote generically $\hat{\mathcal{P}} = \sum_n |n\rangle\langle n|$. This term exactly cancels out the third addendum.

This means that if $\hat{f}^\dagger_{k,\alpha}$ is the operator that creates an electron in the Floquet-Bloch mode $|\phi_{k,\alpha}\rangle$, we have (the time dependence of Floquet modes is implicit)

$$|\Psi(0)\rangle = \prod_{\alpha}^{\text{occ}} \prod_{k_n}^{\text{BZ}} \hat{f}^\dagger_{\alpha,k_n} |0\rangle \ ,$$

or, equivalently

$$\hat{\mathcal{P}} = \sum_{\alpha}^{\text{occ}} \sum_{k_n}^{\text{BZ}} |\phi_{k_n,\alpha}\rangle \langle \phi_{k_n,\alpha}| \ .$$

Inserting this in (4.11), taking the the thermodynamic limit and observing that the off-diagonal terms cancel out leads us to

$$Q(\tau) = \frac{1}{\hbar\omega} \sum_{\alpha}^{\text{occ}} \int_{-\frac{\pi}{a}}^{\frac{\pi}{a}} dk \frac{\partial \varepsilon_{\alpha,k}}{\partial k} \ . \tag{4.12}$$

This is nothing but the Hellman-Feynman theorem of Floquet systems, Eq. E.3, which states

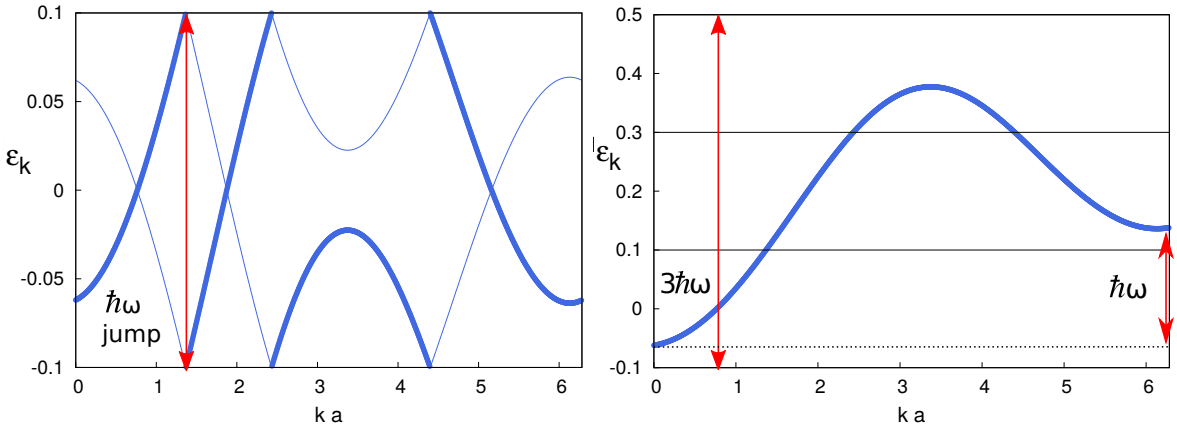

Figure 4.2.: Quasienergies of the Rice-Mele model for $\omega = 0.2J_0/\hbar$, $\delta = J_0$, $\Delta = 3J_0$. On the left: bands restricted to the first FBZ. The thick Floquet band is the populated one and has a winding number equal to 1. Notice that the sum of the winding numbers of the two bands is zero. On the right: the populated band in the extended zone (of size $3\hbar\omega$). $\varepsilon_{k=2\pi/a} - \varepsilon_{k=0} = \hbar\omega$

that the period-averaged current carried by a Floquet state is given by $\partial_k \varepsilon_{\alpha,k}/\hbar$. We have replaced the κ-derivative with a k-derivative, since in the equation for Bloch wavefunctions the Hamiltonian depend on $\kappa + k$ [2], so the two derivatives are equivalent.
Now, if the quantities $\varepsilon_{\alpha,k}$, were the *energy* bands of an ordinary insulator, the integral of Eq. (4.12) would give zero, since $\varepsilon_{\alpha,k}$ would be smooth, periodic function of k. However, *quasienergies* have a different behaviour from ordinary energies, since they have a $\hbar\omega$-periodicity. Let us consider the extended FBZ scheme and the particular case where the

[2] For instance in the continuum $\hat{H}(k,\kappa,t) = (\hat{p} + \hbar k + \hbar\kappa)^2/(2m) + \hat{V}(x,t)$

filled $\varepsilon_{\alpha,k}$ are *continuous* across the extended FBZ. In this case, the bands do not have to be a periodic function of k, since it can happen that $\varepsilon_{k=2\pi/a} - \varepsilon_{k=0} = n\hbar\omega, n \in \mathbb{Z}$. This is shown in the right panel of Fig. 4.2, where we plot the the extended zone scheme for the populated quasienergy band in the adiabatic regime of the Rice-Model, which is a prototypical tight-binding realization of the Thouless pump. Conversely, in the reduced Floquet zone scheme (left panel), the populated quasienergy band, having a total bandwidth bigger than $\hbar\omega$, will show jumps of size $\hbar\omega$. Therefore the integral (4.12) counts how many times the quasienergies cross the top-bottom border of the first FBZ (that has a size $\hbar\omega$) as k sweeps over the momentum BZ. In other words, this is the *winding number* of the quasienergies over the FBZ, e.g. the momentum quasienergy torus $[0, 2\pi] \times [-\hbar\omega/2, \hbar\omega/2]$. Thus we arrive at the conclusion that the charge pumped by a filled Floquet band that is continuous across the extended FBZ must be topologically quantized because it is given by a winding number.

4.2.1. Adiabatic driving and Thouless formula

Here we analyse the usual case [23] where the initial state is the band insulating ground state of some Hamiltonian in the thermodynamic limit that is *adiabatically* driven:

$$|\Psi(0)\rangle = \prod_{\nu}^{\text{occ}} \prod_{k}^{\text{BZ}} \hat{c}^{\dagger}_{\nu,k} \, |0\rangle \, , \tag{4.13}$$

where $\hat{c}^{\dagger}_{\nu,k}$ creates a particle in the initial Hamiltonian eigenstate, being spatially periodic Bloch orbital $u_{\nu,k}(x,t) = \langle x|\hat{c}^{\dagger}_{\nu,k}(t)|0\rangle$. For a perfect adiabatic evolution, the time-evolved many body state would differ from the initial one just for the dynamical and geometrical phases. In particular, the total Berry phase is given by the sum of the Berry phases of the single orbitals [123], so

$$|\Psi(\tau)\rangle = \prod_{\nu}^{\text{occ}} \prod_{k}^{\text{BZ}} e^{-i\int_0^\tau E_{\nu,k}(t)dt} e^{i\gamma_{\nu,k}} \hat{c}^{\dagger}_{\nu,k} \, |0\rangle \, .$$

In this adiabatic limit, the single particle orbitals are eigenstates of the evolution operator, therefore the Floquet modes of the system are the Hamiltonian eigenstates, while the quasienergies are given by the sum of dynamical and geometrical phases[3], $\varepsilon_{\alpha,k} = \varepsilon^0_{\alpha,k} + \mathcal{O}(1/\tau^2)$, with

$$\varepsilon^0_{\alpha,k} = \frac{1}{\tau}\int_0^\tau \left(E_\alpha(t) + \hbar\mathcal{A}_\alpha(t)\right) dt \, . \tag{4.14}$$

Here $\mathcal{A}^\alpha(t) = i\,\langle u_\alpha|\,\partial_t u_\alpha\rangle$ is the Berry connection of the α-th Hamiltonian eigenstate. This means that Thouless pumping is an example of what we discussed in the previous paragraph and we can apply formula (4.12). In the adiabatic limit $\tau \to \infty$ the Berry phase contribution

[3] In general quasienergies are given by the sum of a dynamical phase and an Aharonov-Anadan phase, see App. G

to the quasienergy goes to zero. We must anyway consider it because of the $\hbar\omega$ factor dividing the integral in Eq. (4.12). Indeed the Berry phase is the one that does the job:

$$\begin{aligned} Q(\tau) &= \frac{1}{\hbar}\sum_{\nu}^{\text{occ}} \int_{-\frac{\pi}{a}}^{\frac{\pi}{a}} \frac{dk}{2\pi} \int_0^\tau \left(\frac{\partial E_{\nu,k}(t)}{\partial k} + i\hbar \langle u_{\nu,k}| \partial_{tk}^2 u_{\nu,k}\rangle + i\hbar \langle \partial_\kappa u_{\nu,k}| \partial_t u_{\nu,k}\rangle \right) = \\ &= \sum_{\nu}^{\text{occ}} \int_{-\frac{\pi}{a}}^{\frac{\pi}{a}} \frac{dk}{2\pi} \int_0^\tau \underbrace{i\Big(\langle \partial_\kappa u_{\nu,k}| \partial_t u_{\nu,k}\rangle - \text{c.c.} \Big)}_{\mathcal{F}^\nu_{k,t}} , \end{aligned} \tag{4.15}$$

which is nothing but the Thouless formula [23] that we have already seen in Sec. 2.3.2. The last expression was obtained by noticing that the integral over k of the derivative of the energy bands is 0 because of their periodicity (in k) and that the term coming from integration by parts, $\int_0^\tau \partial_t \langle u_{\nu,k}| \partial_\kappa u_{\nu,k}\rangle$, is zero because the instantaneous Hamiltonian eigenstates are periodic in time. The quantization of the charge descends from the fact that $\mathcal{F}^\nu_{k,t}$ is the Berry curvature of the ν-th Bloch orbital in the quasimomentum-time torus. The winding number of quasienergies in the FBZ in the Rice-Mele model for $\Delta = 3J_0$ and $\delta_0 = J_0$ are shown in Fig. 4.2 for a frequency $\hbar\omega = 0.2J_0$. The band corresponding to the ground state wraps in the positive direction, giving a winding number $+1$, while the one corresponding to the excited eigenstates of $\hat{H}(t)$ wraps in the opposite way. This is consistent with the fact that the sum of the Chern numbers of a finite-dimensional Hamiltonian must be zero [124].

4.2.2. Generic driving frequency

The first question that arises in the analysis of non adiabatic effects in Thouless pumping is for which range of frequencies there exist a Floquet quasienergy band that wraps around the FBZ. Of course when ω becomes too large, e.g. larger than the maximum eigenvalue of $\hat{H}(t)$, the FBZ will become much larger than the quasienergy bandwidth, thus there can be no band winding. Still, this happens much sooner, actually for any frequency $\omega > 0$. To see this, we give a general argument from Ref. [122]. Since, as we said before, the sum of winding numbers is zero, there must be at least one k-point where the quasienergy bands cross if at least one quasienergy band has non vanishing winding number. However, these crossings are not stable: according to Wigner-Von Neumann theorem, a crossing of the eigenvalues of a 2×2 complex Hermitean matrix (the Floquet Hamiltonian $\hat{H}_F$) requires the tuning of at least three real parameters [122, 125]. In this case the parameters are only 2, namely the period τ and the quasimomentum k. Hence one expects, generically, that crossings turn into avoided crossings with opening of gaps for any finite τ, implying the absence of winding numbers different from 0. For this reason, quasienergy winding numbers are a *fragile* topological quantity [122]. We expect therefore deviations from perfect quantization of the pumped charge for the Floquet band under consideration as soon as $\omega > 0$.

It turns out that it is always possible to select the band whose pumped charge is close to an integer value as much as possible, e.g. that it winds around the FBZ continuously, apart

from a finite number of discontinuities that are as small as possible. In the case of Thouless pumping, this condition can be realized by ordering the Floquet states at each k-point by their period-averaged expectation energy [41]. The lowest energy band is the so called *Floquet adiabatic band* $\varepsilon_{\mathrm{ad,k}}$. Indeed, the thick band in Fig. 4.2 is actually the adiabatic band: We reproduce it here in the left panel of Fig. 4.3. In the right panel we zoom in the region around an avoided crossing in the quasienergy spectrum (solid line), comparing it to the perfect crossing occurring for the adiabatic solution $\varepsilon^0_{\alpha,k}$ of Eq. (4.14). The gap that occurs

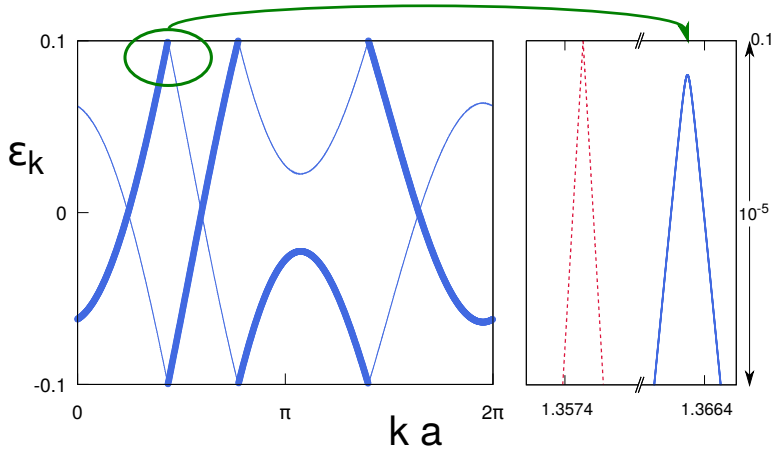

Figure 4.3.: Left: quasienergy spectrum of Rice-Mele model $\Delta_0 = 3J_0$, $\delta_0 = J_0$, $\omega = 0.2J_0/\hbar$. The thick band is the adiabatic one $\varepsilon_{\mathrm{ad},k}$. Right: (solid line) zoom of the previous figure close to the upper border of the FBZ around $ka = 1.3664$; the dashed line denotes $\varepsilon^0_{\alpha,k}$. Notice the gap of order 10^{-6}.

is exponentially small in $1/\omega$. As noticed in Ref. [119], this can be explained through the Fourier space mapping of Floquet modes. Indeed, as we discussed in Sec. 2.2, as soon as $\omega > 0$ the Floquet modes get exponentially localized on each harmonic site m. This means that there will be an exponentially small matrix element between the two originally crossing bands that gives rise to an exponentially small gap. This, in turn, reflects itself in the properties of the charge $Q_{\mathrm{ad}} = (\hbar\omega)^{-1} \int_{-\frac{\pi}{a}}^{\frac{\pi}{a}} \mathrm{d}k \frac{\partial \varepsilon_{\mathrm{ad},k}}{\partial k}$ pumped by the Floquet adiabatic band: for $\omega > 0$ it deviates from an integer by terms proportional to the sum of the gaps. This deviation is therefore exponentially small in $1/\omega$ (a similar result was found in Ref. [41] for a different model), see Fig. 4.4 and accompanying text.

Summarizing, if we were able to prepare an initial state that coincides with the Floquet adiabatic band, the deviation from perfect quantization would be exponentially small.

4.3. Charge pumped with a generic initial state

Contrary to what we have discussed so far, in any real situation, the initial state $|\Psi(0)\rangle$ of the system is *not* a Floquet state. A more reasonable assumption is to assume that the

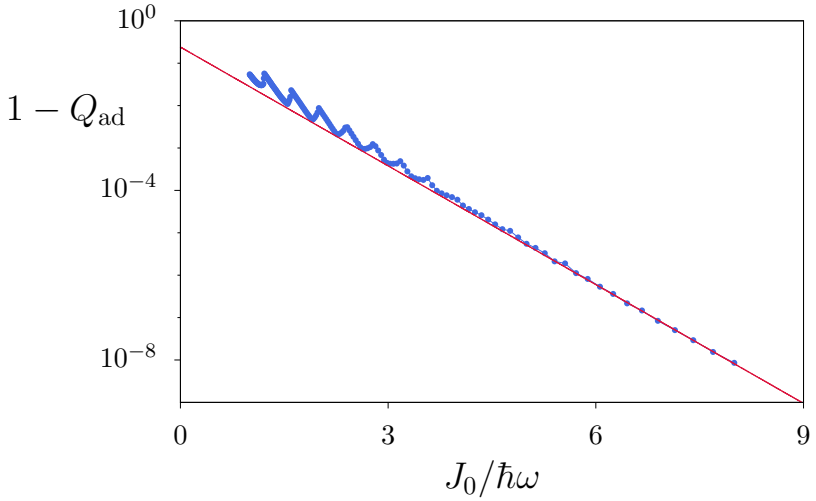

Figure 4.4.: The charge Q_{ad} pumped by the adiabatic band pumped for $\Delta_0 = 3J_0$ $\delta_0 = J_0$. The fit (red line) is $0.25 \cdot \exp(-2.15 J_0/(\hbar\omega))$.

initial stae is the ground state of the initial Hamiltonian $\hat{H}(0)$. As we have discussed in Sec. 2.1.1, after many driving cycles the expectation values of the system tend to synchronize with the driving, reaching the so called diagonal ensemble value. Since the system that we are analysing is integrable, the asymptotic value of the pumped charge, which we will refer to as *diagonal charge* for brevity, is given by

$$Q_{diag} = \frac{1}{\hbar\omega} \sum_{\alpha} \int_{-\frac{\pi}{a}}^{\frac{\pi}{a}} dk \; n_{\alpha,k} \frac{\partial \varepsilon_{\alpha,k}}{\partial k} \; . \tag{4.16}$$

Here $n_{\alpha,k}$ is the occupation of the mode $|\phi_{\alpha,k}\rangle$: $n_{\alpha,k} = \langle \Psi(0)| \hat{f}^{\dagger}_{\alpha,k} \hat{f}_{\alpha,k} |\Psi(0)\rangle$. If $|\Psi(0)\rangle$ is the ground state of a translationally invariant Hamiltonian as in Eq. (4.13),

$$n_{\alpha,k} = \sum_{\nu}^{occ} |\langle u_{\nu,k}(0)| \, \phi_{\alpha,k}(0)\rangle|^2 \; .$$

We can derive Eq. (4.16) by writing Eq. (4.11) for the case of the pumped charge after m periods. This means that we just need to replace $\hat{U}(\tau, 0)$ with $\hat{U}(m\tau, 0)$ and then apply

Floquet theorem: $\hat{U}(m\tau,0)=\left[\hat{U}(\tau,0)\right]^m$. Thus we have

$$\begin{aligned}Q(m\tau)=&\frac{1}{L}\,\mathrm{Tr}\left\{\mathcal{P}\sum_\alpha\left(\frac{m\tau}{\hbar}\partial_\kappa\varepsilon_\alpha\left|\phi_\alpha\right\rangle\left\langle\phi_\alpha\right|+\sum_{\alpha'\neq\alpha}\mathrm{e}^{\frac{i}{\hbar}(\varepsilon_{\alpha'}-\varepsilon_\alpha)m\tau}\left|\phi_{\alpha'}\right\rangle\left\langle\phi_{\alpha'}\right|\partial_\kappa\phi_\alpha\rangle\left\langle\phi_\alpha\right|\right)\right\}=\\
=&\int_{-\frac{\pi}{a}}^{\frac{\pi}{a}}\frac{dk}{2\pi}\sum_\alpha\left(\frac{m\tau}{\hbar}n_{\alpha,k}\partial_k\varepsilon_{\alpha,k}+\right.\\
&\left.+\sum_{\alpha'\neq\alpha}\mathrm{e}^{\frac{i}{\hbar}(\varepsilon_{\alpha',k}-\varepsilon_{\alpha,k})m\tau}\sum_\nu^{occ}\left\langle\phi_{\alpha,k}\right|u_{\nu,k}\rangle\left\langle u_{\nu,k}\right|\phi_{\alpha',k}\rangle\left\langle\phi_{\alpha',k}\right|\partial_k\phi_{\alpha,k}\rangle\right).\end{aligned}\tag{4.17}$$

The large oscillatory terms go to zero for $m\to\infty$ as the integral over k is performed, because of Riemann-Lebesgue lemma. In this large m limit, the charge pumped between the (m)-th and the $(m+1)$-th period will then be

$$\lim_{m\to\infty}Q((m+1)\tau)-Q(m\tau)=Q_{\mathrm{diag}}.$$

which is of course equivalent to averaging over many cycles:

$$Q_{\mathrm{diag}}\overset{m\to\infty}{=}\frac{1}{m}Q(m\tau)\,.\tag{4.18}$$

In Fig. 4.5 we compare Eq. (4.16) and (4.18), finding a good convergence already after $m\simeq 10$

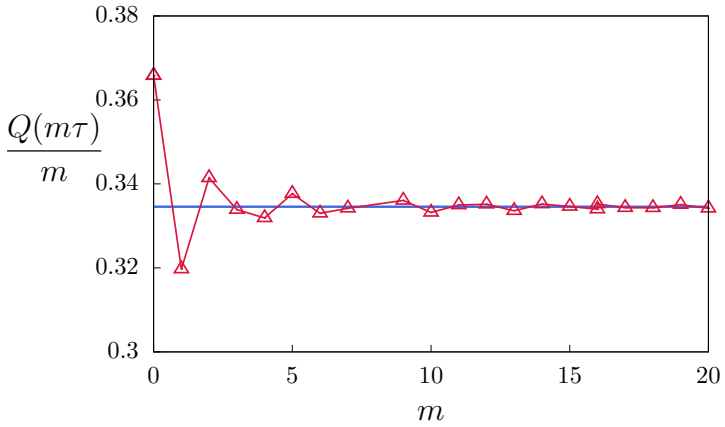

Figure 4.5.: Diagonal charge calculated with (4.16) (straight blue line) and with the average formula (4.18) as a function of the number of periods m. The Rice-Mele parameters are $\omega=5.0J_0/\hbar$, $\delta_0=J_0$, $\Delta_0=3J_0$.

pumping cycles. Formula (4.16), albeit simple, can be a starting point for investigating the behaviour at non-adiabatic frequencies. In the case of the Rice-Mele model, given the fact that $\varepsilon_0=-\varepsilon_1$, we can write it as

$$Q_{diag}=\frac{2}{\hbar\omega}\int_{-\frac{\pi}{a}}^{\frac{\pi}{a}}\mathrm{d}k\;n_{\alpha,k}\frac{\partial\varepsilon_{\alpha,k}}{\partial k}\,,\tag{4.19}$$

where α stands for one of the two bands.

4.3.1. Non-adiabatic breaking of Thouless pumping

The two ingredients of formula (4.16) are the quasienergies dispersion and their occupation function $n_{\alpha,k}$. The occupations lead to stronger deviations than the gaps, as we are going to explain now. Indeed, as shown in Fig. 4.6, the deviations grow *quadratically* in ω. To explain this we focus on the adiabatic band. In the adiabatic limit $\omega \to 0$ its occupation $n_{\mathrm{ad},k}$ is 1, but, as we discuss in detail in Appendix F, an adiabatic perturbation theory in ω can be built. The result is that in the case of the Rice-Mele model the calculation can be carried out very easily and we reproduce the final formula (EQ. (F.24)) here

$$n_{ad,k} = 1 - \frac{\hbar^2\omega^2\Delta_0^2}{64J_0^4}\left(\frac{1}{1+\delta_0^2/J_0^2+(1-\delta_0^2/J_0^2)\cos(ka)}\right)^2 + \mathcal{O}\left(\omega^3\right) . \tag{4.20}$$

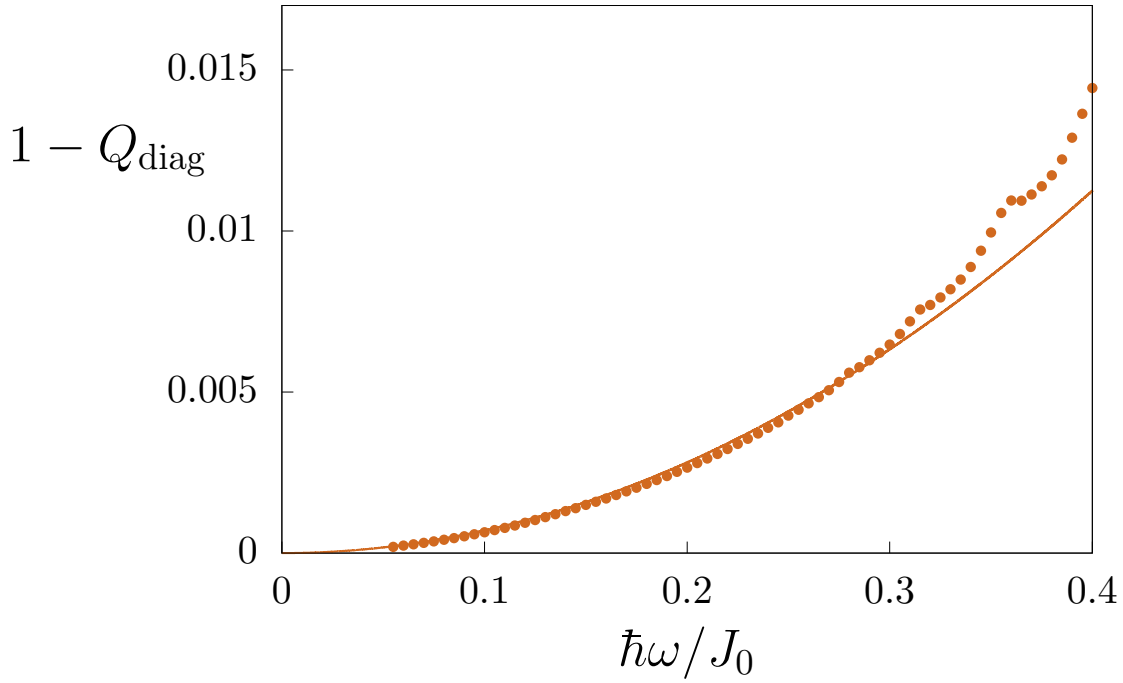

Figure 4.6.: Deviations from integer of the diagonal pumped charge Q_{diag} in the Rice-Mele model. The smooth curve is $\frac{9}{128}(\hbar\omega/J_0)^2$ and is obtained with the perturbative calculation in Eq. (4.20), described in the text. The model parameters are $\Delta_0 = 3J_0$, $\delta_0 = J_0$.

When substituted in Eq. (4.19), this expression clearly implies quadratic corrections for the diagonal charge. In the particular case where $\delta_0 = J_0$, the corrections to occupations become k-independent and Eq. (4.19) predicts that $Q_{diag} = 1 - \frac{1}{128}(\hbar\omega\Delta_0/J_0^2)^2$, since

$\int \mathrm{d}k\, \partial_k \varepsilon_{\mathrm{ad},k}/(\hbar\omega) = 1 - \mathcal{O}(\exp(-\alpha/\omega))$. This formula fits well the numerical data of Fig.4.6.

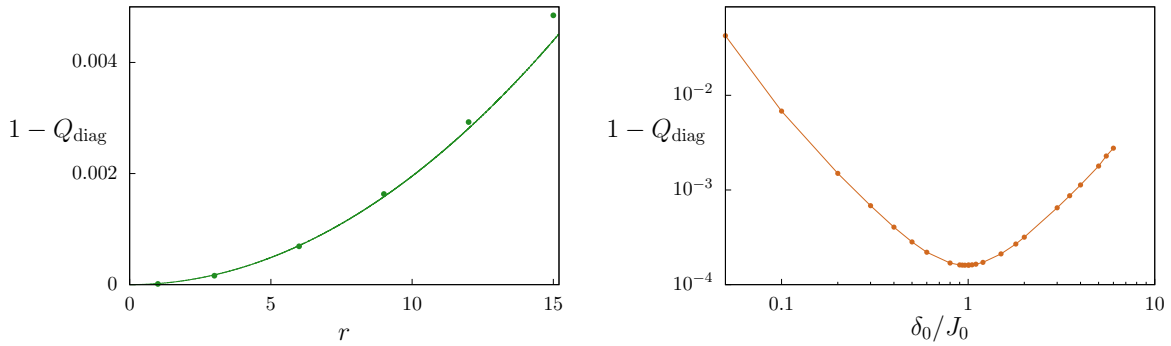

Figure 4.7.: Deviations from integer of the diagonal pumped charge Q_{diag} in the Rice-Mele model versus the model parameters for fixed frequency $\omega = 0.05 J_0/\hbar$. Left: $1 - Q_{\mathrm{diag}}$ for $\delta_0 = J_0$ as a function of the aspect ratio $r = \Delta_0/\delta_0$. The smooth curve is $\frac{1}{128}(\hbar\omega/J_0)^2\, r^2$ and it was calculated with the first order perturbative calculation of the main text. Right: $1 - Q_{\mathrm{diag}}$ for $r = 3$ as a function of δ_0: The minimum sits at $\delta_0 = J_0$.

It is manifest from Eq. (4.20) that the non-adiabatic corrections can be more or less pronounced, depending on the parameters of the driving (Δ_0, δ_0). Figure 4.7 illustrates how the deviations from quantization for a fixed value of frequency, $\omega = 0.05 J_0/\hbar$, depend on (Δ_0, δ_0). In the left plot, we fix the value $\delta_0 = J_0$ as before and we vary the dimensionless ratio $r = \Delta_0/\delta_0$. According to Eq. (4.20), the deviations increase with r as $\frac{\hbar^2\omega^2}{128 J_0^2} r^2$. The agreement with the numerical data for this choice of ω is very good up to $r \lesssim 12$, where higher orders of the perturbation theory (F.16) become relevant. Conversely, in the right plot of Fig. 4.7 we fix $r = \Delta_0/\delta_0 = 3$ and we consider the dependence on δ_0/J_0: we see that the deviations have a minimum around $\delta_0 = J_0$. This is indeed compatible with formula (F.25), which tells that the deviations from 1 of $n_{\mathrm{ad,k}}$ show a minimum at $\delta_0 = J_0$ for fixed r, when averaged over k. Summarizing, deviations should be more noticeable for paths in parameters space that are flattened on the Δ axis and far from the point $\delta_0 = J_0$. Notice that a small δ_0/J_0 corresponds to a weak pumping regime: quite surprisingly, this seems to be one of the regimes where the deviations from adiabaticity are stronger.

We now address the issue of non-adiabatic deviations for a finite number of pumping cycles. Diagonal expectation values are indeed attained after some transient and become exact only after an infinite number of pumping cycles. In Fig. 4.8 we plot the charge pumped after a single pumping cycle, $Q(\tau)$, as a function of ω: we see that $Q(\tau)$ exhibits remarkable beating-like oscillations on top of the overall quadratic decrease of Q_{diag} that grow faster and faster as $\omega \to 0$. The theoretical prediction, according to a theorem of Ref. [122] that we discuss in appendix H, is that the finite-time pumped charge must have an essential singularity in $\omega = 0$. The behaviour that we find is indeed compatible with the presence of non-analyticities of the

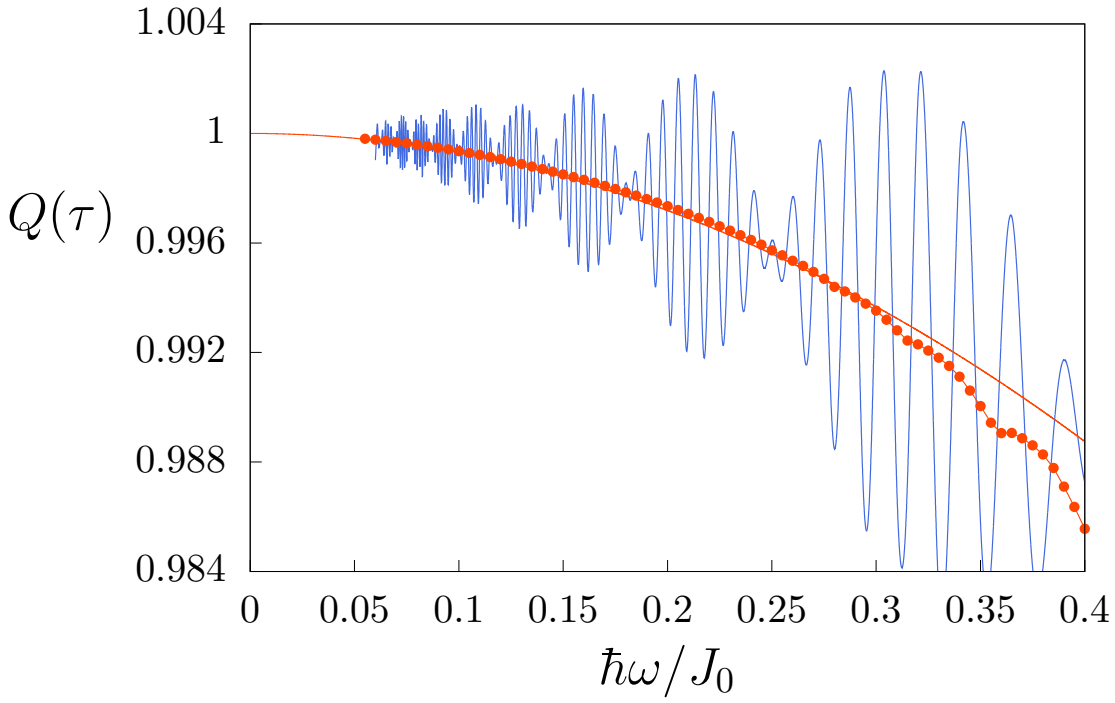

Figure 4.8.: Smooth (blue) line: the charge pumped after the first period, $Q(\tau)$, as a function of the driving frequency ω. The (red) line with dots is the corresponding diagonal ensemble value Q_{diag} reported in Fig. 4.6. The Rice-Mele model parameters are $\Delta_0 = 3J_0$, $\delta_0 = J_0$.

kind of $\sin(c/\omega)$. The theorem was originally formulated for the Integer Quantum Hall effect: there the current, seen as a function of the electric field E, has an essentially singularity in $E = 0$. This should be of the kind $\exp(-c/E)$, which results in exponentially small corrections to the Kubo formula at zero field.

4.3.2. Behaviour at higher frequencies

Through the analysis of the diagonal charge we can study Thouless pumping also far from the adiabatic region. In Fig. 4.9 we plot Q_{diag} in a larger range of frequencies. We should expect a decrease towards 0 as the frequency is increased because of the $1/\omega$ factor in front of Eq. (4.16) and the Magnus expansion that dictates the independence of quasienergies and occupations from ω at lowest order in $1/\omega$. The decrease is not monotonic, because of sudden dips appearing along the curve. This behaviour of the observables was already linked in other works [54] to the appearance of resonances in the Floquet spectrum and this is indeed what we find: each dip is associated with a specific part of the two bands coming close at $\pm\hbar\omega/2$ (the two bands have particle-hole symmetry). Fig. 4.10 helps understanding this process. In panel **(a)**, we plot the quasienergy bands for a frequency which is a bit smaller than the ones

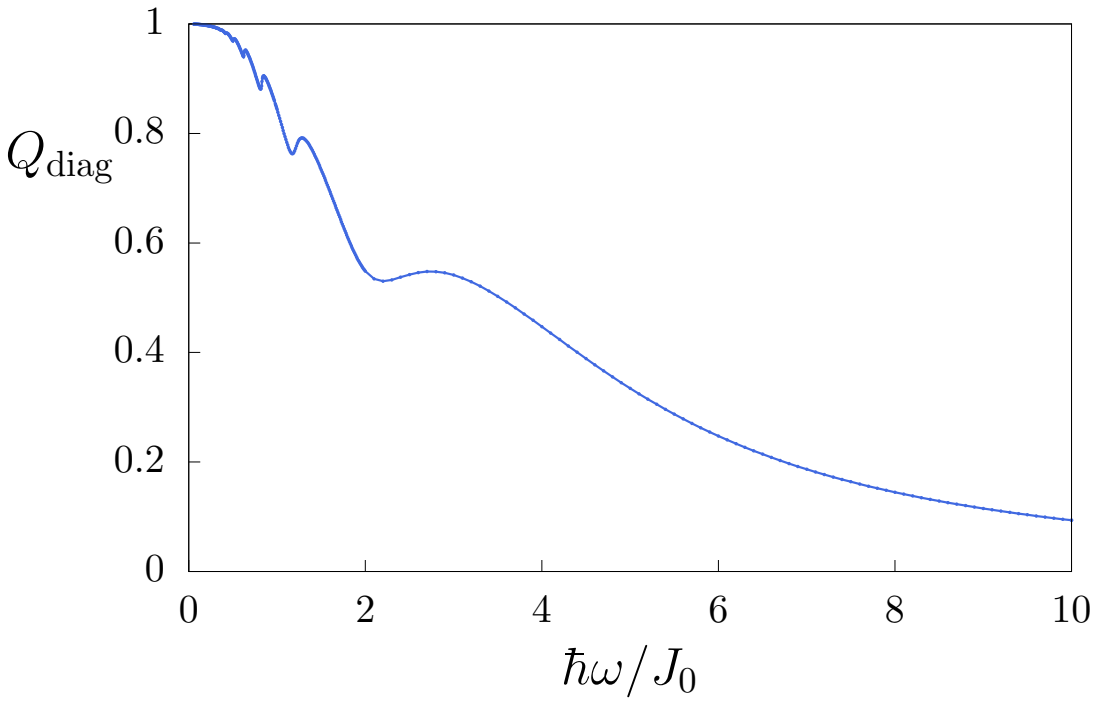

Figure 4.9.: Diagonal charge for $\Delta_0 = 3J_0$, $\delta = J_0$.

where one of such oscillations happen. The thicker band, which is the most populated one, tends to go up as ω increases, while the other goes of course down: when they come close to the borders of the FBZ the levels will start to interact giving rise to avoided crossings in a large region of k-space, as shown in panel **(b)**, where the ω corresponds to the one of the local minimum. Here the two bands are flattened, which means they carry less current and their occupations are scrambled. In panel **(c)**, ω has become big enough to make the two bands cross the FBZ border and get separated: this point corresponds to the local maximum. For larger frequencies the diagonal charge decrease monotonically until the next resonance happen. These oscillations become apparent only for high enough ω because, as we have seen, gaps grow exponentially in $1/\omega$.

When ω becomes very large, Q_{diag} starts to decrease monotonically. The plot in Fig. 4.11 shows that in the end, Q_{diag} goes to zero as $1/\omega^2$, which should be expected on the basis of the Magnus expansion of App. B. Indeed $\hat{H}_F = \hat{H}_0 + \mathcal{O}(1/\omega)$, where $\hat{H}_0$ is nothing but the time average of $\hat{H}_{\text{RM}}(t)$ of Eq. (4.1). Since $\hat{H}_{\text{RM}}(t)$ is time-reversal symmetric at any instant of time, so will be $\hat{H}_0$ and, consequently, $\hat{H}_0(k) = \hat{H}_0^*(-k)$. For this reason, the occupations will be even functions of k, while the derivatives $\partial_k \varepsilon_{\alpha,k}$ will be odd, making vanish the integral of Eq. (4.16) at lowest order. Therefore the first non-zero contribution must come from the $1/\omega$ term of the $\hat{H}_F$ expansion, that breaks time-reversal symmetry, as we have checked in App. F.2.2. Because of the $1/\hbar\omega$ factor in Eq. (4.16) we recover the ω^{-2} decrease.

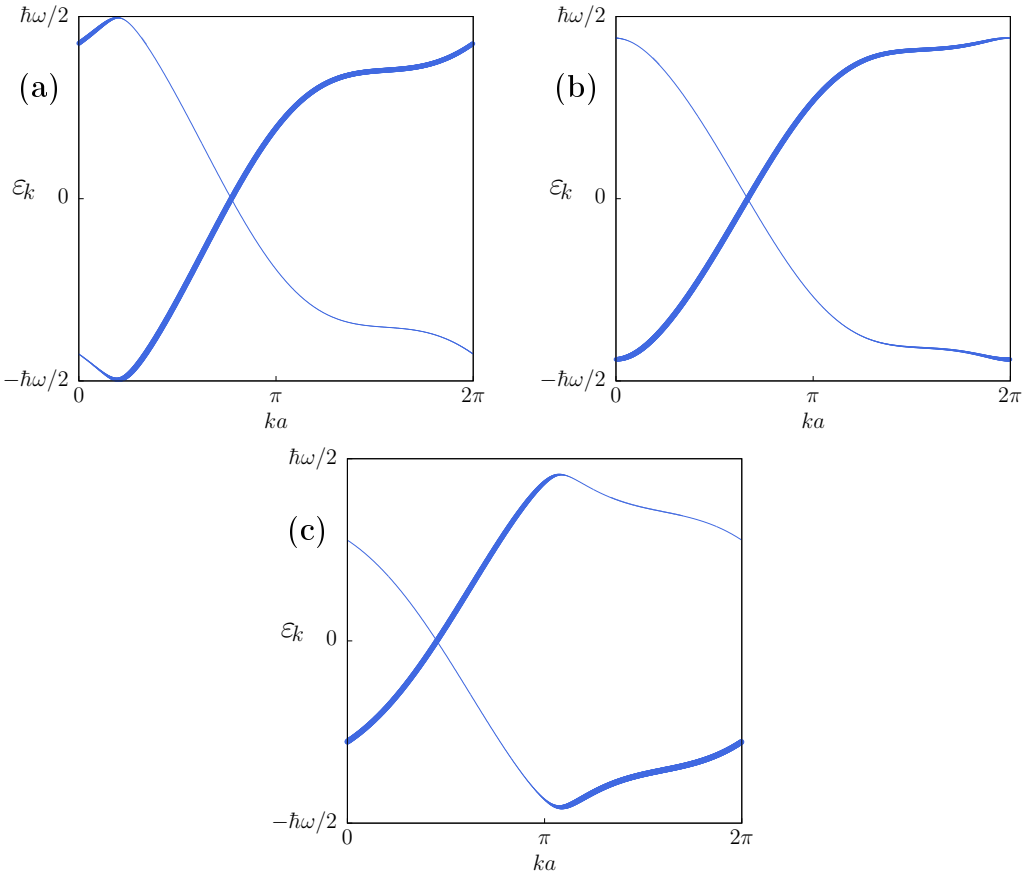

Figure 4.10.: Quasienergy spectra for various frequencies close to an oscillation of Q_{diag} in ω for $\delta = J_0$, $\Delta_0 = 3J_0$. The line thickness is proportional to the occupation. **(a)**: $\omega = 1.12J_0/\hbar$. The levels in the right part of the BZ do not interact. **(b)**: $\omega = 1.17J_0/\hbar$, a local minimum of Q_{diag} as a function of ω. The gap at $\pm\hbar\omega/2$ for $k \in [\pi, 2\pi]$ has become smaller: the levels interact and the related avoided crossings in the right part of the BZ have provoked a flattening of the bands and a scrambling of the occupations. **(c)**: $\omega = 1.28J_0/\hbar$, a local maximum of Q_{diag} as a function of ω. The bands on the right have exchanged and they do not interact any more around the gap at $\varepsilon = \pm\hbar\omega/2$.

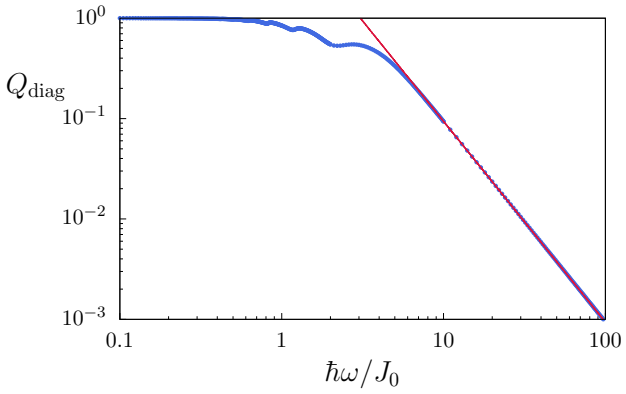

Figure 4.11.: A logarithmic plot version of Fig.4.9. The smooth (red line) is $Q_{\rm diag} = 9.3J_0^2/(\hbar\omega)^2$.

4.4. Effects of a thermal initial state

Another source of deviation from perfect quantization is finite temperature. In this section we want to disentangle this contribution from the non-adiabatic one. In the framework of ultracold atoms experiments, it is reasonable to consider the dynamics to be coherent and the initial density matrix $\hat{\rho}(t=0)$ to be a thermal. If $\beta = 1/K_BT$ we have

$$\hat{\rho}(0) \equiv \hat{\rho}_T = \frac{1}{Z}\sum_n e^{-\beta E_n(0)}\hat{\mathcal{P}}_n(0), \tag{4.21}$$

where $E_n(0)$ and $\mathcal{P}_n(0)$ are respectively the Hamiltonian eigenvalues and eigenprojectors at time $t = 0$ and $Z = \sum_n e^{-\beta E_n(0)}$. The density matrix will then evolve according to the Von-Neumann equation [126], or equivalently as

$$\hat{\rho}(t) = \hat{U}(t,0)\hat{\rho}(0)\hat{U}^\dagger(t,0). \tag{4.22}$$

Expectation values are given by $\langle\hat{O}\rangle(t) = \mathrm{Tr}\left(\rho(t)\hat{O}(t)\right)$. Clearly, for translationally invariant models the density matrix factorizes as $\hat{\rho} = \prod_k \hat{\rho}_k$. If we substitute $\hat{\rho(0)}$ in Eq. (4.10) for the pure state projector $\mathcal{P}$ and repeat the steps of Eq. (4.17), the diagonal charge gets modified only through the replacement of ground-state occupations $n_{\alpha,k}$ with thermal ones $n^T_{\alpha,k}$

$$Q^T_{diag} = \frac{1}{\hbar\omega}\sum_\alpha \int_{-\frac{\pi}{a}}^{+\frac{\pi}{a}} dk\, n^T_{\alpha,k}\frac{\partial\varepsilon_{\alpha,k}}{\partial k}, \tag{4.23}$$

where

$$n^T_{\alpha,k} = \mathrm{Tr}(\hat{\rho}_{T,k}\hat{f}^\dagger_{\alpha,k}\hat{f}_{\alpha,k}) = \frac{1}{Z_k}\sum_n e^{-\beta E_{n,k}(0)}\left|\langle u_{n,k}|\,\phi_{\alpha,k}\rangle\right|^2. \tag{4.24}$$

and Z_k is the partition function at a given k-point. We consider now the case of the Rice-Mele model, e.g. two bands with $E_{0,k}(0) = -E_{1,k}(0)$ and $\varepsilon_{0,k} = -\varepsilon_{1,k}$. This means that $Z_k = 2\cosh(\beta E_{n,k})$, implying

$$n^T_{\alpha,k} = \tanh(-\beta E_{0,k}(0)) n_{\alpha,k} + \frac{e^{\beta E_{0,k}(0)}}{2\cosh(-\beta E_{0,k}(0))} \tag{4.25}$$

and

$$Q^T_{diag} = \frac{2}{\hbar\omega} \int_{-\frac{\pi}{a}}^{+\frac{\pi}{a}} dk \left(\tanh(-\beta E_{0,k}(0)) n_{\alpha,k} + \frac{e^{\beta E_{0,k}(0)}}{2\cosh(-\beta E_{0,k}(0))} \right) \frac{\partial \varepsilon_{\alpha,k}}{\partial k} \ , \tag{4.26}$$

where α stands for one of the two bands. Comparing this equation with (4.19), we notice that the influence of the initial thermal state resides in the $\tanh(-\beta E_{0,k})$ factor, which multiplies the zero temperature integrand of the diagonal charge at each $k-$point. The ω^2 behaviour of the deviations is preserved, but can be hidden by thermal effects. These indeed are exponentially small when the temperature T is much smaller than the initial gap. In the case where $\delta_0 = J_0$, $E_{0,k}(0) = -2J_0$ is k-independent and thermal effects only amount to multiplying the $T = 0$ result by $\tanh(2\beta J_0)$. At first order in ω is

$$Q^T_{diag} = \tanh(2\beta J_0) \cdot \left(1 - \frac{\hbar^2 \Delta_0^2}{128 J_0^4} \omega^2 + \mathcal{O}(\omega^3) \right) \ . \tag{4.27}$$

Thus when $K_B T \approx J_0$ thermal effects dominate over the non-adiabatic ones. This is confirmed by the left plot in Fig. 4.12. We compare this simple case to a generic one with $\delta_0 = 1.5 J_0$ and $\Delta_0 = 9 J_0$. In this case $E_{0,k}(0)$ goes from $-2J_0$ to $-3J_0$ as k varies. Again thermal effects dominate over non-adiabatic ones when $K_B T$ is of the order of the gap.

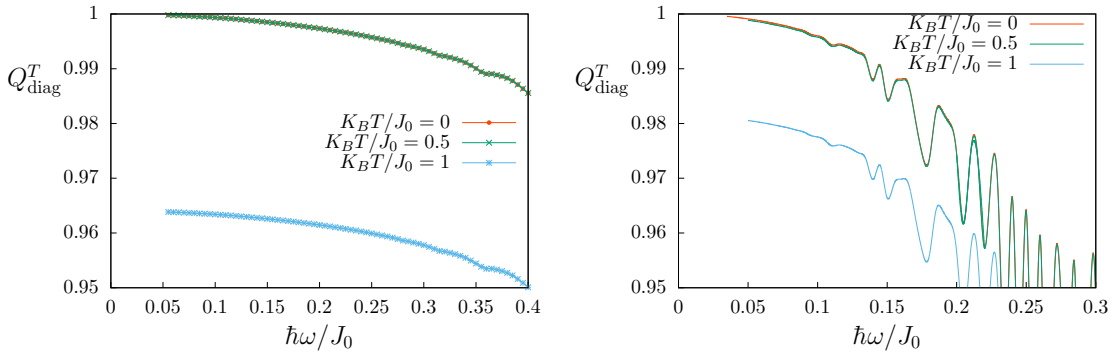

Figure 4.12.: $Q_{\rm diag}$ as a function of $\hbar\omega/J_0$ model versus for various initial temperatures. Left: The simple case $\delta_0 = J_0$, $\Delta = 3J_0$. The $T = 0$ and $T = 0.5 J_0/K_B$ practically coincide. Right: Same plot for $\delta_0 = 1.5 J_0$, $\Delta = 9 J_0$.

4.5. Dynamical and geometrical contributions to pumped charge

The study of the diagonal pumped charge makes it possible to separate the transported charge into two contributions, one dynamical and one geometrical. This comes from the fact, explained in detail in appendix G, that quasienergies are given by the sum of the dynamical phase and the geometrical Aharonov-Anandan phase, $\varepsilon_\alpha = \hbar(\zeta_\alpha - \gamma_\alpha)/\tau$. Substituting in Eq. (4.16) we get

$$Q_{diag} = Q^d_{diag} + Q^g_{diag} \,, \tag{4.28}$$

where

$$\begin{aligned} Q^d_{diag} =& \sum_\alpha \frac{1}{2\pi} \int_{-\frac{\pi}{a}}^{+\frac{\pi}{a}} \mathrm{d}k \; n_{\alpha,k} \frac{\partial \zeta_{\alpha,k}}{\partial k} = \\ =& \frac{1}{\hbar} \sum_\alpha \frac{1}{2\pi} \int_{-\frac{\pi}{a}}^{+\frac{\pi}{a}} \mathrm{d}k \; n_{\alpha,k} \, \partial_k \int_0^\tau \langle \phi_{\alpha,k}(t)| \, \hat{H}(t) \, |\phi_{\alpha,k}(t)\rangle \, \mathrm{d}t \,. \end{aligned} \tag{4.29a}$$

$$\begin{aligned} Q^g_{diag} =& - \sum_\alpha \frac{1}{2\pi} \int_{-\frac{\pi}{a}}^{+\frac{\pi}{a}} \mathrm{d}k \; n_{\alpha,k} \frac{\partial \gamma_{\alpha,k}}{\partial k} = \\ =& - \sum_\alpha \frac{1}{2\pi} \int_{-\frac{\pi}{a}}^{+\frac{\pi}{a}} \mathrm{d}k \; n_{\alpha,k} \, \partial_k \int_0^\tau i \, \langle \phi_\alpha(t)| \, \partial_t \phi_\alpha(t)\rangle \mathrm{d}t \,. \end{aligned} \tag{4.29b}$$

As we have seen in the Sec. 4.2.1, this separation is capable of reproducing Thouless formula in the adiabatic limit: the dynamical charge vanishes and the geometrical one is an integer, corresponding to the Chern number of the ground state of $\hat{H}$ in k, t space. For a generic ω the numerical computation of Eq. (4.29a) and (4.29b) can be very difficult due to the wild behaviour of $\gamma_{\alpha,k}$ and $\zeta_{\alpha,k}$ and as k varies. We show in Fig. 4.13 some results for the geometrical and dynamical components close to the adiabatic limit and at high frequency. As expected, close to $\omega \to 0$ the geometrical contribution is predominant and both components vary quadratically. Quite surprisingly, charge transport is dominated by geometrical effects also at high-frequencies ($\omega \gtrsim 10 J_0/\hbar$): the dynamical diagonal charge vanishes as $1/\omega^4$, rather than $1/\omega^2$ as the geometrical one does.

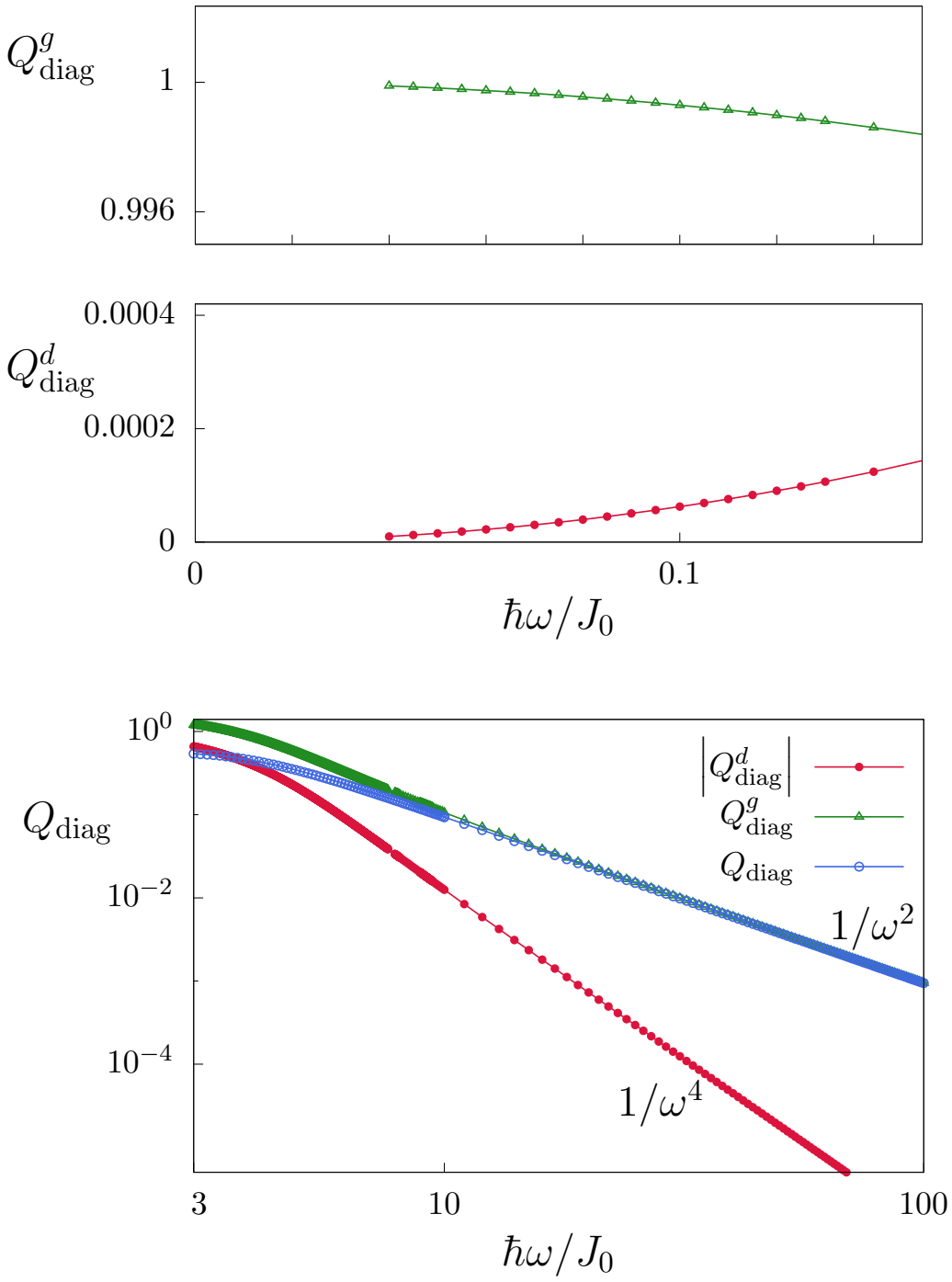

Figure 4.13.: Top: Geometric and dynamical diagonal pumped charge in the Rice-Mele model for $\delta = 1.0\ J_0$, $\Delta = 3.0\ J_0$, calculated with formulas Eq. (4.29a) and (4.29b) close to the adiabatic limit. Both curves vary quadratically. Down: Geometric (green triangles) and absolute value of dynamical (filled red dots) components and total diagonal pumped charge (empty blue dots) for the same parameters of the plot above, but at high frequencies. The geometrical part, decreasing as $1/\omega^2$, dominates over the dynamical one, which decreases as $1/\omega^4$.

4.6. Conclusions

We have studied what happens to the quantization of the Thouless pumped charge out of the perfect adiabatic limit. Within a Floquet framework, we have found that this transport phenomenon is not robust with respect to non-adiabatic effects despite its topological nature. Preparing the system in a realistic state and waiting for relaxation to the diagonal ensemble, we see that the pumped charge deviates from the quantized value in a polynomial fashion, i.e. quadratically in the driving frequency. This observation is, we believe, model-independent, since it requires only that the initial state is the ground state (or any other eigenstate) of the initial Hamiltonian. The fact that a topologically robust property is ruined by the occupation factors of the Floquet bands is in line with what was found in a resonantly driven graphene layer in Sec. 3.5. The ω^2-corrections appear also before the relaxation to the diagonal ensemble, but they are apparently hidden under a non-analytic behaviour. The possible hiding of the polynomial corrections by thermal effects was discussed in Sec. 4.4. We have then analysed the pumped charge far from the adiabatic limit. As ω increases, there is a region where Q_{diag} exhibits oscillations as a function of ω on top of an overall decrease because of quasienergy resonances, and then a final smooth decrease to 0 as $1/\omega^2$. Our findings are of experimental interest because the deviation from adiabaticity we predict should be in principle observable in ultracold atoms experiments (for instance with the methods used in [27, 28]). Finally we have discussed how the diagonal charge can be split into a dynamical component and a geometrical one. Our numerical results, show that at high frequencies the pumping is dominated by the geometrical contribution. It would be interesting to device a method to measure the two components in experiments.

5. Conclusions and perspectives

Periodically driven quantum systems can show remarkable topological features. In the present thesis, within the framework of Floquet theory, we have analysed the dynamics of such systems to find what is the real impact of topology. In the prototypical models that we studied, we have found that there exists an "optimal" Slater determinant of Floquet modes that exploits as much as possible the effects of topology, but it is generally difficult to realise in a closed quantum system.

In Chapter 3 we have dealt with a minimal model for a graphene strip irradiated by circularly polarised electric field, a standard model of a Floquet Chern insulator. It is of great importance because its Floquet Hamiltonian at high driving frequencies is equivalent to the celebrated Haldane model [74] for a Chern Insulator and it has been experimentally realised with ultracold atoms [35]. In this case, we wanted to understand to what degree it is possible to adiabatically prepare the *Floquet ground state* by slowly ramping the amplitude of the periodic perturbation. We have found that while the bulk states get populated in a controlled way, there are always unavoidable excitations of edge states. These excitations manifest themselves through nonequilibrium currents that, upon time averaging, flow solely at the edges. Thus in the end the system finds itself in a situation where its bulk is in a topological phase, while there are non-adiabatic defects on its boundaries. We believe that this mechanism is quite general and should apply whenever a quantum system, starting in the ground state of an Hamiltonian, undergoes (dynamically) a topological phase transition. In the case where the frequency is smaller then the unperturbed energy bandwidth, there can be Floquet ground states with high Chern numbers and no analogue in static systems: an adiabatic preparation with a ramp of the driving amplitude is however impossible as we have shown in Sec. 3.5.

In Chapter 4 we have instead tackled the problem of non-adiabatic effects in Thouless pumping, by studying the Rice-Mele model. Floquet theory facilitates the study of the long-time limit of Thouless pumping for a finite driving frequency ω. Our findings show that the quantization of transported charge is not robust with respect to non-adiabatic effects: it displays corrections that are polynomial in ω, quadratic at lowest order, when the system is initially prepared in the initial ground state. Indeed, for each ω there is a Slater determinant of Flouet states that is intrinsically robust to non-adiabaticities, showing corrections that are exponentialy small in ω but this is practically hard to prepare. We have then extended the study of the (long-time) pumped charge to frequencies far from the adiabatic region. We have

found, after the low-ω regime described before, oscillations in ω due to Floquet quasienergy resonances and then a decrease towards zero as $1/\omega^2$. These behaviours, we believe, are not specific of the Rice-Mele model and could be observed in ultracold atomic gases.

Concerning future work, there are some issues that we would like to mention.

First of all, in this thesis we treated only integrable models, but it is fundamentally important to address the role of interactions in topological Floquet systems. As we briefly discussed in Sec. 2.1.1 any isolated non-integrable periodically driven quantum system will eventually reach a trivial infinite temperature state. Therefore if we simply add interactions to our Floquet models, topological effects can only be seen in a transient, which usually goes under the name of *prethermalisation*. In some regimes the time scale over which the system is not trivial and can display topological features can be exponentially long in the parameters of the system [127, 128]. In our driven graphene model this should happen in the high-frequency regime. Interacting Rice-Mele model with partial filling of the initial lower band has been studied in Ref. [119], where it was found that in some regimes there is an exponentially long time where there is non-trivial particle transport. Apart from the thermalisation problem, it is not understood how the presence of interactions affects the preparation of topological Floquet states, e.g. if they facilitate or obstruct the adiabatic preparation of a Floquet Chern insulator or whether non-adiabatic effects in Thouless pumping are enhanced or suppressed. We have to mention however that the infinite temperature state can be avoided if the system is in a many-body localized phase [129] which usually appears in disordered systems. Recently the study of Floquet topological phases in many-body localized systems has begun to attract some interest [130, 131, 132]. The study of the dynamics in these very peculiar Floquet phases is still in its infancy.

Finally, the impact of dissipation in topological Floquet systems has been the subject of many studies[133, 134, 135, 136, 137], but the role of bosonic or fermionic baths in the stabilisation of topological Floquet phases is not completely understood. For example, it would be interesting to clarify whether edge states in Floquet topological insulators are robust after being coupled to external leads [138] and whether the nonequilibrium excitation mechanism that we have found breaks down in this setting. Another interesting issue is whether the presence of a bosonic bath can improve the preparation of the Floquet ground state when the driving frequency is resonant and higher Chern numbers come into play. The robustness of Thouless pumping in a dissipative environment is instead a completely unexplored question and the interplay between non-adiabatic effects and dissipation is a very important issue for experiments in solid state systems.

A. Floquet adiabatic perturbation theory and Hall conductivity

In this section we derive an expression for the conductivity in the case of a time-periodic system as it is done in Ref. [29]. The approach is very similar to the one by Thouless [94] for the equilibrium case, which is based on adiabatic perturbation theory.

A.1. Floquet adiabatic perturbation theory

We suppose now that at $t = 0$ a slowly varying term $\mathbf{A_E}(t)$ is added to our time-periodic Hamiltonian, e.g. an external perturbation acting on our system is slowly turned on. Clearly the system won't be strictly periodic any more, but if $\mathbf{A_E}(t)$ can be considered to be approximately constant during one period, we can still use the Floquet approach. This consideration leads us to the so called *two-times formalism* [139], e.g. we consider the two time scales to be two different parameters of $\hat{\mathcal{K}}$. In particular, if t is the "slow" time scale and t the fast one, $\hat{\mathcal{K}}$ will depend explicitly on t and implicitly on t through $\mathbf{A_E}(t)$. For a generic state $|\Psi(\mathbf{A_E}(t'), t)\rangle$ the Schrödinger equation reads

$$\hat{\mathcal{K}}\left(\mathbf{A_E}\left(t'\right), t\right)\left|\Psi\left(\mathbf{A_E}\left(t'\right), t\right)\right\rangle = i\hbar\frac{\partial}{\partial t'}\left|\Psi\left(\mathbf{A_E}\left(t'\right), t\right)\right\rangle \ . \tag{A.1}$$

Until now we have not performed any approximation. For any fixed value of $\mathbf{A_E}$ the Floquet theorem holds and we can find N Floquet states solutions to the Schrödinger equation

$$|\psi_\alpha(\mathbf{A_E}, t)\rangle = e^{-i\epsilon_{\alpha,\mathbf{k}}(\mathbf{A_E})t/\hbar}\,|\phi_\alpha(\mathbf{A_E}, t)\rangle \ . \tag{A.2}$$

Since they constitute a basis we can write generically

$$\left|\Psi\left(\mathbf{A_E}\left(t'\right), t\right)\right\rangle = \sum_\alpha c_\alpha\left(\mathbf{A_E}\left(t'\right)\right) e^{-(i/\hbar)\int_0^{t'}\varepsilon_{\alpha,\mathbf{k}}(\mathbf{A_E}(t''))dt''}\left|\phi_\alpha\left(\mathbf{A_E}\left(t'\right), t\right)\right\rangle \ . \tag{A.3}$$

The coefficients are defined as [1]

$$c_\alpha\left(A_\mathbf{E}\left(t'\right)\right) = \langle\phi_\alpha\left(A_\mathbf{E}\left(t'\right), t\right)|\Psi\left(A_\mathbf{E}\left(t'\right), t\right)\rangle \ . \tag{A.4}$$

[1] Floquet modes are an orthonormal basis at each instant of time; so in the absence of any non-periodic perturbations, the coefficients would be time-independent.

At this point we can find an expression for the c_α's at first order in $\dot{A}_{\mathbf{E}}$ in terms of the Floquet modes and the quasienergies. The calculation follows exactly the same steps of the non-driven case, provided that stationary eigenstates are replaced by Floquet modes through Eq. (2.6), the time-dependent Schrödinger equation is now Eq. (A.1), quasienergies take the place of energies and the scalar product is the extended one of Eq. (2.7). Inserting Eq. (A.3) into the Schrödinger equation and multiplying on the left by some $\langle\phi_\beta|$, we get [2]

$$\dot{c}_\beta\left(t'\right) = -\sum_\alpha e^{(i/\hbar)\int_0^{t'}\left(\varepsilon_\beta(t'')-\varepsilon_\alpha(t'')\right)dt''} c_\alpha\left(t'\right)\langle\langle\phi_\beta\left(t';t\right)|\frac{\partial}{\partial t'}\phi_\alpha\left(t';t\right)\rangle\rangle\ , \tag{A.5}$$

where we have omitted $\mathbf{A_E}$ and written directly the t'-dependence. Analogously to the static case, a "Berry phase" term can be defined as $\gamma_\beta\left(t'\right) = \int_0^{t'} dt''\langle\langle\phi_\beta(t'';t)|\frac{\partial}{\partial t''}\phi_\beta(t'';t)\rangle\rangle$. Then

$$\dot{C}_\beta\left(t'\right) = \sum_{\alpha\neq\beta} F_{\beta\alpha} e^{(i/\hbar)\int_0^{t'}\left(\varepsilon_\beta(t'')-\varepsilon_\alpha(t'')\right)dt''} C_\alpha\left(t'\right)\ , \tag{A.6}$$

with the definitions $C_\beta(t') = e^{i\gamma_\beta(t')}c_\beta(t')$ and

$$F_{\beta\alpha}\left(t'\right) = -e^{i\left(\gamma_\beta(t')-\gamma_\alpha(t')\right)}\langle\langle\phi_\beta\left(\mathbf{A_E}(t')\right)|\frac{\partial}{\partial\mathbf{A_E}}\phi_\alpha\left(\mathbf{A_E}(t')\right)\rangle\rangle\ \dot{\mathbf{A}}_{\mathbf{E}}(t')\ . \tag{A.7}$$

If our initial condition is $c_\alpha(0) = \delta_{\alpha 0}$, where "0" denotes an arbitary Floquet state we are willing to describe, then

$$\dot{C}_\beta\left(t'\right) = \left(1-\delta_{\beta 0}\right) e^{(i/\hbar)\int_0^{t'}\left(\varepsilon_\beta(t'')-\varepsilon_0(t'')\right)dt''}\ F_{\beta 0}\left(t'\right)\ . \tag{A.8}$$

Integration by parts gives us the final expression or the first order correction in $\dot{\mathbf{A}}_{\mathbf{E}}$ to perfect adiabatic dynamics in Floquet systems

$$C_\beta\left(t'\right) \simeq -i\hbar\left(1-\delta_{\beta 0}\right)\frac{e^{(i/\hbar)\int_0^{t'}\left(\varepsilon_\beta(t'')-\varepsilon_0(t'')\right)dt''}}{\varepsilon_\beta\left(t'\right)-\varepsilon_0(t')}\ F_{\beta 0}\left(t'\right)\ , \tag{A.9}$$

$$\begin{aligned}\left|\Psi\left(t';t\right)\right\rangle =& e^{(i/\hbar)\gamma_0(\mathbf{A_E}(t'))}e^{-(i/\hbar)\int_0^{t'}\varepsilon_0(\mathbf{A_E}(t''))dt''}\Bigg[\left|\phi_0\left(\mathbf{A_E}\left(t'\right);t\right)\right\rangle + i\hbar\sum_{\beta\neq 0}\left|\phi_\beta\left(\mathbf{A_E}\left(t'\right);t\right)\right\rangle\times\\ &\times\frac{\langle\langle\phi_\beta\left(\mathbf{A_E}\left(t'\right);t\right)|\frac{\partial}{\partial\mathbf{A_E}}\phi_0\left(\mathbf{A_E}\left(t'\right);t\right)\rangle\rangle}{\varepsilon_\beta\left(\mathbf{A_E}\left(t'\right)\right)-\varepsilon_0\left(\mathbf{A_E}\left(t'\right)\right)}\cdot\frac{\partial}{\partial t'}\mathbf{A_E}\left(t'\right)\Bigg]\Bigg|_{t'=t}\end{aligned} \tag{A.10}$$

[2] Here we have used the fact that the coefficients are approximately constant during one period and therefore are not affected by the time average of the inner product.

This means that if our initial state is one of the N Floquet solutions ((A.2)) of the Schrödinger equation (e.g. for some fixed value of $\mathbf{A_E}$) it will evolve as

$$|\psi_\alpha(\mathbf{A_E},t)\rangle \to |\psi_\alpha(\mathbf{A_E}(t),t)\rangle = e^{i\gamma_\alpha(t)}e^{-i\int_0^t \varepsilon_\alpha(t')dt'}\Bigg[|\phi_\alpha(\mathbf{A_E}(t);t)\rangle + i\hbar\sum_{\beta\neq\alpha}|\phi_\beta(\mathbf{A_E}(t);t)\rangle \times \\ \times\frac{\langle\langle\phi_\beta(\mathbf{A_E}(t);t)|\dfrac{\partial}{\partial\mathbf{A_E}}\phi_\alpha(\mathbf{A_E}(t);t)\rangle\rangle}{\varepsilon_\beta(\mathbf{A_E}(t))-\varepsilon_\alpha(\mathbf{A}_E(t))}\dot{A}_\mathbf{E}(t)\Bigg]\,. \tag{A.11}$$

Through the application of perturbation theory in the extended Hilbert space, we can resort to the textbook trick used in writing Berry curvature[3]

$$\left\langle\left\langle\phi_\beta\middle|\frac{\partial}{\partial\mathbf{A_E}}\phi_\alpha\right\rangle\right\rangle = \sum_{\eta\neq\alpha}\langle\langle\phi_\beta|\phi_\eta\rangle\rangle\frac{\left\langle\left\langle\phi_\eta\middle|\dfrac{\partial\hat{H}}{\partial\mathbf{A_E}}\middle|\phi_\alpha\right\rangle\right\rangle}{\varepsilon_\beta-\varepsilon_\alpha} = \frac{\left\langle\left\langle\phi_\beta\middle|\dfrac{\partial\hat{H}}{\partial\mathbf{A_E}}\middle|\phi_\alpha\right\rangle\right\rangle}{\varepsilon_\beta-\varepsilon_\alpha}\,. \tag{A.12}$$

A.2. Calculation of the conductivity

We suppose to have a non-interacting (spinless) fermions in $2d$ and to have translational invariance so that we can introduce the momentum $\mathbf{k}$ as a good quantum number. We suppose moreover that there are no degeneracies (modulo $\hbar\omega$) at each $\mathbf{k}$ point between the quasienergies $\varepsilon_{\alpha,\mathbf{k}}$. The initial (pure) density matrix of our system, expressed in the basis of Floquet states, is

$$\hat{\rho}(t=0) = \prod_k\sum_{\alpha\alpha'}\rho_{\alpha\alpha',\mathbf{k}}\,|\psi_{\alpha,\mathbf{k}}(0)\rangle\,\langle\psi_{\alpha',\mathbf{k}}(0)|\,. \tag{A.13}$$

We suppose that for each $\mathbf{k}$ there N_p particles, so that $\mathrm{Tr}(\hat{\rho}) = N_p$. We want to calculate the response to a weak constant electric field $\mathbf{E}$. If we make the gauge choice $\mathbf{A_E}(t) = c\mathbf{E}t$ we

[3] If a time-periodic perturbation $V(t)$ is added to a Hamiltonian with the same period, then the first-order correction to the Floquet modes are

$$\left|\phi_\alpha^{(1)}(t)\right\rangle = \sum_{\beta\neq\alpha}\frac{\langle\langle\phi_\beta^{(0)}|V(t)|\phi_\alpha^{(0)}\rangle\rangle}{\varepsilon_\beta^{(0)}-\varepsilon_\alpha^{(0)}}\left|\phi_\beta^{(0)}(t)\right\rangle\,,$$

as in regular perturbation theory. Then if H depends on some parameter λ we can write

$$|\phi_\alpha(\lambda+\delta\lambda;t)\rangle = |\phi_\alpha(\lambda;t)\rangle + \sum_{\beta\neq\alpha}\frac{\langle\langle\phi_\beta(\lambda;t)|\hat{H}(\lambda+\delta\lambda;t)-\hat{H}(\lambda;t)|\phi_\alpha(\lambda;t)\rangle\rangle}{\varepsilon_\beta(\lambda)-\varepsilon_\alpha(\lambda)}|\phi_\beta(\lambda;t)\rangle \implies$$

$$\implies \left|\frac{\partial}{\partial\lambda}\phi_\alpha(\lambda;t)=\right\rangle\sum_{\beta\neq\alpha}\frac{\left\langle\left\langle\phi_\beta(\lambda;t)\middle|\dfrac{\partial\hat{H}}{\partial\lambda}\middle|\phi_\alpha(\lambda;t)\right\rangle\right\rangle}{\varepsilon_\beta(\lambda)-\varepsilon_\alpha(\lambda)}|\phi_\beta(\lambda;t)\rangle\,.$$

can apply our previous results. Since we are doing linear response, we will set $\mathbf{A_E} = 0$ in the quasienergies, the Floquet modes and the current operator in the formula for the adiabatically modified Floquet state. The period-averaged expectation value of the a-th component of the current is

$$\begin{aligned}\langle\langle \hat{J}_a \rangle\rangle &= \frac{1}{\tau}\int_0^\tau \mathrm{Tr}\left[\hat{\rho}\,(t)\,\hat{J}_a\,(t)\right] dt \\ &= \sum_{\mathbf{k}}\sum_{\alpha\alpha'}\frac{1}{\tau}\int_0^\tau \rho_{\alpha\alpha',\mathbf{k}}\,\mathrm{Tr}\left[|\psi_{\alpha,\mathbf{k}}\,(t)\rangle\left\langle\psi_{\alpha',\mathbf{k}}\,(t)\right|\hat{J}_a\,(t)\right] dt\,. \end{aligned} \tag{A.14}$$

Taking the trace over the unperturbed Floquet modes at time t and using Eq. (A.11) and (A.12) give us

$$\begin{aligned}\langle\langle \hat{J}_a \rangle\rangle =& \frac{1}{\tau}\int_0^\tau \sum_{\mathbf{k}}\sum_{\alpha\alpha'\alpha''}\rho_{\alpha\alpha',\mathbf{k}}\left\langle\phi_{\alpha'',\mathbf{k}}\,(t)\right|\left|\psi_{\alpha,\mathbf{k}}\,(t)\right\rangle\left\langle\psi_{\alpha',\mathbf{k}}\,(t)\right|\hat{J}_a\,(t)\left|\phi_{\alpha'',\mathbf{k}}\,(t)\right\rangle dt = \\ =& \frac{1}{\tau}\int_0^\tau \sum_{\mathbf{k}}\sum_{\alpha\alpha'\alpha''}\rho_{\alpha\alpha',\mathbf{k}}e^{i(\gamma_{\alpha,\mathbf{k}}(t)-\gamma_{\alpha',\mathbf{k}}(t))}e^{-i\int_0^t(\varepsilon_{\alpha,\mathbf{k}}(t)-\varepsilon_{\alpha',\mathbf{k}}(t))dt}\left\langle\phi_{\alpha'',\mathbf{k}}\,(t)\right|\times \\ &\times\left\{|\phi_{\alpha,\mathbf{k}}\,(t)\rangle + i\hbar\sum_{\beta\neq\alpha}\sum_b|\phi_{\beta,\mathbf{k}}\,(t)\rangle\,\frac{\langle\langle\phi_{\beta,\mathbf{k}}|\hat{J}_b|\phi_{\alpha,\mathbf{k}}\rangle\rangle}{\left(\varepsilon_{\beta,\mathbf{k}}-\varepsilon_{\alpha,\mathbf{k}}\right)^2}E_b\right\}\times \\ &\times\left\{\left\langle\phi_{\alpha',\mathbf{k}}\,(t)\right| - i\hbar\sum_{\beta'\neq\alpha'}\sum_{b'}\left\langle\phi_{\beta',\mathbf{k}}\,(t)\right|\frac{\langle\langle\phi_{\alpha',\mathbf{k}}|J_{b'}|\phi_{\beta',\mathbf{k}}\rangle\rangle}{\left(\varepsilon_{\beta',\mathbf{k}}-\varepsilon_{\alpha',\mathbf{k}}\right)^2}E_{b'}\right\}\hat{J}_a\left|\phi_{\alpha'',\mathbf{k}}\,(t)\right\rangle dt\,. \end{aligned} \tag{A.15}$$

We have used the fact that $\partial\hat{H}/\partial A_b = \hat{J}_b$. The contributions can be divided in diagonal ($\alpha = \alpha'$) and off-diagonal. The first ones are

$$\begin{aligned}\langle\langle \hat{J}_a \rangle\rangle_{diag} \simeq& \langle\langle \hat{\hat{J}}_a \rangle\rangle^{(0)}_{diag} - i\hbar\sum_{\mathbf{k}}\sum_{\alpha}\delta_{\alpha\alpha''}\rho_{\alpha\alpha,\mathbf{k}}\sum_{\beta'\neq\alpha}\sum_{b'}\langle\langle\phi_{\beta',\mathbf{k}}|\hat{\hat{J}}_a|\phi_{\alpha,\mathbf{k}}\rangle\rangle\frac{\langle\langle\phi_{\alpha,\mathbf{k}}|J_{b'}|\phi_{\beta',\mathbf{k}}\rangle\rangle}{\left(\varepsilon_{\beta',\mathbf{k}}-\varepsilon_{\alpha',\mathbf{k}}\right)^2}E_{b'} + \\ &+ i\hbar\sum_{\mathbf{k}}\sum_{\alpha}\rho_{\alpha\alpha',\mathbf{k}}\sum_{\beta\neq\alpha}\sum_b\delta_{\alpha''\beta}\langle\langle\phi_{\alpha,\mathbf{k}}|\hat{\hat{J}}_a|\phi_{\beta,\mathbf{k}}\rangle\rangle\frac{\langle\langle\phi_{\beta}|J_b|\phi_{\alpha,\mathbf{k}}\rangle\rangle}{\left(\varepsilon_{\beta,\mathbf{k}}-\varepsilon_{\alpha,\mathbf{k}}\right)^2}E_b\,. \end{aligned} \tag{A.16}$$

The lowest order term represents the unperturbed value of the current. Using Eq. (E.2), we obtain

$$\begin{aligned}\langle\langle \hat{J}_a \rangle\rangle^{(0)}_{diag} =& \langle\langle\frac{\partial H}{\partial k_a}\rangle\rangle^{(0)}_{diag} = \sum_{\mathbf{k}}\sum_{\alpha}\rho_{\alpha\alpha,\mathbf{k}}\frac{1}{\hbar}\left(\frac{\partial\epsilon_{\alpha,\mathbf{k}}}{\partial\mathbf{k}} + \frac{1}{\tau}\int_0^\tau dt\frac{\partial}{\partial t}\left\langle\phi_\alpha\right|\left|\frac{\partial}{\partial\mathbf{k}}\phi_\alpha\right\rangle\right) = \\ =& \sum_{\mathbf{k}}\sum_{\alpha}\rho_{\alpha\alpha,\mathbf{k}}\frac{1}{\hbar}\left(\frac{\partial\epsilon_{\alpha,\mathbf{k}}}{\partial\mathbf{k}}\right)\,. \end{aligned} \tag{A.17}$$

The second term in the equation disappears because of the periodicity of the Floquet modes over a period. The first order diagonal correction in $|\mathbf{E}|$ is then given by:

$$\langle\langle \hat{J}_a \rangle\rangle^{(1)}_{diag} = i\hbar \sum_{\mathbf{k}} \sum_{\alpha} \sum_{\beta\neq\alpha} \sum_{b} \frac{\rho_{\beta\beta,\mathbf{k}} - \rho_{\alpha\alpha,\mathbf{k}}}{\varepsilon_{\beta,\mathbf{k}} - \varepsilon_{\alpha,\mathbf{k}}} \frac{\langle\langle \phi_{\alpha,\mathbf{k}} | \hat{J}_b | \phi_{\beta,\mathbf{k}} \rangle\rangle \langle\langle \phi_{\beta,\mathbf{k}} | J_a | \phi_{\alpha,\mathbf{k}} \rangle\rangle}{\varepsilon_{\beta,\mathbf{k}} - \varepsilon_{\alpha,\mathbf{k}}} E_b \,. \tag{A.18}$$

To obtain this result we have relabelled $\beta' \to \beta$ and $b' \to b$ in the first term, while in the second one we have exchanged the indices $\alpha \rightleftarrows \beta$.
The off-diagonal contribution is instead

$$\begin{aligned}\langle\langle \hat{J}_a \rangle\rangle^{(1)}_{o-d} \simeq \sum_{\mathbf{k}} \sum_{\alpha\neq\alpha'} \frac{1}{\tau} \int_0^\tau dt e^{i(\gamma_{\alpha,\mathbf{k}}(t) - \gamma_{\alpha',\mathbf{k}}(t))} e^{-i\int_0^t (\varepsilon_{\alpha,\mathbf{k}}(t) - \varepsilon_{\alpha'}(t))dt} \rho_{\alpha\alpha',\mathbf{k}} \times \\ \times \Bigg(-i\hbar\delta_{\alpha\alpha''} \sum_{\beta'\neq\alpha'} \sum_{b'} \langle \phi_{\beta',\mathbf{k}} | \hat{\hat{J}}_a | \phi_{\alpha,\mathbf{k}} \rangle \frac{\langle\langle \phi_{\alpha',\mathbf{k}} | J_{b'} | \phi_{\beta',\mathbf{k}} \rangle\rangle}{\left(\varepsilon_{\beta',\mathbf{k}} - \varepsilon_{\alpha',\mathbf{k}}\right)^2} E_{b'} + \\ + i\hbar\delta_{\alpha''\beta} \sum_{\beta\neq\alpha} \sum_{b} \langle \phi_{\alpha',\mathbf{k}} | \hat{\hat{J}}_a | \phi_{\beta} \rangle \frac{\langle\langle \phi_{\beta,\mathbf{k}} | J_b | \phi_{\alpha,\mathbf{k}} \rangle\rangle}{\left(\varepsilon_{\beta,\mathbf{k}} - \varepsilon_{\alpha,\mathbf{k}}\right)^2} E_b \Bigg) \,.\end{aligned} \tag{A.19}$$

Let us concentrate only on the first order term, assuming the zero-th order one gives no contribution. If we concentrate only on the diagonal part, which in many cases is the value to which the expectation value converges (see Sec. 2.1.1, we get for the transverse conductivity, defined as $\sigma_{ab} = (\langle\langle \hat{J}_a \rangle\rangle / E_b)/\mathrm{Vol}$ the expression

$$\sigma_{ab} = \frac{1}{\mathrm{Vol}} \frac{1}{\hbar} \sum_{\alpha} \sum_{\beta\neq\alpha} i \frac{n_{\beta,\mathbf{k}} - n_{\alpha,\mathbf{k}}}{\varepsilon_{\beta,\mathbf{k}} - \varepsilon_{\alpha,\mathbf{k}}} \frac{\langle\langle \phi_{\alpha,\mathbf{k}} | \hat{J}_b | \phi_{\beta,\mathbf{k}} \rangle\rangle \langle\langle \phi_{\beta,\mathbf{k}} | J_a | \phi_{\alpha,\mathbf{k}} \rangle\rangle}{\varepsilon_{\beta,\mathbf{k}} - \varepsilon_{\alpha,\mathbf{k}}} \,, \tag{A.20}$$

where we have used for the occupations $\rho_{\alpha\alpha,\mathbf{k}}$ the notation $n_{\alpha,\mathbf{k}}$ as in the rest of this thesis and Vol is the system volume. This formula can be rewritten in terms of the "Floquet' Berry connection as in the static case. If we consider the case of a bulk crystal, then we have to sum the contributions from all the quasimomenta. Moreover the derivatives with respect to the vector potential become quasimomentum derivatives. At this point it useful to say that the charge current is given by $\hat{J}_a = \mathrm{e}\partial_k \hat{H}/\hbar$, where e is the electron charge. If we also use again Eq.((A.12)) and keep in mind that $\langle\langle \phi_{\alpha,\mathbf{k}} | \frac{\partial \phi_{\beta,\mathbf{k}}}{\partial k_b} \rangle\rangle = -\langle\langle \frac{\partial \phi_{\alpha,\mathbf{k}}}{\partial k_a} | \phi_{\beta,\mathbf{k}} \rangle\rangle$ we get

$$\begin{aligned}\sigma_{ab} =& \frac{1}{\mathrm{Vol}} \sum_{\mathbf{k}} \sum_{\alpha} \sum_{\beta\neq\alpha} i\hbar \frac{n_{\beta,\mathbf{k}} - n_{\alpha,\mathbf{k}}}{\varepsilon_{\beta,\mathbf{k}} - \varepsilon_{\alpha,\mathbf{k}}} \frac{\langle\langle \phi_{\alpha,\mathbf{k}} | \hat{J}_b | \phi_{\beta,\mathbf{k}} \rangle\rangle \langle\langle \phi_{\beta,\mathbf{k}} | J_a | \phi_{\alpha} \rangle\rangle}{\varepsilon_{\beta,\mathbf{k}} - \varepsilon_{\alpha,\mathbf{k}}} = \\ =& \sum_{\mathbf{k}} \sum_{\alpha} \sum_{\beta\neq\alpha} -\frac{i\mathrm{e}^2}{\hbar} \left[n_{\beta,\mathbf{k}} - n_{\alpha,\mathbf{k}} \right] \langle\langle \frac{\partial \phi_{\alpha,\mathbf{k}}}{\partial k_b} | \phi_{\beta,\mathbf{k}} \rangle\rangle \langle\langle \phi_{\beta,\mathbf{k}} | \frac{\partial \phi_{\alpha,\mathbf{k}}}{\partial k_a} \rangle\rangle = \\ =& \sum_{\mathbf{k}} \sum_{\alpha} \sum_{\beta\neq\alpha} -\frac{i\mathrm{e}^2}{\hbar} \Bigg[n_{\beta,\mathbf{k}} \langle\langle \frac{\partial \phi_{\beta,\mathbf{k}}}{\partial k_a} | \phi_{\alpha,\mathbf{k}} \rangle\rangle \langle\langle \phi_{\alpha,\mathbf{k}} | \frac{\partial \phi_{\beta,\mathbf{k}}}{\partial k_b} \rangle\rangle + \\ & - n_{\alpha,\mathbf{k}} \langle\langle \frac{\partial \phi_{\alpha,\mathbf{k}}}{\partial k_b} | \phi_{\beta,\mathbf{k}} \rangle\rangle \langle\langle \phi_{\beta,\mathbf{k}} | \frac{\partial \phi_{\alpha,\mathbf{k}}}{\partial k_a} \rangle\rangle \Bigg] \,.\end{aligned} \tag{A.21}$$

Adding and subtracting $\sum_\alpha n_{\alpha,\mathbf{k}}\langle\langle\frac{\partial\phi_{\alpha,\mathbf{k}}}{\partial k_b}|\phi_{\alpha,\mathbf{k}}\rangle\rangle\langle\langle\phi_{\alpha,\mathbf{k}}|\frac{\partial\phi_{\alpha,\mathbf{k}}}{\partial k_a}\rangle\rangle$ allow us to simplify the identity operator in the middle of the two terms. Relabelling indices $\beta \leftrightarrow \alpha$ in the first term gives us

$$\begin{aligned}\sigma_{ab} =& -i\frac{1}{\mathrm{Vol}}\frac{\mathrm{e}^2}{\hbar}\sum_{\mathbf{k}}\sum_{\alpha} n_{\alpha,\mathbf{k}}\left[\langle\langle\frac{\partial\phi_{\alpha,\mathbf{k}}}{\partial k_a}|\frac{\partial\phi_{\alpha,\mathbf{k}}}{\partial k_b}\rangle\rangle - \langle\langle\frac{\partial\phi_{\alpha,\mathbf{k}}}{\partial k_b}|\frac{\partial\phi_{\alpha,\mathbf{k}}}{\partial k_a}\rangle\rangle\right] = \\ =&\frac{1}{\mathrm{Vol}}\frac{\mathrm{e}^2}{\hbar}\sum_{\mathbf{k}}\sum_{\alpha} n_{\alpha,\mathbf{k}}\left[\nabla_{\mathbf{k}}\times\mathcal{A}_\alpha(\mathbf{k})\right]_z \overset{\mathrm{Vol}\to\infty}{=} \frac{\mathrm{e}^2}{h}\frac{1}{2\pi}\sum_{\alpha}\int_{\mathrm{BZ}} n_{\alpha,\mathbf{k}}\left[\nabla_{\mathbf{k}}\times\mathcal{A}_\alpha(\mathbf{k})\right]_z ,\end{aligned} \tag{A.22}$$

where $\mathcal{A}_\alpha(\mathbf{k}) = -i\langle\langle\frac{\partial\phi_{\alpha,\mathbf{k}}}{\partial\mathbf{k}}|\phi_{\alpha,\mathbf{k}}\rangle\rangle$ is the period-averaged Berry connection of the α-th Floquet mode. We conclude that if $n_{\alpha,\mathbf{k}} = 1/0$ in such a way that N_p bands separated in quasienergy from the others are filled, we would get the quantization in units of e/h of the (period averaged) Hall conductivity as in the equilibrium case, since the integrand in the last expression is a Berry curvature of (Floquet-) Bloch bands , $[\nabla_{\mathbf{k}}\times\mathcal{A}_\alpha]_z$ and the integral is equal to a Chern number. Moreover if the bands are filled in this way, the zero-th order term of Eq. (A.17) disappears because of the periodicity in $\mathbf{k}$ of the bands. Thus the Hall response is exactly quantised.

B. The Magnus expansion

We give here some hints on how to derive to derive a $1/\hbar\omega$ expansion for the Floquet Hamiltonian $\hat{H}_F$ [140], the so called Magnus expansion. It is not the only way to derive an effective Hamiltonian for the dynamics [141, 142] at high frequencies and has some small drawbacks [141] but it includes all the elements that are necessary for our analysis.
The starting point is the Dyson series for the evolution operator [143] over one generic period

$$\begin{aligned}\hat{U}(\tau+t_0,t_0) &= \mathcal{T}\mathrm{e}^{-\frac{i}{\hbar}\int_{t_0}^{t_0+\tau}\hat{H}(t)dt} = \\ &= \mathcal{T}\left\{1-\frac{i}{\hbar}\int_{t_0}^{t_0+\tau}\hat{H}(t)dt-\frac{1}{2\hbar^2}\int_{t_0}^{t_0+\tau}\hat{H}(t_1)dt_1\int_{t_0}^{t_0+\tau}\hat{H}(t_2)dt_2+..\right\} \qquad \text{(B.1)}\\ &= 1-\frac{i}{\hbar}\int_{t_0}^{t_0+\tau}\hat{H}(t)dt-\frac{1}{\hbar^2}\int_{t_0}^{t_0+\tau}\hat{H}(t_1)dt_1\int_{t_0}^{t_1}\hat{H}(t_2)dt_2+\dots\ .\end{aligned}$$

Substituting the Fourier series for the Hamiltonian $\hat{H}(t)=\sum_n \hat{H}_n \mathrm{e}^{in\omega t}$ and focusing only on corrections up to second order we have

$$\begin{aligned}\hat{U}(\tau+t_0,t_0) &= \mathbb{1}-\frac{i}{\hbar}\hat{H}_0\tau-\frac{1}{\hbar^2}\int_{t_0}^{t_0+\tau}\mathrm{d}t_1\Bigg(\sum_{n=-\infty}^{\infty}\hat{H}_n e^{in\omega t_1}\Bigg(H_0(t_1-t_0)+\\ &\qquad +\sum_{\substack{n'=-\infty\\ n'\neq 0}}^{\infty}H_{n'}\frac{e^{in'\omega t_1}-e^{in'\omega t_0}}{in'\omega}\Bigg)\Bigg)+\mathcal{O}\left(\frac{1}{(\hbar\omega)^3}\right)=\\ &= \mathbb{1}-\frac{i}{\hbar}H_0\tau-\frac{1}{\hbar^2}\Bigg(\sum_{\substack{n,n'=-\infty\\ n,n'\neq 0}}^{\infty}\delta_{n-n'}\frac{H_nH_{n'}}{in'\omega}\tau-H_0\sum_{\substack{n'=-\infty\\ n'\neq 0}}^{\infty}+\frac{H_{n'}}{in'\omega}e^{in'\omega t_0}\tau+\\ &\qquad +\sum_{\substack{n=-\infty\\ n\neq 0}}^{\infty}\frac{H_nH_0}{in\omega}e^{in\omega t_0}\tau\Bigg)+\mathcal{O}\left(\frac{1}{(\hbar\omega)^3}\right).\end{aligned}$$

On the other hand we can expand the Floquet operator in powers of the Floquet Hamiltonian:

$$\hat{U}(\tau+t_0,t_0)=\ \mathbb{1}-\frac{i}{\hbar}\hat{H}_F(t_0)\tau-\frac{1}{2\hbar^2}\hat{H}_F^2(t_0)\tau^2+... \qquad \text{(B.2)}$$

In the last expression we have explicitly written the dependence of the Floquet Hamiltonian on the initial time t_0. By equating terms at same order in $1/\hbar\omega$, we get up to first order

$$\hat{H}_F(t_0) = \hat{H}_0 + \sum_{n\neq 0} \frac{1}{n\hbar\omega} \left\{ \hat{H}_n \hat{H}_{-n} + \mathrm{e}^{in\omega t_0} \left[\hat{H}_0, \hat{H}_n \right] \right\} + \mathcal{O}\left(\frac{1}{\hbar^2\omega^2} \right) . \tag{B.3}$$

This expansion brings an apparent contradiction, because the spectrum of our approximation of H_F depends on the initial time t_0. Notice that this fact would be hidden if we had set $t_0 = 0$ as we have done in the rest of this thesis. This is in contrast with the fact that Floquet Hamiltonians at different initial times are related by a unitary transformation. To see this, we first notice that the following representation for a generic evolution operator holds:

$$\begin{aligned} \hat{U}(t_2,t_1) = \hat{U}(t_2,t_1) \sum_\alpha |\phi_\alpha(t_1)\rangle \langle\phi_\alpha(t_1)| = \hat{U}(t_2,t_1) \sum_\alpha \mathrm{e}^{\frac{i}{\hbar}\varepsilon_\alpha t_1} |\psi_\alpha(t_1)\rangle \langle\phi_\alpha(t_1)| \implies \\ \implies \hat{U}(t_2,t_1) = \sum_\alpha \mathrm{e}^{-\frac{i}{\hbar}\varepsilon_\alpha(t_2-t_1)} |\phi_\alpha(t_2)\rangle \langle\phi_\alpha(t_1)| . \end{aligned} \tag{B.4}$$

In the the first line, we have used the fact that the Floquet modes $|\phi_\alpha(t)\rangle$ are a basis at all times. From this relation and the periodicity of the Floquet modes, it follows that a generic evolution operator is invariant under simultaneous τ translations of both arguments

$$\hat{U}(t_1,t_2) \;=\; \hat{U}(t_1+n\tau, t_2+n\tau) . \tag{B.5}$$

Therefore we can write

$$\begin{aligned} \hat{U}(t_0'+\tau,t_0') = \mathrm{e}^{-\frac{i}{\hbar}H_F(t_0')\tau} = \hat{U}(t_0'+\tau,t_0+\tau)\, \hat{U}(t_0+\tau,t_0)\, \hat{U}(t_0,t_0') \\ = \hat{U}(t_0',t_0)\, \mathrm{e}^{-\frac{i}{\hbar}H_F(t_0)\tau}\, \hat{U}(t_0,t_0') \implies \end{aligned}$$

$$\implies H_F(t_0') = \hat{U}^\dagger(t_0',t_0)\, H_F(t_0)\, \hat{U}(t_0,t_0') . \tag{B.6}$$

This paradox is resolved with a more refined analysis of the expansion [141]. What it turns out is that while the corrections to the eigenstates coming from the $[H_0, H_n]$ term in equation (B.3) are of the same order of the ones from the H_n, H_{-n} term, the corrections to the quasienergies are of higher order. Thus in the case of eq.(B.3), the $[H_0, H_n]$ term gives corrections to the quasienergies of order $1/(\hbar\omega)^2$ which must be discarded to make the approximation consistent.

This is one of the reasons why the Magnus expansion must be handled with care. Among the others, convergence of the series is also a serious issue [140].

C. Chern number as a local quantity

In this appendix we follow the work of Bianco and Resta [36, 144] and show how to calculate locally the Chern number and, consequently, the Hall conductivity of insulators. This technique enables to topologically characterize the ground state of a Hamiltonian defined in geometries with boundaries. We start from the definition of the Chern number in an infinite crystal with PBC having its first N_p bands fully occupied [144, 145]:

$$\begin{aligned}\mathcal{C} =&\frac{i}{2\pi}\sum_{p}^{\text{occ}}\sum_{q}^{\text{unocc}}\int_{\text{BZ}}d\mathbf{k}\Big(\langle\partial_{k_x}u_{p\mathbf{k}}|\,u_{q\mathbf{k}}\rangle\,\langle u_{q\mathbf{k}}|\,\partial_{k_y}u_{p\mathbf{k}}\rangle-\text{c.c.}\Big)\\ =&2\pi i\sum_{p}^{\text{occ}}\sum_{q}^{\text{unocc}}\int_{\text{BZ}}\frac{d\mathbf{k}}{(2\pi)^2}\Big(\,(\hat{x}_{\mathcal{P}}(\mathbf{k}))_{pq}\,(\hat{y}_{\mathcal{Q}}(\mathbf{k}))_{qp}-\text{c.c.}\Big)\\ =&2\pi i\ \text{Tr}\left(\hat{x}_{\mathcal{P}}\hat{y}_{\mathcal{Q}}-\hat{y}_{\mathcal{P}}\hat{x}_{\mathcal{Q}}\right).\end{aligned}$$

Here $|u_{p/q\,\mathbf{k}}\rangle$ denote the periodic part of a set of occupied/empty Bloch states. The second form is obtained by using $\langle\partial_{k_x}u_{p\mathbf{k}}|\,u_{q\mathbf{k}}\rangle = -\langle u_{p\mathbf{k}}|\,\partial_{k_x}u_{q\mathbf{k}}\rangle$ and re-expressing the result in terms of momentum-space matrix element of the position operators $\hat{x}_{\mathcal{P}}=\mathcal{P}\hat{x}\mathcal{Q}$ and $\hat{y}_{\mathcal{Q}}=\mathcal{Q}\hat{y}\mathcal{P}$ sandwiched between the projectors $\hat{\mathcal{P}}$ and $\hat{\mathcal{Q}}$ on occupied and empty bands: $(\hat{x}_{\mathcal{P}}(\mathbf{k}))_{pq} = \langle u_{p\mathbf{k}}|\,i\partial_{k_x}u_{q\mathbf{k}}\rangle$ and $(\hat{y}_{\mathcal{Q}}(\mathbf{k}))_{qp}=\langle u_{q\mathbf{k}}|\,i\partial_{k_y}u_{p\mathbf{k}}\rangle$. The final form makes it explicit that the sums over p and q and the momentum space integral yield simply a *trace* expression in terms of projected position operators.

Now, in the thermodynamic limit, we can equivalently compute the trace in real space (Wannier) representation [1]. Hence, switching to real space we can extract a *local Chern marker* (CM) $\mathcal{C}(\mathbf{r})$ as:

$$\mathcal{C}(\mathbf{r}) = 2\pi i\,\langle\mathbf{r}|\left(\hat{x}_{\mathcal{P}}\hat{y}_{\mathcal{Q}}-\hat{y}_{\mathcal{P}}\hat{x}_{\mathcal{Q}}\right)|\mathbf{r}\rangle\ , \tag{C.1}$$

in terms of which the Chern number is written as

$$\mathcal{C}\overset{TL}{=}\frac{1}{V}\,\text{Tr}\left[\hat{\mathfrak{C}}\right]=\frac{1}{V}\int_{V}\mathfrak{C}(\mathbf{r})d\mathbf{r}, \tag{C.2}$$

This local expression can be used also for an open boundary (OB) geometry, and even when translational invariance is broken by disorder. Interestingly, when one considers open boundary conditions (OBC), where $\hat{x}$ and $\hat{y}$ are well defined operators even without projectors

[1] $\frac{1}{V}\,\text{Tr}\,\hat{A}=\int\frac{d\mathbf{k}}{(2\pi)^d}\,\text{Tr}\,\mathbb{A}(\mathbf{k})$, where $\mathbb{A}(\mathbf{k})$ is a matrix representation of $\hat{A}$ in the subspaced labelled by $\mathbf{k}$.

[146], we can rewrite $\mathcal{C}(\mathbf{r})$ in a more appealing form in terms of standard commutators[36]. Indeed $\hat{x}_{\mathcal{P}}\hat{y}_{\mathcal{Q}} - \hat{y}_{\mathcal{P}}\hat{x}_{\mathcal{Q}} = \mathcal{P}(\hat{x}\mathcal{Q}\hat{y} - \hat{y}\mathcal{Q}\hat{x})\mathcal{P} = -[\hat{x}_{\mathcal{P}}, \hat{y}_{\mathcal{P}}]$, where we used $\mathcal{Q} = 1 - \mathcal{P}$, $[\hat{x}, \hat{y}] = 0$, and standard properties of projectors. Hence, a physically equivalent way of writing the local Chern marker is:

$$\mathcal{C}(\mathbf{r}) = -2\pi i \langle \mathbf{r} | \left[\hat{x}_{\mathcal{P}}, \hat{y}_{\mathcal{P}} \right] | \mathbf{r} \rangle \ , \tag{C.3}$$

which involves the *commutator* of $\mathcal{P}$-projected position operators. Now we consider the case where OBC are applied. Clearly, in this last form, $\int_V d\mathbf{r}\ \mathcal{C}(\mathbf{r}) = 0$, but the local "bulk" physics is well reproduced, due to "Kohn's nearsightedness" of electrons in insulators [112]. This fact means, among other things that the ground state projector is exponentially localized, e.g. $\langle \mathbf{r}' | \hat{\mathcal{P}} | \mathbf{r} \rangle \sim \exp(|\mathbf{r} - \mathbf{r}'|)$. This would mean that averaging the LCM over the bulk gives the same result as in the PBC and that the boundaries give an extensive contribution that makes the total average zero:

$$\mathfrak{C}(\mathbf{r})|_{boun} \overset{TL}{\simeq} -\mathcal{C} \times \mathcal{O}(L) \implies \frac{\int_{boun} \mathfrak{C}(\mathbf{r})\, d\mathbf{r}}{\int_{bulk} \mathfrak{C}(\mathbf{r})\, d\mathbf{r}} \overset{TL}{\simeq} \mathcal{O}(L^{-1}) \tag{C.4}$$

Indeed in ref.[36] simple numerical experiments on different Haldane model samples confirm this reasoning. Even more remarkably, in situations with no disorder, it is evident from numerical experiments on tight binding models that in the bulk the Local Chern Marker approaches the quantized value in the thermodynamic limit *point by point*, with very small fluctuations.

D. Details for chapter 3

D.1. Technical details on the numerical implementation.

We summarize here the main technicalities involved in doing QA dynamics for the Hamiltonians we have considered. The crucial ingredient is that an initial Slater determinant remains a Slater determinant under an arbitrary unitary time-evolution, as long as the driving Hamiltonian is quadratic in the fermionic operators. As we explained in Sec. (3.1.1), the Hamiltonian can be expressed as

$$\hat{H}(t) = \sum_{k}^{\mathrm{BZ}_y} \sum_{i,i'=1}^{N_x} \mathbb{H}_{ii'}(k,t)\ \hat{c}^{\dagger}_{i,k}\hat{c}_{i',k}\ , \tag{D.1}$$

after Fourier-Bloch transforming along y. Here $\mathbb{H}(k,t)$ is an $N_x \times N_x$ Hermitean matrix with elements on the diagonal (the on-site terms) and at nn (for the Haldane model there are also second-neighbor terms). The initial Slater determinant $|\Psi(0)\rangle$ is constructed by diagonalizing $\mathbb{H}(k,0)$ for each k, obtaining the eigenvectors $u_{i,\alpha}(k)$ and forming the corresponding eigenmode combinations $\hat{a}^{\dagger}_{\alpha,k} = \sum_i u_{i,\alpha}(k)\,\hat{c}^{\dagger}_{i,k}$, which are then occupied according to Pauli principle. Any relevant translationally invariant operator can be decomposed in terms of the Bloch combinations $\hat{c}^{\dagger}_{i,k}$ as we did for $\hat{H}(t)$. For instance, the y-component of the current flowing along the bond $(\mathbf{r}_{i,j}, \mathbf{r}_{i',j})$, averaged over j, — for the Haldane case there are also second-neighbor currents along bond $(\mathbf{r}_{i,j}, \mathbf{r}_{i,j+1})$ — can be expressed as:

$$\hat{J}_{ii'}(t) = \sum_{k}^{\mathrm{BZ}_y} \mathbb{J}_{ii'}(k,t)\ \hat{c}^{\dagger}_{i,k}\hat{c}_{i',k}\ , \tag{D.2}$$

with $\mathbb{J} = \frac{1}{\hbar}\frac{\partial \mathbb{H}}{\partial \kappa_y}\big|_{\kappa_y=0}$, where $\kappa_y = \frac{2\pi}{aN_y}\frac{\Phi_L}{\phi_0}$ is related to the Laughlin flux Φ_L, in units of the flux quantum ϕ_0, piercing the PBC-cylinder along the x-axis. If $|\Psi(t)\rangle$ denotes the time-evolved Slater determinant state of the system, then all physically relevant observables can be extracted from the knowledge of the single-particle Green's function:

$$\mathbb{G}_{i'i}(k,t) \equiv \langle\Psi(t)|\hat{c}^{\dagger}_{i,k}\hat{c}_{i',k}|\Psi(t)\rangle = \langle\Psi(0)|\hat{c}^{\dagger}_{i,k}(t)\hat{c}_{i',k}(t)|\Psi(0)\rangle\ , \tag{D.3}$$

where the second form involves switching to the Heisenberg representation. Due to the absence of interactions, The Schrödinger unitary dynamics implies a simple *linear* equation of motion for the Heisenberg's operators $\hat{c}^{\dagger}_{i,k}(t)$ and $\hat{c}_{i',k}(t)$, which can be solved as follows.

The initial eigenstate wavefunctions at given k are conveniently organized into an $N_x \times N_x$ unitary matrix $\mathbb{S}^0(k) = [u_{i,\alpha}]$, with k-eigenvectors by columns. One can show that the Heisenberg's equations for $\hat{c}_{i,k}(t)$ are solved by

$$\hat{c}_{i,k}(t) = \sum_{\alpha} \mathbb{S}_{i,\alpha}(k,t)\, \hat{a}_{\alpha,k} \ ,$$

where the matrix $\mathbb{S}(k,t)$ obeys the Schrödinger equation:

$$i\hbar \frac{d}{dt}\mathbb{S}(k,t) = \mathbb{H}(k,t) \cdot \mathbb{S}(k,t) \ . \tag{D.4}$$

This matrix differential equation is solved, for each k, with initial value $\mathbb{S}(k,0) = \mathbb{S}^0(k)$, through a standard 4^{th}-order Runge-Kutta numerical integration. The integration is carried-on up to time $t = \tau_{\rm QA} = n_{\rm QA}\tau$ where the adiabatic switching-on of the periodic perturbation is completed; we take $\tau_{\rm QA}$ to be an integer multiple $n_{\rm QA}$ of the period of the driving $\tau = 2\pi/\omega$. Following that, we carry-on an evolution governed by the final periodic Hamiltonian with fixed $\lambda_{\rm f}$ for a time $\tau_{\rm f} = n_{\rm f}\tau$; the unitary evolution operator allows us to write, at any later time, $\mathbb{S}(k,t) = \mathbb{U}_k(t, n_{\rm QA}\tau)\, \mathbb{S}(k, n_{\rm QA}\tau)$. This periodic evolution is greatly simplified by using the Floquet theorem, which guarantees that the evolution operator $\mathbb{U}_k(t, n_{\rm QA}\tau)$ can be written as

$$\mathbb{U}_k(t, n_{\rm QA}\tau) = \mathbb{U}_k(\delta t, 0)[\mathbb{U}_k(\tau, 0)]^n \ ,$$

where $t = (n + n_{\rm QA})\tau + \delta t$ with $0 \leq \delta t < \tau$. The evolution operator over a period $\mathbb{U}_k(\tau, 0)$, the so-called Floquet operator, plays then a crucial role: its eigenvectors are the Floquet modes $|\phi_{k,\alpha}(0)\rangle$, with phase-eigenvalues $\mathrm{e}^{-i\varepsilon_{k,\alpha}\tau/\hbar}$ expressed in terms of quasienergies $\varepsilon_{k,\alpha}$. The resulting periodic dynamics can be then followed up to large times by simply solving the one-period Floquet problem. Once $\mathbb{S}(k,t)$ is constructed, the physical Green's function is obtained from:

$$\mathbb{G}_{i'i}(k,t) = \langle \Psi(0)|\hat{c}^{\dagger}_{i,k}(t)\hat{c}_{i',k}(t)|\Psi(0)\rangle = \sum_{\alpha}^{\rm occ} \mathbb{S}_{i'\alpha}(k,t)\ \mathbb{S}^{\dagger}_{\alpha i}(k,t) \ . \tag{D.5}$$

The Green's function $\mathbb{G}_{i'i}(k,t)$ directly provides a real-space representation for the projector $\mathcal{P}(t)$ on occupied states used in the construction of the Chern marker $\mathcal{C}(\mathbf{r})$ (see Sec. 3.4):

$$\langle \mathbf{r}_{i',j'}|\mathcal{P}(t)|\mathbf{r}_{i,j}\rangle = \frac{1}{N_y}\sum_{k}^{\mathrm{BZ}_y} \mathrm{e}^{-ika(j-j')}\ \mathbb{G}_{i'i}(k,t) \ . \tag{D.6}$$

The occupations are instead calculated from

$$n_{k,\alpha} = \langle \Psi(n\tau)|\hat{f}^{\dagger}_{k,\alpha}\hat{f}_{k,\alpha}|\Psi(n\tau)\rangle \ , \tag{D.7}$$

with $n \leq n_f$ since they are constant for $n > n_f$.

D.2. Scaling of the residual energy in the Haldane model

We give here some computational details on the finite size scaling of the residual energy $E_{\rm res}(t) = \langle\Psi(t)|\hat{H}(t)|\Psi(t)\rangle - E_{\rm GS}(t)$ for the Haldane model. As we explained in the main text in Sec. 3.2, for square sample $N_x = N_y \equiv L$, the final residual energy has the form $E_{\rm res}(t = \tau_{\rm QA}) = \mathscr{E}_{\rm bulk}(\tau_{\rm QA})L^2 + \mathscr{E}_{\rm edge}(\tau_{\rm QA})L$. We computed the coefficients $\mathscr{E}_{\rm bulk}$ and $\mathscr{E}_{\rm edge}$ from the bare data of $E_{\rm res}(t)$ in the following way. First of all we calculated numerically $\mathscr{E}_{\rm bulk}(\tau_{\rm QA})$ by

$$\mathscr{E}_{\rm bulk}(\tau_{\rm QA}) = \frac{1}{2}\frac{\partial^2}{\partial L^2} E_{\rm res}(L;\tau_{\rm QA}) \,, \tag{D.8}$$

with a finite difference method of order 2, for a given $\tau_{\rm QA}$. To obtain $\mathscr{E}_{\rm bulk}(\tau_{\rm QA})$, Ideally one would need the thermodynamic limit $\lim_{L\to\infty}$ in order that $\mathscr{E}_{\rm bulk}(\tau_{\rm QA})$ does not depend on L. However, we checked the convergence to this limit for finite size samples for every value of $\tau_{\rm QA}$, obtaining the derivatives up to $L = 96$. In the left panel of Fig. D.1, we plotted of $\mathscr{E}_{\rm bulk}$ as a function of the system size for a given annealing time and the Haldane model parameters of 3.2 and the convergence is clear. At this point, having obtained $\mathscr{E}_{\rm bulk}(\tau_{\rm QA})$, we computed $\mathscr{E}_{\rm edge}(\tau_{\rm QA})$ by

$$\mathscr{E}_{\rm edge}(\tau_{\rm QA}) = \frac{\partial}{\partial L}\left(E_{\rm res}(L;\tau_{\rm QA}) - \mathscr{E}_{\rm bulk}(\tau_{\rm QA})L^2\right) \,. \tag{D.9}$$

taking as $\mathscr{E}_{\rm bulk}(\tau_{\rm QA})$ the value for $L = 96$ and using a finite difference method of order 2. Again, we checked the convergence to a thermodynamic limit, as it can be seen from the right panel of figure D.1.

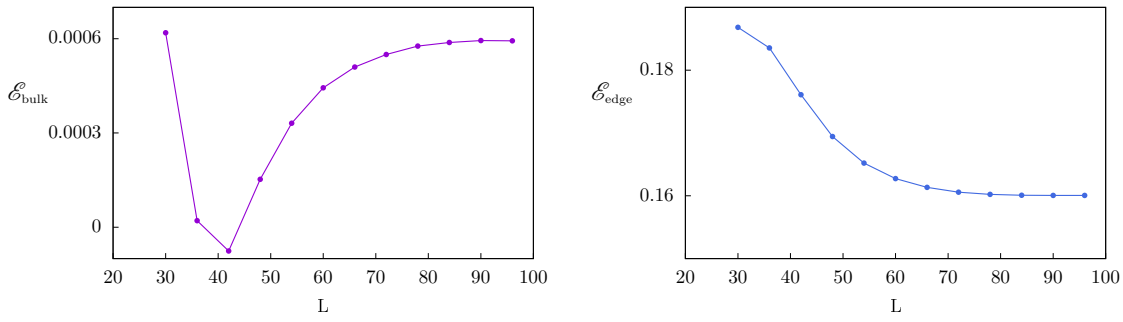

Figure D.1.: Convergence of $\mathscr{E}_{\rm bulk}$ and $\mathscr{E}_{\rm edge}$ as a function of the system size L. The parameters of the dynamics of the Haldane model are $\Delta_{AB}(0) = 2.1t_1$, $\Delta_{AB}(\tau_{\rm QA}) = 0$, $t_2 = 0.3t_1$, $\phi_H = \frac{\pi}{2}$, $\tau_{\rm QA} = 180\hbar/t_1$.

Finally, as reported in main text, we analysed the scaling of the now determined coefficients $\mathscr{E}_{\rm bulk}(\tau_{\rm QA})$ for $L = 96$ with the annealing time $\tau_{\rm QA}$. As a last check, we verified that indeed

$E_{\rm res}(t=\tau_{\rm QA}) = \mathscr{E}_{\rm bulk}(\tau_{\rm QA})L^2 + \mathscr{E}_{\rm edge}(\tau_{\rm QA})L$ and found an excellent agreement (see figure D.2).

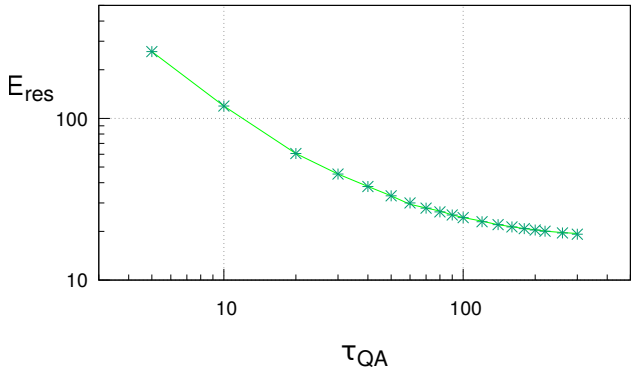

Figure D.2.: Dots: $E_{\rm res}(L;\tau_{\rm QA})$ for $L = 96$. The Haldane parameters are the same of Fig.]D.1 and paragrpah 3.2. The smooth line is the ansatz $E_{\rm res}(t=\tau_{\rm QA}) = \mathscr{E}_{\rm bulk}(\tau_{\rm QA})L^2 + \mathscr{E}_{\rm edge}(\tau_{\rm QA})L$, with the coefficients calculated through the procedure described in this paragraph.

E. Matrix elements of derivatives of the Hamiltonian in the Floquet basis

We want to calculate the matrix element of the operator $\partial\hat{H}/\partial\xi$, where ξ is a generic parameter (e.g. the inaccessible flux in the case of the current) between the Floquet modes $|\phi_\alpha(t)\rangle$. In what follows we will repeatedly make use of the Schrödinger equation for the modes,

$$\left(\hat{H} - i\hbar\frac{\partial}{\partial t}\right)|\phi_\alpha(t)\rangle = \varepsilon_\alpha\,|\phi_\alpha(t)\rangle\,, \tag{E.1}$$

where ε_α are the quasienergies. Therefore

$$\begin{aligned}
&\langle\phi_\alpha(t)|\partial_\xi\hat{H}(t)\,|\phi_\beta(t)\rangle = \\
&\quad=\partial_\xi\left[\langle\phi_\alpha(t)|\,\hat{H}(t)\,|\phi_\beta(t)\rangle\right] - \langle\partial_\xi\phi_\alpha(t)|\,\hat{H}(t)\,|\phi_\beta(t)\rangle - \langle\phi_\alpha(t)|\,\hat{H}(t)\,|\partial_\xi\phi_\beta(t)\rangle = \\
&\quad=\partial_\xi\left[\varepsilon_\alpha\delta_{\alpha\beta} + i\hbar\,\langle\phi_\alpha(t)|\,\partial_t\phi_\beta(t)\rangle\right] - i\hbar\,\langle\partial_\xi\phi_\alpha(t)|\,\partial_t\phi_\beta(t)\rangle - \varepsilon_\beta\,\langle\partial_\xi\phi_\alpha(t)|\,\phi_\beta(t)\rangle + \\
&\qquad- \varepsilon_\alpha\,\langle\phi_\alpha(t)|\,\partial_\xi\phi_\beta(t)\rangle + i\hbar\,\langle\partial_t\phi_\alpha(t)|\,\partial_\xi\phi_\beta(t)\rangle.
\end{aligned}$$

Making use of $\langle\partial_\xi\phi_\alpha(t)|\,\phi_\beta(t)\rangle = -\,\langle\phi_\alpha(t)|\,\partial_\xi\phi_\beta(t)\rangle$, we arrive at

$$\langle\phi_\alpha(t)|\,\partial_\xi\hat{H}(t)\,|\phi_\beta(t)\rangle = \partial_\xi\varepsilon_\alpha\delta_{\alpha\beta} + (\varepsilon_\beta - \varepsilon_\alpha)\,\langle\phi_\alpha(t)|\,\partial_\xi\phi_\beta(t)\rangle + i\hbar\partial_t\left[\langle\phi_\alpha(t)|\,\partial_\xi\phi_\beta(t)\rangle\right]. \tag{E.2}$$

If an average over one period, the third term vanishes because of the periodicity of the modes. Moreover, if $\alpha = \beta$, we get the Hellmann-Feynman theorem for Floquet systems, that is

$$\langle\langle\phi_\alpha(t)\left|\frac{\partial\hat{\mathcal{K}}(t)}{\partial\xi}\right|\phi_\alpha(t)\rangle\rangle = \partial_\xi\varepsilon_\alpha. \tag{E.3}$$

F. Details for chapter 4

F.1. Current operator of the Rice-Mele model

We imagine to put our 1D chain on a circular geometry, in such a way that $\hat{c}^\dagger_{N+1,A/B} \equiv \hat{c}^\dagger_{1,A/B}$, i.e., the cell number $N+1$ coincides with cell number 1. If we thread the ring with a magnetic flux $\Phi = \widetilde{A}L$, where $\widetilde{A}$ is a constant vector potential parallel to the ring, the hoppings get modified through Peierls substitution, e.g. $-J_1\hat{c}^\dagger_{j,B}\hat{c}_{j,A} \to -\mathrm{e}^{-ia\kappa_y/2}J_1\hat{c}^\dagger_{j,B}\hat{c}_{j,A}$, where we have defined, as usual $\kappa = \frac{L}{2\pi}\frac{\Phi}{\phi_0}$. Therefore the current operator can be calculated through $\hat{J}(t) = \frac{1}{\hbar}\partial_\kappa \hat{H}(t)|_{\kappa=0}$, which gives, in real space, the matrix elements

$$\widehat{J}_{\mathrm{RM}}(t) = \frac{a}{2\hbar}J_1(t)\sum_{j=1}^{N}\left(i\hat{c}^\dagger_{j,B}\hat{c}_{j,A} + \mathrm{H.c.}\right) + \frac{a}{2\hbar}J_2(t)\sum_{j=1}^{N}\left(i\hat{c}^\dagger_{j+1,A}\hat{c}_{j,B} + \mathrm{H.c.}\right) . \tag{F.1}$$

When PBC are employed, we can switch to momentum space. Here we have a 2×2 matrix for each k-point: $\hat{J}(t) = \sum_k^{BZ}\hat{J}(k,t) = \sum_{\mathbf{k}}^{\mathrm{BZ}}\left[\hat{c}^\dagger_{kA}\ \hat{c}^\dagger_{kB}\right]\left[\mathbb{J}(k,t)\right]\begin{bmatrix}\hat{c}_{kA}\\ \hat{c}_{kB}\end{bmatrix}$, with

$$\mathbb{J}(k,t) = \begin{pmatrix} 0 & -i\frac{a}{2\hbar}J_1(t) + i\frac{a}{2\hbar}J_2(t)\cos(k) + \frac{a}{2\hbar}J_2(t)\sin(k) \\ c.c. & 0 \end{pmatrix} . \tag{F.2}$$

The total current is then given by

$$\langle\hat{J}(t)\rangle = \mathrm{Tr}\left[\mathbb{J}(k,t)\mathbb{G}(k,t)\right] , \tag{F.3}$$

where we have defined, as usual

$$\mathbb{G}_{\alpha\beta}(k,t) = \langle\Psi(t)|\,\hat{c}^\dagger_{k,\beta}\hat{c}_{k,\alpha}\,|\Psi(t)\rangle \quad \alpha,\beta = A,B \tag{F.4}$$

F.2. Adiabatic perturbation theory for Rice-Mele Floquet modes

In this section, we make use of ref. [147] to calculate the occupation of the non-adiabatic band in the Rice Mele model at first order in ω. Using a rescaled time $s = t/\tau$, we make use of the following definitions:

$$M_{nm}(s) \equiv \langle u_n(s)| \dot{u}_m(s)\rangle \tag{F.5a}$$
$$\Lambda_{mn}(s) \equiv E_m(s) - E_n(s) \tag{F.5b}$$
$$\gamma_n(s) \equiv i\int_0^s \langle u_n(s')\big| \dot{u}_n(s')\rangle \mathrm{d}s' \tag{F.5c}$$
$$\zeta_n(s) \equiv \frac{1}{\hbar}\int_0^s \langle u_n(s')\big| \hat{H}(s') \big|u_n(s')\big\rangle \,\mathrm{d}s' \tag{F.5d}$$
$$J_{mn}(s) = \int_0^s \frac{|M_{mn}(s')|^2}{\Lambda_{mn}(s')}\mathrm{d}s' \,. \tag{F.5e}$$

Here $E_n(t)$ and $|u_n(t)\rangle$ are n-th eigenvalue and eigenstate of $\hat{H}(t)$ respectively. In the case of the Rice-Mele model $n = 0, 1$ for a given k-point (there are only two bands). Ref. [147] builds an adiabatic perturbation theory in $1/\tau$ for the time evolved state $|\Psi(s)\rangle$ as

$$|\Psi(s)\rangle = \sum_{p=0}^{\infty} \frac{1}{\tau^p} |\Psi^p(s)\rangle \,. \tag{F.6}$$

We suppose from now on that the initial state is the n-th eigenstate of the Hamiltonian and that the gaps are always non-zero. Therefore we indicate by $|\Psi_n(s)\rangle$ the evolved state at scaled time s after being initially prepared in the n-th eigenstate. The zero-th order term is the usual adiabatic approximation

$$\big|\Psi_n^0(s)\big\rangle = e^{i\gamma_n(s)} e^{-i\zeta_n(s)\tau} |u_n(s)\rangle \,. \tag{F.7}$$

The first order correction reads

$$\begin{aligned}\big|\Psi_n^1(s)\big\rangle =& i\hbar \sum_{m\neq n} e^{i\gamma_n(s)} e^{-i\zeta_n(s)\tau} J_{mn} |u_n(s)\rangle + \\ &+ i\hbar \sum_{m\neq n} e^{i\gamma_n(s)} e^{-i\zeta_n(s)\tau} \frac{M_{mn}(s)}{\Lambda_{mn}(s)} |u_m(s)\rangle + \\ &- i\hbar \sum_{m\neq n} e^{i\gamma_m(s)} e^{-i\zeta_m(s)\tau} \frac{M_{mn}(0)}{\Lambda_{mn}(0)} |u_m(s)\rangle \,.\end{aligned} \tag{F.8}$$

Let us write the evolution operator over one period at first order in $1/\tau$ for the Rice-Mele model. From now on we will omit the s-dependence of M, γ, ζ, J and Λ, since we will need them only at $s = 0$ and $s = \tau$ where they are equal thanks to the τ periodicity of the Hamiltonian.

$$\hat{U}(\tau, 0) = \begin{pmatrix} e^{i\gamma_0} e^{-i\zeta_0\tau} + i\hbar\, e^{i\gamma_0} e^{-i\zeta_0\tau} \dfrac{J_{10}}{\tau} & i\hbar\, e^{i\gamma_0} e^{-i\zeta_0\tau} \dfrac{M_{10}}{\tau\Lambda_{10}} - i\hbar\, e^{i\gamma_1} e^{-i\zeta_1\tau} \dfrac{M_{10}}{\tau\Lambda_{10}} \\ i\hbar\, e^{i\gamma_1} e^{-i\zeta_1\tau} \dfrac{M_{01}}{\tau\Lambda_{01}} - i\hbar\, e^{i\gamma_0} e^{-i\zeta_0\tau} \dfrac{M_{01}}{\tau\Lambda_{01}} & e^{i\gamma_1} e^{-i\zeta_1\tau} + i\hbar\, e^{i\gamma_1} e^{-i\zeta_1\tau} \dfrac{J_{01}}{\tau} \end{pmatrix} + \mathcal{O}(\frac{1}{\tau^2}) \,.$$

Now this expression is simplified by the fact that for the RM model we have $\zeta_0 = -\zeta_1$, $\gamma_0 = -\gamma_1$, $\Lambda_{10} = -\Lambda_{01}$. Moreover since we can always choose the instantaneous eigenstates to be real, follows $M_{01} = M_{10}$. From these facts it follows also that $J_{10} = -J_{01}$. Thus we can write

$$\hat{U}(\tau,0) = \begin{pmatrix} e^{i\gamma_0}e^{-i\zeta_0\tau}\left(1+i\hbar\,\frac{J_{10}}{\tau}\right) & -2\hbar\,\sin\left(\gamma_0-\zeta_0\tau\right)\frac{M_{10}}{\tau\Lambda_{10}} \\ 2\hbar\sin\left(\gamma_0-\zeta_0\tau\right)\,\frac{M_{10}}{\tau\Lambda_{10}} & e^{-i\gamma_0}e^{i\zeta_0\tau}\left(1-i\hbar\frac{J_{10}}{\tau}\right) \end{pmatrix} + \mathcal{O}(\frac{1}{\tau^2})\,, \tag{F.9}$$

or, in a more compact form

$$\begin{aligned} \hat{U}(\tau,0) = &\left[\cos\left(\gamma_0-\zeta_0\tau\right)-\hbar\sin\left(\gamma_0-\zeta_0\tau\,\right)\frac{J_{10}}{\tau}\right]\mathbb{1}+ \\ &+i\left[\sin\left(\gamma_0-\zeta_0\tau\right)+\hbar\cos\left(\gamma_0-\zeta_0\tau\,\right)\frac{J_{10}}{\tau}\right]\hat{\sigma}_z+ \\ &-2i\,\hbar\sin\left(\gamma_0-\zeta_0\tau\right)\,\frac{M_{10}}{\tau\Lambda_{10}}\hat{\sigma}_y\,. \end{aligned} \tag{F.10}$$

The eigenvalues are given by

$$\begin{aligned} \mu_\alpha = &\cos\left(\gamma_0-\zeta_0\tau\right)-\hbar\sin\left(\gamma_0-\zeta_0\tau\,\right)\frac{J_{10}}{\tau}\;\pm\;\left(-\sin^2\left(\gamma_0-\zeta_0\tau\,\right)\left(1+\frac{4\hbar^2M_{10}^2}{\tau^2\Lambda_{10}^2}\right)+\right. \\ &\left.-\hbar^2\frac{J_{10}^2}{\tau^2}\cos^2\left(\gamma_0-\zeta_0\tau\,\right)-2\hbar\frac{J_{10}}{\tau}\sin\left(\gamma_0-\zeta_0\tau\,\right)\cos(\gamma_0-\zeta_0)\right)^{1/2}. \end{aligned} \tag{F.11}$$

Notice that since we did not go to a further order in perturbation theory, we might be missing some term proportional to $1/\tau^2$. We will see later that this is not the case. If moreover $\sin\left(\gamma_0-\zeta_0\right)\neq 0$ we have[1]

$$\begin{aligned} \mu_\alpha =&\cos\left(\gamma_0-\zeta_0\tau\right)-\hbar\sin\left(\gamma_0-\zeta_0\tau\,\right)\frac{J_{10}}{\tau}\;\pm\;i\sin\left(\gamma_0-\zeta_0\tau\,\right)\left(1+\frac{4\hbar^2M_{10}^2}{\tau^2\Lambda_{10}^2}+\right. \\ &\left.+\hbar^2\frac{J_{10}^2}{\tau^2}\cot^2\left(\gamma_0-\zeta_0\tau\right)+2\hbar\frac{J_{10}}{\tau}\cot(\gamma_0-\zeta_0\tau)\right)^{1/2}= \\ =&\cos\left(\gamma_0-\zeta_0\tau\tau\right)-\hbar\sin\left(\gamma_0-\zeta_0\tau\right)\frac{J_{10}}{\tau}\pm \\ &\pm i\sin\left(\gamma_0-\zeta_0\tau\right)\left(1+\hbar\frac{J_{10}}{\tau}\cot(\gamma_0-\zeta_0\tau)+\hbar^2\frac{J_{10}^2}{2\tau^2}\cot^2\left(\gamma_0-\zeta_0\tau\right)+\right. \\ &\left.+\frac{2\hbar^2M_{10}^2}{\tau^2\Lambda_{10}^2}-\frac{1}{2}\hbar^2\frac{J_{10}^2}{2\tau^2}\cot^2\left(\gamma_0-\zeta_0\tau\right)+\mathcal{O}\left(\frac{1}{\tau^3}\right)\right)= \\ =&\cos\left(\gamma_0-\zeta_0\tau\right)-\hbar\sin\left(\gamma_0-\zeta_0\tau\right)\frac{J_{10}}{\tau}\pm \\ &\pm i\sin\left(\gamma_0-\zeta_0\tau\right)\left(1+\hbar\frac{J_{10}}{\tau}\cot(\gamma_0-\zeta_0\tau)+\frac{2\hbar^2M_{10}^2}{\tau^2\Lambda_{10}^2}+\mathcal{O}\left(\frac{1}{\tau^3}\right)\right)\,. \end{aligned} \tag{F.12}$$

[1] We use $(1+x)^{1/2} = 1+\frac{1}{2}x-\frac{1}{8}x^2+...$

The equation for the Floquet modes $|\phi_\alpha(0)\rangle = (v \;\; w)^{\mathrm{T}}$ is given by

$$\hat{U}(\tau,0)\,|\phi_\alpha(0)\rangle = \mu_\alpha\,|\phi_\alpha(0)\rangle \;\; .$$

Substituting eq. (F.9) and eq. (F.12) we get

$$\begin{cases} i\left[\sin(\gamma_0-\zeta_0\tau)+\hbar\cos(\gamma_0-\zeta_0\tau)\,\dfrac{J_{10}}{\tau}\right]v - 2\,\hbar\sin(\gamma_0-\zeta_0\tau)\;\dfrac{M_{10}}{\tau\Lambda_{10}}w = \\ \qquad = \pm i\sin(\gamma_0-\zeta_0\tau)\left(1+\hbar\dfrac{J_{10}}{\tau}\cot(\gamma_0-\zeta_0\tau)+\dfrac{2\hbar^2M_{10}^2}{\tau^2\Lambda_{10}^2}\right)v & \text{(F.13a)} \\ -i\left[\sin(\gamma_0-\zeta_0\tau)+\hbar\cos(\gamma_0-\zeta_0\tau)\,\dfrac{J_{10}}{\tau}\right]w + 2\,\hbar\sin(\gamma_0-\zeta_0\tau)\;\dfrac{M_{10}}{\tau\Lambda_{10}}v = \\ \qquad = \pm i\sin(\gamma_0-\zeta_0\tau)\left(1+\hbar\dfrac{J_{10}}{\tau}\cot(\gamma_0-\zeta_0\tau)+\dfrac{2\hbar^2M_{10}^2}{\tau^2\Lambda_{10}^2}\right)w\;. & \text{(F.13b)} \end{cases}$$

In the adiabatic approximation the eigenvectors are given by $(1 \;\; 0)^{\mathrm{T}}$ and $(0 \;\; 1)^{\mathrm{T}}$. Let us choose the eigenvalue with + sign, which goes to $(1 \;\; 0)^{\mathrm{T}}$ when $\tau \to \infty$. Eq.(F.13a) then gives

$$\frac{w}{v} = -\frac{\hbar M_{10}}{\tau\Lambda_{10}} + \mathcal{O}\left(\frac{1}{\tau^2}\right) \;\; . \tag{F.14}$$

The same result can of course be obtained through eq.(F.13b). The ratio w/v, even if now the vector is not normalized, is equal to w of the normalized vector at first order. Therefore is a good quantity to calculate the variation of the occupation.
However we have to check what are the effects of the inclusion of $\dfrac{1}{\tau^2}\left|\Psi_n^2(\tau)\right\rangle$ in the calculation of the evolution operator $\hat{U}(\tau,0)$. Following ref. [147], the additional terms in $\hat{U}(\tau,0)$ will be of the form

$$\frac{1}{\tau^2}(\cos(\gamma_0-\zeta_0\tau)+i\sin(\gamma_0-\zeta_0\tau))\,[A\hat{\sigma}_z+B\hat{\sigma}_y+C\hat{\sigma}_x] \;\; . \tag{F.15}$$

The only additional correction of order $1/\tau^2$ to the eigenvalues will come from the $\hat{\sigma}_z$ term thanks to the double product with the constant term multiplying $\hat{\sigma}_z$ in (F.10), e.g. $\mu_\alpha = \sqrt{\ldots + 2i\dfrac{A}{\tau^2}\sin(\gamma_0-\zeta_0)\,(\cos(\gamma_0-\zeta_0)+i\sin(\gamma_0-\zeta_0))}$. Anyway after the expansion of the square root, the resulting term will exactly cancel out the $\hat{\sigma}_z$ term on the left hand side. $\hat{\sigma}_y$ and $\hat{\sigma}_y$ terms instead just give higher order contributions. Therefore formula (F.14) for the corrections to eigenstates is correct. An immediate consequence is that the corrections to the population of the adiabatic band for a given k are:

$$n_{ad,k} = 1 - \left|\frac{\hbar^2 M_{10}(k,0)}{\tau\Lambda_{10}(k,0)}\right|^2 + \mathcal{O}\left(\frac{1}{\tau^3}\right) \;\; , \tag{F.16}$$

where we have restored the time dependence and added a k-dependence to the various terms. This last quantity can be conveniently calculated by rewriting M_{10} as

$$M_{10}(k,0) = \langle u_{1,k}(0)|\,\dot{u}_{0,k}(0)\rangle = -\frac{\langle u_{1,k}(0)|\,\partial_s\hat{H}(k,s)|_{s=0}\,|u_{0,k}(0)\rangle}{\Lambda_{10}(k,0)} \;\; . \tag{F.17}$$

F.2.1. Explicit calculation

Formula (F.16) can be explicitly calculated. Using eq. (4.5) and (4.7) we easily see that

$$\partial_s \hat{H}(k,s)|_{s=0} = \partial_s R_z(k,s)|_{s=0}\hat{\sigma}_z = 2\pi\Delta_0\hat{\sigma}_z \ . \tag{F.18}$$

This fact tells us immediately that at first order in $1/\tau$, the non adiabatic corrections to the populations are quadratic in Δ_0. The gap is equal to $\Lambda_{10} = 2E_{1,k}(t)$. At the initial time $s = 0$ the eigenvectors are given by

$$|u_{1,k}(0)\rangle = \frac{1}{\sqrt{2}E_{1,k}(0)} \begin{pmatrix} E_{1,k}(0) \\ R_x(k,0) + iR_y(k,0) \end{pmatrix}; \tag{F.19}$$

$$|u_{0,k}(0)\rangle = \frac{1}{\sqrt{2}E_{1,k}(0)} \begin{pmatrix} iR_y(k,0) - R_x(k,0) \\ E_{1,k}(0) \end{pmatrix} \ . \tag{F.20}$$

Substituting these last expressions in eq.(F.17), we obtain

$$M_{10}(k,0) = -\frac{\pi\Delta_0}{E_{1,k}^2(0)}(iR_y(k,0) - R_x(k,0)) \ . \tag{F.21}$$

Now since $E_{1,k}^2(0) = R_x^2(k,0) + R_y^2(k,0)$,

$$n_{ad,k} = 1 - \frac{\hbar^2\pi^2\Delta_0^2}{4\tau^2 E_{1,k}^4(0)} + \mathcal{O}(\frac{1}{\tau^3}) = \tag{F.22}$$

$$= 1 - \frac{\hbar^2\pi^2\Delta_0^2}{4\tau^2 J_0^4}\left(\frac{1}{2 + 2\delta_0^2/J_0^2 + 2(1-\delta_0^2/J_0^2)\cos(ka)}\right)^2 + \mathcal{O}\left(\frac{1}{\tau^3}\right) \tag{F.23}$$

$$= 1 - \frac{\hbar^2\omega^2\Delta_0^2}{64 J_0^4}\left(\frac{1}{1 + \delta_0^2/J_0^2 + (1-\delta_0^2/J_0^2)\cos(ka)}\right)^2 + \mathcal{O}\left(\omega^3\right) \ . \tag{F.24}$$

In figure F.1 we compare the numerical calculations and formula (F.22) for $\delta_0 = 1.2J_0$, $\Delta_0 = 3.6J_0$, $\omega = 0.05J_0/\hbar$. The agreement is excellent. We notice also that when $\delta_0 = J_0$ the corrections become k-independent as shown in Fig. F.2, but the agreement is still very good. It is interesting at this point to consider the average $\bar{n}_{ad}$ of the population of the adiabatic band over the BZ.

$$\bar{n}_{ad} = \int_0^{2\pi} \frac{\mathrm{d}k}{2\pi} n_{ad,k} = 1 - \frac{\pi^2\hbar^2\Delta_0^2\left(J_0^2 + \delta_0^2\right)}{128\ \tau^2 J_0^3\ \delta_0^3} + \mathcal{O}\left(\frac{1}{\tau^3}\right) \ . \tag{F.25}$$

If we express Δ_0 in terms of δ_0 as $\Delta_0 = r\delta_0$ and compute the derivative with respect to δ_0 we get $\mathrm{d}\bar{n}_{ad}/\mathrm{d}\delta_0 \propto (\delta_0^2 - J_0^2)/\delta_0^2$. Therefore the average corrections to the occupations for fixed J_0 and r have a minimum at $|\delta_0| = |J_0|$.

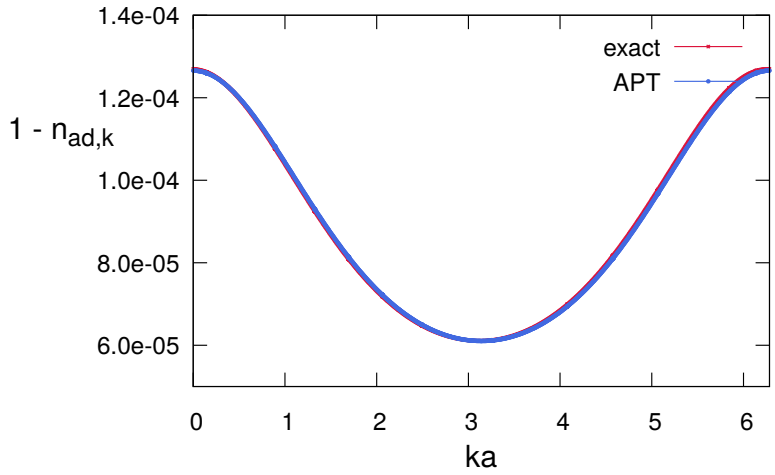

Figure F.1.: Deviations from 1 of the occupations of the adiabatic band. Comparisons between numerical results and formula (F.22) for $\delta_0 = 1.2J_0$, $\Delta_0 = 3.6J_0$, $\omega = 0.05J_0/\hbar$.

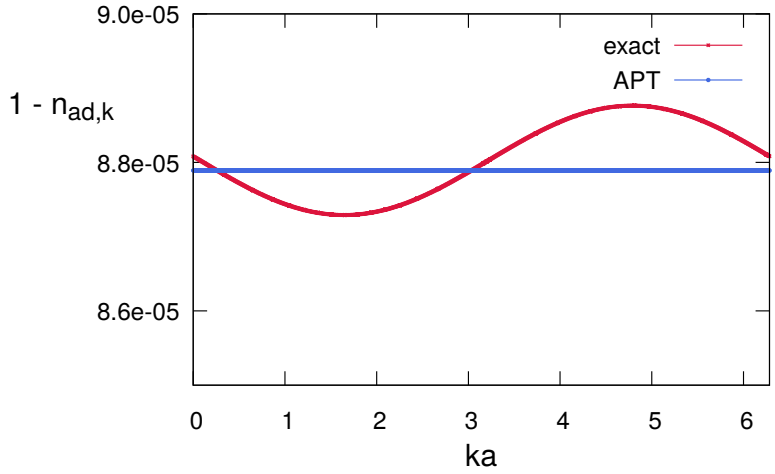

Figure F.2.: Deviations from 1 of the occupations of the adiabatic band. Comparisons between numerical results and formula (F.22) for $\delta_0 = J_0$, $\Delta_0 = 3.0J_0$, $\omega = 0.05J_0/\hbar$. Notice that the analytical curve is k-independent.

F.2.2. High frequency expansion for the Floquet Hamiltonian

If the frequency ω is bigger than any other energy scale in the system, we can get some analytical insight into the properties of the Floquet Hamiltonian $\hat{H}_F$ through the high-frequency expansion of appendix B. In this case, since the monochromatic driving appears in the Hamiltonian with a single frequency (i.e the driving term is not an exponential as in the case of driven graphene), the only Fourier components of the Hamiltonian are H_0 and $H_{\pm 1}$. We are interested only in the quasienergy spectrum and therefore we compute only the gauge-independent terms. At first order we have

$$\hat{H}_F^{(1)} \approx \hat{H}_0 + \frac{1}{\hbar\omega}\left[\hat{H}_{+1}, \hat{H}_{-1}\right] \ . \tag{F.26}$$

The 0-th component gives only a uniform n.n. hopping

$$\hat{H}_0 = -J_0 \sum_{j=1}^{N} \left(\hat{c}^\dagger_{j,B}\hat{c}_{j,A} + \hat{c}^\dagger_{j+1,A}\hat{c}_{j,B} + \text{h.c.}\right) \ , \tag{F.27}$$

e.g. the average Hamiltonian is the one of a band metal. We notice that at lowest order time-reversal invariance hold and $\hat{H}_F^{*(0)}(k) = \hat{H}_F^{(0)}(-k)$ [2].
The +1-th Fourier component reads instead

$$\hat{H}_1 = \underbrace{-\frac{\delta_0}{2}\sum_{j=1}^{N}\left(\hat{c}^\dagger_{j,B}\hat{c}_{j,A} + \text{h.c.}\right)}_{I} + \underbrace{\frac{\delta_0}{2}\sum_{j=1}^{N}\left(\hat{c}^\dagger_{j+1,A}\hat{c}_{j,B} + \text{h.c.}\right)}_{II} - \underbrace{\frac{i\Delta_0}{2}\sum_{j=1}^{N}\left(\hat{c}^\dagger_{j,A}\hat{c}_{j,A} - \hat{c}^\dagger_{\text{j,B}}\hat{c}_{\text{j,B}}\right)}_{III} \ . \tag{F.28}$$

The -1 one, being the hermitian conjugate of H_1, e.g. $H_{-1} = H_1^\dagger$, changes only by a sign in the on-site term.
We will repeatedly make use of the following fermion commutator identity

$$\begin{aligned}\left[\hat{a}^\dagger_\alpha\hat{a}_\beta, \hat{a}^\dagger_\gamma\hat{a}_\delta\right] =& \hat{a}^\dagger_\alpha\left[\hat{a}_\beta, \hat{a}^\dagger_\gamma\hat{a}_\delta\right] + \left[\hat{a}^\dagger_\alpha, \hat{a}^\dagger_\gamma\hat{a}_\delta\right]\hat{a}_\beta = \\ =& \hat{a}^\dagger_\alpha\left(\left\{\hat{a}_\beta, \hat{a}^\dagger_\gamma\right\}\hat{a}_\delta + \hat{a}^\dagger_\gamma\left\{\hat{a}_\beta, \hat{a}_\delta\right\}\right) + \left(\left\{\hat{a}^\dagger_\alpha, \hat{a}^\dagger_\gamma\right\}\hat{a}_\delta - \hat{a}^\dagger_\gamma\left\{\hat{a}^\dagger_\alpha, \hat{a}_\delta\right\}\right)\hat{a}_\beta = \\ =& \hat{a}^\dagger_\alpha\hat{a}_\delta\delta_{\beta\gamma} - \hat{a}^\dagger_\gamma\hat{a}_\beta\delta_{\alpha\delta} \ .\end{aligned} \tag{F.29}$$

Now the commutator involving the two hopping terms I and II gives 0, since they are equal in H_1 and H_{-1}, e.g. $[I_1 + II_1, I_{-1} + II_{-1}] = 0$. We only have to compute then, the terms involving both hopping and on-site terms.

$$\begin{aligned}[I_1, III_{-1}] =& -i\frac{\delta_0\Delta_0}{4}\sum_{j,j'=1}^{N}\left[\hat{c}^\dagger_{j,B}\hat{c}_{j,A} + \text{h.c.}, \hat{c}^\dagger_{j,A}\hat{c}_{j,A} - \hat{c}^\dagger_{j,B}\hat{c}_{j,B}\right] = \\ =& -i\frac{\delta_0\Delta_0}{4}\sum_{j=1}^{N}\left(2\hat{c}^\dagger_{j,B}\hat{c}_{j,A} - 2\hat{c}^\dagger_{j,A}\hat{c}_{j,B}\right) \ ;\end{aligned} \tag{F.30a}$$

[2] $\hat{H}_F^{(0)}(k) = \sum_k^{BZ}\left(-J_0\left(1 + e^{-ikx}\right)\hat{c}^\dagger_{kA}\hat{c}_{kB} + \text{h.c.}\right)$

$$
\begin{aligned}
[II_1, III_{-1}] &= i\frac{\delta_0\Delta_0}{4}\sum_{j,j'=1}^{N}\left[\hat{c}^\dagger_{j+1,A}\hat{c}_{j,B} + \text{h.c.}\,, \hat{c}^\dagger_{j,A}\hat{c}_{j,A} - \hat{c}^\dagger_{j,B}\hat{c}_{j,B}\right] = \\
&= i\frac{\delta_0\Delta_0}{4}\sum_{j=1}^{N}\left(-2\hat{c}^\dagger_{j+1,A}\hat{c}_{j,B} + 2\hat{c}^\dagger_{j,B}\hat{c}_{j+1,A}\right)\,.
\end{aligned}
\tag{F.30b}
$$

Since the on site term differs from one Fourier component to the other only by a sign, we have $[III_1, I_{-1}] = [I_1, III_{-1}]$ and $[III_1, II_{-1}] = [II_1, III_{-1}]$.
After gathering together all the contributions, we obtain

$$
\hat{H}_F = -\left(J_0 + i\frac{\delta_0\Delta_0}{\hbar\omega}\right)\sum_{j=1}^{N}\left(\hat{c}^\dagger_{j,B}\hat{c}_{j,A} + \hat{c}^\dagger_{j+1,A}\hat{c}_{j,B}\right) + \text{h.c.} + \mathcal{O}\left(\frac{1}{\omega^2}\right)\,. \tag{F.31}
$$

At first order in $1/\omega$ we still have metal, but the Hamiltonian has become complex. This implies the breaking of time-reversal symmetry.

G. Aharonov-Anandan phase and Floquet systems

G.1. Aharanov-Anandan phase

In their 1987 paper [148], Aharonov and Anandan generalized the notion of geometric phase to any state undergoing a cyclic evolution, without the necessity for an adiabatic driving of the system. By cyclic evolution, we mean that after a time τ, the state $|\Psi\rangle$ goes back to itself apart from a phase factor:

$$|\Psi(\tau)\rangle = e^{i\phi} |\Psi(0)\rangle \ . \tag{G.1}$$

The mathematical arena to study this phenomenon is the *projective* Hilbert space $\mathscr{P}$. This is constructed by identifying all the vectors in $\mathscr{H}$ that differ by a multiplicative complex number (different from zero). This identification defines an equivalence relation and its classes are the elements of $\mathscr{P}$ and are called *rays*[1]. Therefore we have defined the map $\Pi : \mathscr{H} \to \mathscr{P}$, such that $\Pi(|\psi\rangle) = \{|\psi'\rangle = c\,|\psi\rangle\,, c \in \mathbb{C} \setminus \{0\}\}$.

At first glance, it could seem paradoxical to describe the effect of a phase by going into a space in which phases do not matter. What we are going to prove, is that the phase acquired by the time evolved cyclic state depend only on the path swept in $\mathscr{P}$, which is closed because of eq. (G.1). More formally, if $C(t)$ with $t \in [0, \tau]$ is the curve described by the state $|\psi(t)\rangle$ satisfying eq. (G.1), $\Pi(C) \equiv \tilde{C}$ is such that $\tilde{C}(\tau) = \tilde{C}(0)$.
Now we define $\left|\tilde{\psi}(t)\right\rangle = e^{-if(t)} |\psi(t)\rangle$, with the constraint $f(\tau) - f(0) = \phi$, implying $\left|\tilde{\psi}(\tau)\right\rangle = \left|\tilde{\psi}(0)\right\rangle$. Then the Schrödinger equation for $|\psi\rangle$ reads

$$-\frac{df}{dt} = \frac{1}{\hbar} \langle\psi(t)| \hat{H}(t) |\psi(t)\rangle - i \left\langle\tilde{\psi}(t)\right| \frac{d}{dt} \left|\tilde{\psi}(t)\right\rangle \Longrightarrow \tag{G.2}$$

$$\Longrightarrow \phi = f(\tau) - f(0) = -\frac{1}{\hbar} \int_0^\tau \langle\psi(t)| \hat{H}(t) |\psi(t)\rangle + i \int_0^\tau \left\langle\tilde{\psi}(t)\right| \frac{d}{dt} \left|\tilde{\psi}(t)\right\rangle \ . \tag{G.3}$$

Therefore we can extract the geometrical part of the phase by subtracting the dynamical one

[1] Otherwise we could have said that a ray is the set of all the elements of $\mathscr{H}$ having the same projector.

$\zeta(\tau)$:

$$\gamma \equiv \phi + \zeta(\tau) = \phi + \frac{1}{\hbar}\int_0^\tau \langle\psi(t)|\,\hat{H}(t)\,|\psi(t)\rangle\,dt \tag{G.4}$$

$$= i\int_0^\tau \left\langle\tilde{\psi}(t)\right|\frac{d}{dt}\left|\tilde{\psi}(t)\right\rangle dt = i\oint \left\langle\tilde{\psi}\right| d\tilde{\psi}\rangle\ . \tag{G.5}$$

Eq. (G.4) and (G.5) are two possible definitions of the Aharonov-Anandan phase. Let us see why it has a geometric nature.
First of all, on the contrary of the dynamical phase, γ is independent of the rate at which the curve, as seen from eq. (G.5). Secondly, it is universal in the sense that for every Hamiltonian $\hat{H}(t)$ generating the same $\tilde{C}$ in $\mathscr{P}$, γ does not change. Indeed, an appropriate choice of $f(t)$ that accounts for the different dynamical phase, leads to the same $\left|\tilde{\psi}(t)\right\rangle$. Conversely, different choices of $\left|\tilde{\psi}\right\rangle$, lead to the same γ. For example, considering $\left|\tilde{\psi}_2(t)\right\rangle = e^{-i\alpha(t)}\left|\tilde{\psi}_1(t)\right\rangle$, with $\alpha(\tau) = \alpha(0) + 2\pi n$ implies

$$\gamma_2 = \int_0^\tau \left\langle\tilde{\psi}_2(t)\right|\frac{d}{dt}\tilde{\psi}_2(t)\rangle dt = 2\pi n + \gamma_1\ . \tag{G.6}$$

All these three facts confirm the geometrical nature of γ. This means that the geometrical part of the phase accumulated by two states, defined by eq. (G.4), whose curves in $\mathscr{P}$ are identical, will be the same.

Clearly, Berry phase [73] is a special case of Aharonov-Anandan phase [148]. In that case the adiabatic evoution is a mean to ensure the cyclicity of the time evolved state, which is at any time an eigenstate of the Hamiltonian.

G.2. Dynamical and geometrical contributions to quasienergies

A Floquet state is a special case of the cyclic evolution discussed before. In this case the time-periodicity of the Hamiltonian guarantees the existence of solutions of the Schrödinger equation that undergo a cyclic evolution, e.g. the Foquet states: $|\psi_\alpha(\tau)\rangle = e^{-\frac{i}{\hbar}\varepsilon_\alpha\tau}\,|\psi_\alpha(0)\rangle$. From the discussion above, we deduce that the quasienergy has two contributions, one dynamical and one geometrical. In particular, to obtain the geometrical part, we must multiply the states $|\psi_\alpha(t)\rangle$ by a phase $\exp(-if(t))$ such that $f(\tau) - f(0) = -\varepsilon_\alpha\tau/\hbar$. The simplest choice is of course $f(t) = -\varepsilon_\alpha t/\hbar$. This means that for each point in the projective Hilbert space along the curve, we take the Floquet modes [2] as the representative of the specific ray

[2] We remark that the Floquet modes by themselves do not satisfy the time-dependent Schrödinger equation. The unitary evolution generates also the phase factors.

equivalence class. Therefore, using formulas (G.4) and (G.5)

$$\frac{\tau}{\hbar}\,\varepsilon_\alpha = \zeta_\alpha - \gamma_\alpha \;; \tag{G.7a}$$

$$\zeta_\alpha = \frac{1}{\hbar}\int_0^\tau \langle\phi_\alpha(t)|\,\hat{H}(t)\,|\phi_\alpha(t)\rangle\,dt \;; \tag{G.7b}$$

$$\gamma_\alpha = i\int_0^\tau \langle\phi_\alpha(t)|\,\partial_t\phi_\alpha(t)\rangle dt \;. \tag{G.7c}$$

We could have naively obtained these equations by projecting over $\langle\phi_\alpha|$ the Schrödinger equation (E.1) for the mode $|\phi_\alpha\rangle$ and averaging over one period. However, the Aharonov-Anandan construction give to them a clear interpretation. Eq. (G.7c) is a perfect analogous of the Berry phase for a band insulator. The difference is that the Floquet modes have taken the place of the periodic part of the Bloch wavefunctions and we derivate with respect to time rather than quasimomentum.
The AA phase can be calculated numerically with the usual Berry phase trick [145]

$$\gamma_\alpha = -\mathrm{Im}\log\prod_{j=0}^{N-1}\langle\phi_\alpha(t_j)|\,\phi_\alpha(t_{j+1})\rangle \;, \tag{G.8}$$

where $t_j \in [0,\tau]$, $t_0 = 0, t_N = \tau$. It can be justified by inserting $|\phi(t+dt)\rangle = |\phi(t)\rangle + dt\,|\partial_t\phi(t)\rangle + O(dt^2)$ and keeping only the leading term. One should be careful in a direct calculation of equations G.7 because of quasienergy folding.

We derive now equivalent expressions for the geometrical and dynamical contributions [46, 149]. First of all, if we insert the Fourier expansion for the modes

$$|\phi_\alpha(t)\rangle = \sum_{m=-\infty}^{+\infty}|\chi_{\alpha,m}\rangle\,\mathrm{e}^{im\omega t} \tag{G.9}$$

in eq. (G.7a) we get

$$\zeta\alpha = \frac{\tau}{\hbar}\bar{H}_\alpha = \frac{\tau}{\hbar}\varepsilon_\alpha \; - \hbar\omega\sum_{m=-\infty}^{+\infty} m\langle\chi_{\alpha,m}\,|\chi_{\alpha,m}\rangle \;, \tag{G.10}$$

where we have defined $\bar{H}_\alpha$ to be the mean energy of a Floquet mode, e.g. $\bar{H}_\alpha \equiv \langle\langle\phi_\alpha|\hat{H}(t)|\phi_\alpha\rangle\rangle = \hbar\zeta_\alpha/\tau$. Now we can massage also the expression for the geometric phase. Defining $\lambda \equiv \omega t$, we make the periodic boundary condition for the modes frequency independent, $|\phi_\alpha(\lambda+2\pi)\rangle = |\phi_\alpha\rangle$. Moreover $\hat{\mathcal{K}} = \hat{H} - i\hbar\partial_t = \hat{H} - i\hbar\omega\partial_\lambda$: Now we can apply the Hellmann-Feynman theorem (E.3) to the derivative with respect to ω and use $\partial_\omega\hat{\mathcal{K}(\lambda)} = -i\hbar\partial_\lambda = -i\hbar\partial_t/\omega$

$$\partial_\omega\varepsilon_\alpha = \langle\langle\phi_\alpha\left|\partial_\omega\hat{\mathcal{K}}\right|\phi_\alpha\rangle\rangle = -i\frac{\hbar}{\omega}\frac{1}{\tau}\int_0^\tau\langle\phi_\alpha(t)|\,\partial_t\phi_\alpha(t)\rangle dt \implies$$

$$\implies \gamma_\alpha = -\frac{2\pi}{\hbar}\frac{\partial\varepsilon_\alpha}{\partial\omega} \;. \tag{G.11}$$

From this point of view Berry's adiabatic phase is special case of the situation described above. There the frequency of the driving is much smaller than the gap that separates the ground state from the excited ones. Then for the adiabatic theorem, the Floquet state (that is also an eigenstate of $\hat{H}$) and the actual time-evolved state $|\Psi(t)\rangle$ coincide. We stress that apart from the aforementioned adiabatic case, there is no general recipe to prepare a Floquet state in a closed system.

H. The theorem by Avron and Kons on the zero-ω limit of transported charge

We reproduce here the theorem of Avron and Kons [122] on the analytical properties of the transported charge in a constant electric field. We make some small formal adaptation to our case of pumping in time dependent systems. We start with a time-periodic Hamiltonian $\hat{H}(t)$, of period $\tau = 2\pi/\omega$, such as the one of the driven Rice-Mele model of eq. (4.1). If we rescale time as $s = t/\tau$, the Schrödinger equation for the evolution operator for a given period τ, that we call $\hat{U}_\tau(s, s')$, becomes

$$i\hbar \frac{d}{ds}\hat{U}_\tau(s, s') = \tau \hat{H}(s)\hat{U}_\tau(s, s'). \tag{H.1}$$

With this simple rewriting we get this preliminary result on the analytic properties of the evolution operator:

Proposition. *Given a bounded Hamiltonian $\hat{H}$, $\hat{U}_\tau(s, 0)$ and $\hat{U}^\dagger_\tau(s, 0)$ are entire functions of τ.*

Proof. This fact fact comes from the absolute convergence of the Dyson series. This can be proven by using the fact that $\hat{H}$ is a bounded operator. For simplicity we consider the Dyson series evolution operator over one period

$$\hat{U}_\tau(1, 0) = \sum_{n=0}^{\infty} \frac{(-i)^n \tau^n}{n!} \int_0^1 dt_1 \cdots \int_0^{t_n - 1} dt_n \hat{H}(t_1) \cdot \hat{H}(t_2) \cdots \hat{H}(t_n)$$

If the Hamiltonian is bounded by a positive constant M, we can write the inequality

$$\begin{aligned} \hat{U}_\tau(1, 0) \leq & \sum_{n=0}^{\infty} \frac{\tau^n}{n!} \int_0^1 dt_1 \cdots \int_0^{t_n - 1} dt_n \left|\left| \hat{H}(t_1) \cdot \hat{H}(t_2) \cdots \hat{H}(t_n) \right|\right| \leq \\ \leq & \sum_{n=0}^{\infty} \frac{\tau^n}{(n!)^2} M^n \ . \end{aligned}$$

The last series is absolutely convergent for any finite τ. □

This means that if we consider τ to belong to the whole complex plane, $\hat{U}_\tau(s, 0)$ will be analytic everywhere, up to a singularity in $\tau = \infty$. An immediate consequence is the following statement:

Corollary. *If $|\Psi(0)\rangle$ is the initial state of our system (which we take to be τ-independent) then the expectation value of the current operator $\hat{J}$*

$$\langle \hat{J} \rangle(\tau; s) = \langle \Psi_0 | \, \hat{U}_\tau^\dagger(s,0) \hat{J} \, \hat{U}_\tau(s,0) \, | \Psi_0 \rangle \tag{H.2}$$

is an entire function of τ.

Of course the same conclusions can be drawn for the expectation value of any bounded operator. The fact that $\langle \hat{J} \rangle(\tau; s)$ is an entire function means that it must have some kind of singularity (pole or essential) at $\tau = \infty$ or, equivalently, at $\omega = 0$, unless it is constant[1]. The theorem of Avron and Kons clarifies the nature of the singularity.

Theorem. *If the Hamiltonian $\hat{H}$ and the current operator $\hat{J}$ are bounded, the expectation value $\langle \hat{J} \rangle(\omega; s)$ is an analytic function of ω with an isolated essential singularity in $\omega = 0$, unless it is constant for every ω.*

Proof. Because of corollary the Laurent expansion of $\langle \hat{J} \rangle(\tau; s)$ around $\tau = 0$ has infinite radius of convergence. Therefore it cannot have negative powers of τ, or equivalently positive powers of ω around $\omega = 0$. If the singularity at $\omega = 0$ was a pole, $\langle \hat{J} \rangle(\omega; s)$ would diverge as $\omega \to 0$ along any direction in the complex plane. This means that for any constant $M > 0$ there is a $\delta > 0$ such that for any $|\tau| < \delta$, $\langle \hat{J} \rangle(\omega; s) > M$. However, since $\hat{J}$ is a bounded operator, there exists a constant M' such that $\langle \hat{J} \rangle(\omega; s) < M'$ for any real $\omega > 0$ [2]. The contradiction of these inequalities implies that the current cannot have a pole of finite order at $\omega = 0$. □

These considerations are true also for the pumped charge over a finite number m of periods, which is

$$Q(\omega; m) = \lim_{L \to \infty} \frac{1}{L} m\tau \int_0^m \langle \hat{J} \rangle(\omega; s) \mathrm{d}s \; .$$

Indeed, for any finite τ and m, $Q(\omega; m)$ will also be an entire function of ω because it is the integral of an analytic function over a finite domain of s.

[1] Indeed for Liouville's theorem [150] every entire function f that is bounded everywhere including infinity is constant. Thus, if f is a non-constant entire function, the Taylor series $f(z) = \sum_{n=0}^{\infty} a_n z^n$ will have an infinite radius of convergence and at least one $a_n \neq 0$ for $n > 0$. Considering the Taylor series for $f(1/z)$, it is evident how it has a singularity in $1/z = 0$, which implies a singularity for $f(z)$ in $z = \infty$. Specifically, if there are infinitely many a_n different from 0, the singularity is essential, otherwise it is a pole.

[2] Every bounded operator $\hat{A}$ is such that has a finite norm [151], meaning that the expectation value over any vector of finite norm is smaller than some constant. Since for any real ω the states over which we compute the expectation value have norm 1, the inequality holds.

Acknowledgements

I want to express my deepest gratitude to my supervisor Prof. Giuseppe Santoro for his precious guidance and friendly help throughout my PhD.
I am much indebted to Dr. Angelo Russomanno for his kind support and stimulating collaboration.
I warmly thank Dr. Adriano Amaricci for giving me the opportunity to further explore the physics of topological insulators. More recently, Prof. Roberta Citro has been a precious collaborator in my work on quantum pumping, to her I therefore want to address my words of thanks.
Finally, I would like to thank the many colleagues and friends with whom I have shared my journey during these years in Sissa: Caterina, Maja, Francesco, Simone, Tommaso, Mariam and Matteo S. and Matteo W..

Bibliography

[1] N. David Mermin. The topological theory of defects in ordered media. *Reviews of Modern Physics*, 51(3):591, 1979.

[2] David J. Thouless. *Topological quantum numbers in nonrelativistic physics*. World Scientific, 1998.

[3] Grigory E. Volovik. *The universe in a helium droplet*, volume 117. Oxford University Press on Demand, 2003.

[4] Alexander Altland and Ben D. Simons. *Condensed matter field theory*. Cambridge University Press, 2010.

[5] Klaus Von Klitzing, Gerhard Dorda, and Michael Pepper. New method for high-accuracy determination of the fine-structure constant based on quantized Hall resistance. *Physical Review Letters*, 45(6):494, 1980.

[6] D.J. Thouless, M. Kohmoto, M.P. Nightingale, and M. Den Nijs. Quantized Hall conductance in a two-dimensional periodic potential. *Physical Review Letters*, 49(6):405, 1982.

[7] Mahito Kohmoto. Topological invariant and the quantization of the Hall conductance. *Annals of Physics*, 160(2):343–354, 1985.

[8] C. L. Kane and E. J. Mele. Quantum Spin Hall Effect in Graphene. *Phys. Rev. Lett.*, 95:226801, Nov 2005.

[9] C. L. Kane and E. J. Mele. Z_2 Topological Order and the Quantum Spin Hall Effect. *Phys. Rev. Lett.*, 95:146802, Sep 2005.

[10] M. Z. Hasan and C. L. Kane. *Colloquium*: Topological insulators. *Rev. Mod. Phys.*, 82:3045–3067, Nov 2010.

[11] Xiao-Liang Qi and Shou-Cheng Zhang. Topological insulators and superconductors. *Rev. Mod. Phys.*, 83:1057–1110, Oct 2011.

[12] Masatoshi Sato and Yoichi Ando. Topological superconductors: a review. *Reports on Progress in Physics*, 80(7):076501, 2017.

[13] Binghai Yan and Claudia Felser. Topological materials: Weyl semimetals. *Annual Review of Condensed Matter Physics*, 8:337–354, 2017.

[14] Bertrand I Halperin. Quantized Hall conductance, current-carrying edge states, and the existence of extended states in a two-dimensional disordered potential. *Physical Review B*, 25(4):2185, 1982.

[15] Yasuhiro Hatsugai. Chern number and edge states in the integer quantum Hall effect. *Physical review letters*, 71(22):3697, 1993.

[16] Dmytro Pesin and Allan H Macdonald. Spintronics and pseudospintronics in graphene and topological insulators. *Nature Materials*, 11(5):409, 2012.

[17] Hua Chen, Wenguang Zhu, Di Xiao, and Zhenyu Zhang. Co oxidation facilitated by robust surface states on Au-covered topological insulators. *Physical review letters*, 107(5):056804, 2011.

[18] Catherine R Rajamathi, Uttam Gupta, Nitesh Kumar, Hao Yang, Yan Sun, Vicky Süß, Chandra Shekhar, Marcus Schmidt, Horst Blumtritt, Peter Werner, et al. Weyl semimetals as hydrogen evolution catalysts. *Advanced Materials*, 29(19), 2017.

[19] Shou-Cheng Zhang Xiao Zhang. Chiral interconnects based on topological insulators, 2012.

[20] Timothy M Philip and Matthew J Gilbert. High-performance nanoscale topological energy transduction. *Scientific Reports*, 7, 2017.

[21] C.W.J. Beenakker. Search for Majorana fermions in superconductors. *Annual Review of Condensed Matter Physics*, 4(1):113–136, 2013.

[22] Sankar Das Sarma, Michael Freedman, and Chetan Nayak. Majorana zero modes and topological quantum computation. *NPJ Quantum Information*, 1:15001, 2015.

[23] D. J. Thouless. Quantization of particle transport. *Phys. Rev. B*, 27:6083–6087, May 1983.

[24] RD King-Smith and David Vanderbilt. Theory of polarization of crystalline solids. *Physical Review B*, 47(3):1651, 1993.

[25] Gerardo Ortiz and Richard M Martin. Macroscopic polarization as a geometric quantum phase: Many-body formulation. *Physical Review B*, 49(20):14202, 1994.

[26] B. L. Altshuler and I. Glazman. Pumping Electrons. *Science*, 283(5409):1864–1865, 1999.

[27] Shuta Nakajima, Takafumi Tomita, Shintaro Taie, Tomohiro Ichinose, Hideki Ozawa, Lei Wang, Matthias Troyer, and Yoshiro Takahashi. Topological thouless pumping of ultracold fermions. *Nature Physics*, 2016.

[28] Michael Lohse, Christian Schweizer, Oded Zilberberg, Monika Aidelsburger, and Immanuel Bloch. A thouless quantum pump with ultracold bosonic atoms in an optical superlattice. *Nature Physics*, 12(4):350–354, 2016.

[29] Takashi Oka and Hideo Aoki. Photovoltaic Hall effect in graphene. *Physical Review B*, 79(8):081406, 2009.

[30] Takuya Kitagawa, Takashi Oka, Arne Brataas, Liang Fu, and Eugene Demler. Transport properties of nonequilibrium systems under the application of light: Photoinduced quantum Hall insulators without Landau levels. *Physical Review B*, 84(23):235108, 2011.

[31] Netanel H Lindner, Gil Refael, and Victor Galitski. Floquet topological insulator in semiconductor quantum wells. *Nature Physics*, 7(6):490–495, 2011.

[32] Netanel H Lindner, Doron L Bergman, Gil Refael, and Victor Galitski. Topological Floquet spectrum in three dimensions via a two-photon resonance. *Physical Review B*, 87(23):235131, 2013.

[33] Arijit Kundu, HA Fertig, and Babak Seradjeh. Effective theory of Floquet topological transitions. *Physical review letters*, 113(23):236803, 2014.

[34] Y.H. Wang, Hadar Steinberg, Pablo Jarillo-Herrero, and Nuh Gedik. Observation of Floquet-Bloch states on the surface of a topological insulator. *Science*, 342(6157):453–457, 2013.

[35] Gregor Jotzu, Michael Messer, Rémi Desbuquois, Martin Lebrat, Thomas Uehlinger, Daniel Greif, and Tilman Esslinger. Experimental realization of the topological haldane model with ultracold fermions. *Nature*, 515:237–240, 2014.

[36] Raffaello Bianco and Raffaele Resta. Mapping topological order in coordinate space. *Physical Review B*, 84(24):241106, 2011.

[37] Qian Niu and DJ Thouless. Quantised adiabatic charge transport in the presence of substrate disorder and many-body interaction. *Journal of Physics A: Mathematical and General*, 17(12):2453, 1984.

[38] Qian Niu. Theory of the quantized adiabatic particle transport. *Modern Physics Letters B*, 5(14n15):923–931, 1991.

[39] Rui Li and Michael Fleischhauer. Finite-size corrections to quantized particle transport in topological charge pumps. *arXiv preprint arXiv:1705.11179*, 2017.

[40] Q Niu. Towards a quantum pump of electric charges. *Physical review letters*, 64(15):1812, 1990.

[41] Wei-Kai Shih and Qian Niu. Nonadiabatic particle transport in a one-dimensional electron system. *Physical Review B*, 50(16):11902, 1994.

[42] MJ Rice and EJ Mele. Elementary excitations of a linearly conjugated diatomic polymer. *Physical Review Letters*, 49(19):1455, 1982.

[43] Jon H. Shirley. Solution of Schrödinger equation with a hamiltonian periodic in time. *Phys. Rev.*, 138:B979, 1965.

[44] Hideo Sambe. Steady states and quasienergies of a quantum-mechanical system in an oscillating field. *Physical Review A*, 7(6):2203, 1973.

[45] Giulio Casati and Luca Molinari. "Quantum chaos" with time-periodic hamiltonians. *Progress of Theoretical Physics Supplement*, 98:287–322, 1989.

[46] Milena Grifoni and Peter Hänggi. Driven quantum tunneling. *Physics Reports*, 304(5):229–354, 1998.

[47] Heinz Peter Breuer and Martin Holthaus. Quantum phases and Landau-Zener transitions in oscillating fields. *Physics Letters A*, 140(9):507–512, 1989.

[48] HP Breuer and M Holthaus. Adiabatic processes in the ionization of highly excited hydrogen atoms. *Zeitschrift für Physik D Atoms, Molecules and Clusters*, 11(1):1–14, 1989.

[49] Stuart C Althorpe, Donald J Kouri, David K Hoffman, and Nimrod Moiseyev. A time-independent wavepacket approach to the (t, t')-method for treating time-dependent hamiltonian systems. *Chemical physics*, 217(2):289–296, 1997.

[50] Phillip Weinberg, Marin Bukov, Luca D'Alessio, Anatoli Polkovnikov, Szabolcs Vajna, and Michael Kolodrubetz. Adiabatic perturbation theory and geometry of periodically-driven systems. *Physics Reports*, 2017.

[51] Robert S Strichartz. *A guide to distribution theory and Fourier transforms*. World Scientific Publishing Co Inc, 2003.

[52] A. Russomanno. *Periodic driving of a coherent quantum many body system and relaxation to the Floquet diagonal ensemble*. PhD thesis, SISSA, Trieste, 2014.

[53] Achilleas Lazarides, Arnab Das, and Roderich Moessner. Periodic thermodynamics of isolated quantum systems. *Physical review letters*, 112(15):150401, 2014.

[54] Angelo Russomanno, Alessandro Silva, and Giuseppe E Santoro. Periodic steady regime and interference in a periodically driven quantum system. *Physical review letters*, 109(25):257201, 2012.

[55] Mark Srednicki. Chaos and quantum thermalization. *Physical Review E*, 50(2):888, 1994.

[56] Achilleas Lazarides, Arnab Das, and Roderich Moessner. Equilibrium states of generic quantum systems subject to periodic driving. *Phys. Rev. E*, 90:012110, 2014.

[57] Hyungwon Kim, Tatsuhiko N Ikeda, and David A Huse. Testing whether all eigenstates obey the eigenstate thermalization hypothesis. *Physical Review E*, 90(5):052105, 2014.

[58] Luca D'Alessio and Marcos Rigol. Long-time behavior of isolated periodically driven interacting lattice systems. *Physical Review X*, 4(4):041048, 2014.

[59] Angelo Russomanno, Rosario Fazio, and Giuseppe E Santoro. Thermalization in a periodically driven fully connected quantum Ising ferromagnet. *EPL (Europhysics Letters)*, 110(3):37005, 2015.

[60] Gregory H Wannier. Dynamics of band electrons in electric and magnetic fields. *Reviews of Modern Physics*, 34(4):645, 1962.

[61] G. Grosso and G.P. Parravicini. *Solid State Physics*. Academic Press, 2013.

[62] David Emin and CF Hart. Existence of Wannier-Stark localization. *Physical Review B*, 36(14):7353, 1987.

[63] Wannier-Stark ladders and loch oscillations in superlattices, author=Mendez, Emilio E and Bastard, Gérald, journal=Physics Today, volume=46, pages=34–34, year=1993, publisher=American Institute of Physics.

[64] Takeshi Nakanishi, Tomi Ohtsuki, and Motohiko Saitoh. Stark ladders in a two-dimensional tight-binding lattice. *Journal of the Physical Society of Japan*, 62(8):2773–2782, 1993.

[65] Ivar Martin, Gil Refael, and Bertrand Halperin. Topological frequency conversion in strongly driven quantum systems. *arXiv preprint arXiv:1612.02143*, 2016.

[66] Ching-Kai Chiu, Jeffrey CY Teo, Andreas P Schnyder, and Shinsei Ryu. Classification of topological quantum matter with symmetries. *Reviews of Modern Physics*, 88(3):035005, 2016.

[67] Takuya Kitagawa, Erez Berg, Mark Rudner, and Eugene Demler. Topological characterization of periodically driven quantum systems. *Physical Review B*, 82(23):235114, 2010.

[68] Alvaro Gómez-León and Gloria Platero. Floquet-bloch theory and topology in periodically driven lattices. *Physical review letters*, 110(20):200403, 2013.

[69] Frederik Nathan and Mark S. Rudner. Topological singularities and the general classification of Floquet–Bloch systems. *New Journal of Physics*, 17(12):125014, 2015.

[70] Michel Fruchart. Complex classes of periodically driven topological lattice systems. *Physical Review B*, 93(11):115429, 2016.

[71] Rahul Roy and Fenner Harper. Periodic table for floquet topological insulators. *arXiv preprint arXiv:1603.06944*, 2016.

[72] Xiao-Liang Qi, Yong-Shi Wu, and Shou-Cheng Zhang. General theorem relating the bulk topological number to edge states in two-dimensional insulators. *Physical Review B*, 74(4):045125, 2006.

[73] M. V. Berry. Quantal phase factors accompanying adiabatic changes. *Proc. Roy. Soc. Lond. A*, 392:45–57, 1984.

[74] F. D. M. Haldane. Model for a Quantum Hall Effect without Landau Levels: Condensed-Matter Realization of the "Parity Anomaly". *Phys. Rev. Lett.*, 61:2015–2018, Oct 1988.

[75] Realizing Haldane model in e-based honeycomb ferromagnetic insulators, author=Kim, Heung-Sik and Kee, Hae-Young, journal=npj Quantum Materials, volume=2, number=1, pages=20, year=2017, publisher=Nature Publishing Group.

[76] Kush Saha. Photoinduced Chern insulating states in semi-dirac materials. *Physical Review B*, 94(8):081103, 2016.

[77] Shu-Ting Pi and Sergey Savrasov. Polarization induced Z2 and Chern topological phases in a periodically driving field. *Scientific reports*, 6, 2016.

[78] Liang Jiang, Takuya Kitagawa, Jason Alicea, AR Akhmerov, David Pekker, Gil Refael, J Ignacio Cirac, Eugene Demler, Mikhail D Lukin, and Peter Zoller. Majorana fermions in equilibrium and in driven cold-atom quantum wires. *Physical review letters*, 106(22):220402, 2011.

[79] Guocai Liu, Ningning Hao, Shi-Liang Zhu, and W.M. Liu. Topological superfluid transition induced by a periodically driven optical lattice. *Physical Review A*, 86(1):013639, 2012.

[80] Dong E. Liu, Alex Levchenko, and Harold U. Baranger. Floquet Majorana fermions for topological qubits in superconducting devices and cold-atom systems. *Physical review letters*, 111(4):047002, 2013.

[81] Mónica Benito, A. Gómez-León, V.M. Bastidas, Tobias Brandes, and Gloria Platero. Floquet engineering of long-range p-wave superconductivity. *Physical Review B*, 90(20):205127, 2014.

[82] Matthew S. Foster, Victor Gurarie, Maxim Dzero, and Emil A. Yuzbashyan. Quench-induced Floquet topological p-wave superfluids. *Physical review letters*, 113(7):076403, 2014.

[83] Rui Wang, Baigeng Wang, Rui Shen, L. Sheng, and D. Y. Xing. Floquet Weyl semimetal induced by off-resonant light. *EPL (Europhysics Letters)*, 105(1):17004, 2014.

[84] Zhongbo Yan and Zhong Wang. Tunable Weyl points in periodically driven nodal line semimetals. *Phys. Rev. Lett.*, 117:087402, Aug 2016.

[85] Hailong Wang, Longwen Zhou, and Y. D. Chong. Floquet Weyl phases in a three-dimensional network model. *Phys. Rev. B*, 93:144114, Apr 2016.

[86] Ching-Kit Chan, Yun-Tak Oh, Jung Hoon Han, and Patrick A. Lee. Type-II Weyl cone transitions in driven semimetals. *Phys. Rev. B*, 94:121106, Sep 2016.

[87] Jin-Yu Zou and Bang-Gui Liu. Floquet Weyl fermions in three-dimensional stacked graphene systems irradiated by circularly polarized light. *Phys. Rev. B*, 93:205435, May 2016.

[88] Xiao-Xiao Zhang, Tze Tzen Ong, and Naoto Nagaosa. Theory of photoinduced Floquet Weyl semimetal phases. *Phys. Rev. B*, 94:235137, Dec 2016.

[89] Leda Bucciantini, Sthitadhi Roy, Sota Kitamura, and Takashi Oka. Emergent Weyl nodes and Fermi arcs in a Floquet Weyl semimetal. *Phys. Rev. B*, 96:041126, Jul 2017.

[90] Zhongbo Yan and Zhong Wang. Floquet multi-Weyl points in crossing-nodal-line semimetals. *Phys. Rev. B*, 96:041206, Jul 2017.

[91] Motohiko Ezawa. Photoinduced topological phase transition from a crossing-line nodal semimetal to a multiple-Weyl semimetal. *Physical Review B*, 96(4):041205, 2017.

[92] Yunhua Wang, Yulan Liu, and Biao Wang. Effects of light on quantum phases and topological properties of two-dimensional metal-organic frameworks. *Scientific Reports*, 7:41644, 2017.

[93] Zhongbo Yan, Ren Bi, Huitao Shen, Ling Lu, Shou-Cheng Zhang, and Zhong Wang. Nodal-link semimetals. *arXiv preprint arXiv:1704.00655*, 2017.

[94] G.E. Santoro. *Introduction to Topological Insulators*, 2014. Available on request to the author (santoro@sissa.it).

[95] Mark S Rudner, Netanel H Lindner, Erez Berg, and Michael Levin. Anomalous edge states and the bulk-edge correspondence for periodically driven two-dimensional systems. *Physical Review X*, 3(3):031005, 2013.

[96] Philip Richard Wallace. The band theory of graphite. *Physical Review*, 71(9):622, 1947.

[97] B. E. A. Saleh e M. C. Teich. *Fundamentals of Photonics*. John Wiley & sons, Chichester, 1991.

[98] Tadashi Kadowaki and Hidetoshi Nishimori. Quantum annealing in the transverse Ising model. *Physical Review E*, 58(5):5355, 1998.

[99] Giuseppe E Santoro, Roman Martoňák, Erio Tosatti, and Roberto Car. Theory of quantum annealing of an Ising spin glass. *Science*, 295(5564):2427–2430, 2002.

[100] Giuseppe E Santoro and Erio Tosatti. Optimization using quantum mechanics: quantum annealing through adiabatic evolution. *Journal of Physics A: Mathematical and General*, 39(36):R393, 2006.

[101] Amit Dutta, Gabriel Aeppli, Bikas K Chakrabarti, Uma Divakaran, Thomas F Rosenbaum, and Diptiman Sen. Quantum phase transitions in transverse field spin models: from statistical physics to quantum information, 2015.

[102] Lev D Landau. Zur theorie der energieubertragung. ii. *Phys. Z. Sowjetunion*, 2(46):1–13, 1932.

[103] Clarence Zener. Non-adiabatic crossing of energy levels. *Proceedings of the Royal Society of London A*, 137(833):696–702, 1932.

[104] Ettore Majorana. Atomi orientati in campo magnetico variabile. *Il Nuovo Cimento (1924-1942)*, 9(2):43–50, 1932.

[105] Tom WB Kibble. Some implications of a cosmological phase transition. *Physics Reports*, 67(1):183–199, 1980.

[106] Wojciech H Zurek. Cosmological experiments in superfluid helium? *Nature*, 317(6037):505–508, 1985.

[107] Jacek Dziarmaga. Dynamics of a quantum phase transition and relaxation to a steady state. *Advances in Physics*, 59(6):1063–1189, 2010.

[108] R. B. Laughlin. Quantized Hall conductivity in two dimensions. *Phys. Rev. B*, 23:5632, 1981.

[109] M. D. Caio, N. R. Cooper, and M. J. Bhaseen. Quantum quenches in Chern Insulators. *Phys. Rev. Lett.*, 115:236403, Dec 2015.

[110] Jan P. Dahlhaus, Benjamin M. Fregoso, and Joel E. Moore. Magnetization signatures of light-induced quantum Hall edge states. *Physical Review Letters*, 114(24):246802, 2015.

[111] Luca D'Alessio and Marcos Rigol. Dynamical preparation of Floquet Chern insulators. *Nat. Commun.*, 6:8336, 10 2015.

[112] W. Kohn. Density functional and density matrix method scaling linearly with the number of atoms. *Phys. Rev. Lett.*, 76:3168–3171, Apr 1996.

[113] Raffaele Resta. The insulating state of matter: a geometrical theory. *The European Physical Journal B*, 79(2):121–137, 2011.

[114] MA Sentef, M Claassen, AF Kemper, B Moritz, T Oka, JK Freericks, and TP Devereaux. Theory of Floquet band formation and local pseudospin textures in pump-probe photoemission of graphene. *Nature Communications*, 6, 2015.

[115] A. Bermudez, L. Amico, and M.A. Martin-Delgado. Dynamical delocalization of Majorana edge states by sweeping across a quantum critical point. *New Journal of Physics*, 12(5):055014, 2010.

[116] A. Bermudez, D. Patane, L. Amico, and M.A. Martin-Delgado. Topology-induced anomalous defect production by crossing a quantum critical point. *Physical review letters*, 102(13):135702, 2009.

[117] Di Xiao, Ming-Che Chang, and Qian Niu. Berry phase effects on electronic properties. *Reviews of modern physics*, 82(3):1959, 2010.

[118] Dominik Linzner, Lukas Wawer, Fabian Grusdt, and Michael Fleischhauer. Reservoir-induced Thouless pumping and symmetry-protected topological order in open quantum chains. *Physical Review B*, 94(20):201105, 2016.

[119] Netanel H Lindner, Erez Berg, and Mark S Rudner. Universal chiral quasisteady states in periodically driven many-body systems. *Phys. Rev. X*, 7(1):011018, 2017.

[120] Ken-Ichiro Imura, Yukinori Yoshimura, Takahiro Fukui, and Yasuhiro Hatsugai. Bulk-edge correspondence in topological transport and pumping. *arXiv preprint arXiv:1706.04493*, 2017.

[121] Ruggero Ferrari. Floquet energies and quantum Hall effect in a periodic potential. *International Journal of Modern Physics B*, 12(11):1105–1123, 1998.

[122] Joseph E Avron and Zvi Kons. Quantum response at finite fields and breakdown of Chern numbers. *Journal of Physics A: Mathematical and General*, 32(33):6097, 1999.

[123] Raffaele Resta. *Berry's Phase and Geometric Quantum Distance: Macroscopic Polarization and Electron Localization.* Troisième cycle de la physique en Suisse romande, 2000.

[124] J.E. Moore. Topological Aspects of Condensed Matter Physics: Lecture Notes of the Les Houches Summer School: Volume 103, August 2014. volume 103. Oxford University Press, 2017.

[125] J. Von Neumann and E. Wigner. Über merkwürdige diskrete Eigenwerte. *Z. Phys.*, 30:467, 1929.

[126] Heinz-Peter Breuer and Francesco Petruccione. *The theory of open quantum systems.* Oxford University Press on Demand, 2002.

[127] Dmitry A. Abanin, Wojciech De Roeck, Wen Wei Ho, and Fran**c**cois Huveneers. Effective Hamiltonians, prethermalization, and slow energy absorption in periodically driven many-body systems. *Physical Review B*, 95(1):014112, 2017.

[128] Francisco Machado, Gregory D Meyer, Dominic V Else, Chetan Nayak, and Norman Y Yao. Exponentially slow heating in short and long-range interacting Floquet systems. *arXiv preprint arXiv:1708.01620*, 2017.

[129] Pedro Ponte, Z Papić, Fran**c**cois Huveneers, and Dmitry A Abanin. Many-body localization in periodically driven systems. *Physical review letters*, 114(14):140401, 2015.

[130] Dominic V. Else and Chetan Nayak. Classification of topological phases in periodically driven interacting systems. *Physical Review B*, 93(20):201103, 2016.

[131] Hoi Chun Po, Lukasz Fidkowski, Ashvin Vishwanath, and Andrew C. Potter. Radical chiral Floquet phases in a periodically driven Kitaev model and beyond. *arXiv preprint arXiv:1701.01440*, 2017.

[132] Lukasz Fidkowski, Hoi Chun Po, Andrew C. Potter, and Ashvin Vishwanath. Interacting invariants for Floquet phases of fermions in two dimensions. *arXiv preprint arXiv:1703.07360*, 2017.

[133] Hossein Dehghani, Takashi Oka, and Aditi Mitra. Dissipative Floquet topological systems. *Physical Review B*, 90(19):195429, 2014.

[134] Hossein Dehghani, Takashi Oka, and Aditi Mitra. Out-of-equilibrium electrons and the Hall conductance of a Floquet topological insulator. *Physical Review B*, 91(15):155422, 2015.

[135] Hossein Dehghani and Aditi Mitra. Optical Hall conductivity of a Floquet topological insulator. *Physical Review B*, 92(16):165111, 2015.

[136] Thomas Iadecola, Titus Neupert, and Claudio Chamon. Occupation of topological Floquet bands in open systems. *Physical Review B*, 91(23):235133, 2015.

[137] Karthik I. Seetharam, Charles-Edouard Bardyn, Netanel H. Lindner, Mark S. Rudner, and Gil Refael. Controlled population of Floquet-Bloch states via coupling to Bose and Fermi baths. *Physical Review X*, 5(4):041050, 2015.

[138] Zhenghao Gu, HA Fertig, Daniel P Arovas, and Assa Auerbach. Floquet spectrum and transport through an irradiated graphene ribbon. *Physical review letters*, 107(21):216601, 2011.

[139] HP Breuer and M Holthaus. Adiabatic processes in the ionization of highly excited hydrogen atoms. *Zeitschrift für Physik D Atoms, Molecules and Clusters*, 11(1):1–14, 1989.

[140] Marin Bukov, Luca D'Alessio, and Anatoli Polkovnikov. Universal high-frequency behavior of periodically driven systems: from dynamical stabilization to Floquet engineering. *Advances in Physics*, 64(2):139–226, 2015.

[141] André Eckardt and Egidijus Anisimovas. High-frequency approximation for periodically driven quantum systems from a Floquet-space perspective. *New journal of physics*, 17(9):093039, 2015.

[142] Takahiro Mikami, Sota Kitamura, Kenji Yasuda, Naoto Tsuji, Takashi Oka, and Hideo Aoki. Brillouin-Wigner theory for high-frequency expansion in periodically driven systems: Application to Floquet topological insulators. *Physical Review B*, 93(14):144307, 2016.

[143] Jun John Sakurai and Eugene D Commins. *Modern quantum mechanics, revised edition*. AAPT, 1995.

[144] Raffaello Bianco. *Chern invariant and orbital magnetization as local quantities*. PhD thesis, 2014.

[145] R. Resta. *Geometry and Topology in Electronic Structure Theory*, 2015. available at `http://www-dft.ts.infn.it/~resta/gtse/draft.pdf`.

[146] Raffaele Resta. Quantum-mechanical position operator in extended systems. *Physical Review Letters*, 80(9):1800, 1998.

[147] Gustavo Rigolin, Gerardo Ortiz, and Victor Hugo Ponce. Beyond the quantum adiabatic approximation: Adiabatic perturbation theory. *Physical Review A*, 78(5):052508, 2008.

[148] Yakir Aharonov and J Anandan. Phase change during a cyclic quantum evolution. *Physical Review Letters*, 58(16):1593, 1987.

[149] AG Fainshtein, NL Manakov, and LP Rapoport. Some general properties of quasienergetic spectra of quantum systems in classical monochromatic fields. *Journal of Physics B: Atomic and Molecular Physics*, 11(14):2561, 1978.

[150] Mark J Ablowitz and Athanassios S Fokas. *Complex variables: introduction and applications*. Cambridge University Press, 2003.

[151] Francois David. *The Formalisms of Quantum Mechanics*, volume 893. Springer, 2015.